Diese Arbeit wurde vorgelegt am
Lehr- und Forschungsgebiet Theorie der hybriden Systeme

# Optimale Auslegung von Photovoltaikanlagen
## Optimal Design of Photovoltaic Systems

Bachelorarbeit
Informatik

April 2022


| | |
|---|---|
| Vorgelegt von<br>Presented by | Mustafa Alotbah<br>Püngelerstr. 1<br>52074 Aachen<br>Matrikelnummer: 376264<br>mustafa.alotbah@rwth-aachen.de |
| Erstprüfer<br>First examiner | Prof. Dr. rer. nat. Erika Ábrahám<br>Lehr- und Forschungsgebiet: Theorie der hybriden Systeme<br>RWTH Aachen University |
| Zweitprüfer<br>Second examiner | Prof. Dr. rer. nat. Thomas Noll<br>Lehr- und Forschungsgebiet: Software Modellierung und Verifikation<br>RWTH Aachen University |
| Betreuer<br>Supervisor | Dr. rer. nat. Pascal Richter<br>Lehr- und Forschungsgebiet: Theorie der hybriden Systeme<br>RWTH Aachen University |

# Eigenständigkeitserklärung

Hiermit versichere ich, dass ich diese Bachelorarbeit selbständig verfasst und keine anderen als die angegebenen Quellen und Hilfsmittel benutzt habe. Die Stellen meiner Arbeit, die dem Wortlaut oder dem Sinn nach anderen Werken entnommen sind, habe ich in jedem Fall unter Angabe der Quelle als Entlehnung kenntlich gemacht. Dasselbe gilt sinngemäß für Tabellen und Abbildungen. Diese Arbeit hat in dieser oder einer ähnlichen Form noch nicht im Rahmen einer anderen Prüfung vorgelegen.

Aachen, im April 2022

Mustafa Alotbah

*To my wise father, loving mother and adorable sisters*
*who have always supported and encouraged me*

## Acknowledgments

I would like to express my gratitude to my supervisor Dr. Pascal Richter for his guidance, encouragement throughout this thesis. I would also like to Prof. Erika Ábrahám and Prof. Thomas Noll for accepting and taking the time to read and correct this thesis. I am indeed blessed for the opportunity to work on such a captivating topic that combines different fields.
Also many thanks to my friends, who have supported me and listened to my endless talks about solar energy.

# Contents


**1. Introduction** **1**
1.1. Related Work . . . 2
1.2. Contribution . . . 4
1.3. Outline . . . 5

**2. Input Data** **6**
2.1. Meteorological Data . . . 6
2.2. Sun Position . . . 7
2.3. Cadastral Data . . . 11
2.4. Load profile . . . 14

**3. Simulation of a Photovoltaic System** **17**
3.1. Incident Radiation . . . 17
3.2. Photovoltaic Model . . . 19
3.2.1. Single-Diode Model . . . 21
3.2.2. Simple Efficiency Model . . . 29
3.2.3. Annual Energy Output . . . 30
3.3. Battery Storage Model . . . 33
3.4. Model Validation . . . 37
3.4.1. Photovoltaic Model . . . 37
3.4.2. Battery-Coupled Model . . . 42
3.5. Financial Model . . . 47
3.5.1. Levelized Cost of Electricity . . . 47
3.5.2. Levelized Cost of Solar Energy . . . 48
3.5.3. Levelized Cost of Stored Energy . . . 49
3.5.4. Financial Parameters . . . 51
3.5.5. Sensitivity Analysis . . . 53

**4. Optimization of the Photovoltaic Power Plant** **59**
4.1. Objective Function . . . 59
4.2. Constraints . . . 59
4.3. Optimization Routine . . . 61
4.3.1. Heuristic Method . . . 61
4.3.2. Newton's Method . . . 63

**5. Case Study** **66**
5.1. Case study 1 . . . 66
5.2. Case study 2 . . . 69
5.3. Case study 3 . . . 71
5.4. Discussion of Results . . . 73
5.4.1. Comparison with other tools . . . 73
5.4.2. Optimization strategies . . . 74

**6. Conclusion** **76**
6.1. Summary . . . . . . . . . . . . . . . . . . . . . . . . . . . . . . . . . 76
6.2. Future Work . . . . . . . . . . . . . . . . . . . . . . . . . . . . . . . . 77

**References** **78**

**List of Figures** **82**

**List of Tables** **84**

**Nomenclature** **85**

**Acronyms** **90**

**A. Appendix** **91**

# 1. Introduction

With the late awareness of the detrimental impacts that could be caused by the rapid climate change, investment in renewable energy has increased at a great rate. In fact, investment in solar energy alone has grown by roughly fifteen-fold since 2004, leading the way with 49% of global investment in renewable energy[1].

Solar photovoltaic (PV) systems are at the heart of solar energy. In 2020, the global capacity of PV systems has reached 707.5 $GW_p$, the capacity that the world would produce under ideal conditions, and is responsible for actual production of 135 $GW_p$ of electricity worldwide. Some of the drivers behind this unprecedented demand on PV systems is the rapid drop of their costs and reduction of $CO_2$ emissions. Since 2010, the prices of PV modules have declined by 90% as a result of technology advancement. Moreover, a volume of 35 million tons of $CO_2$ emissions has been avoided in Germany (comparable to what was produced by countries such as New Zealand in the same year[2]) thanks to the 5 $\mathrm{GW_p}$ of installed PV systems' capacity [1].

Figure 1.1: PV panels mounted on a roof of a building[3].

To further encourage installing photovoltaic rooftops, in this thesis an output of a virtual PV roof is simulated given an address of a building and few subjective parameters such as the number of residents and the maximum amount to be invested in PV systems, the optimal size and minimum costs of a PV roof panel are estimated. The simulation of PV roofs is also dependant on meteorological data, e.g. solar irradiation, ambient temperature and on cadastral data e.g. the direction, the tilt and the area of the roof.

[1]Global investment in renewables capacity was $303.5 billion in 2020, excluding large hydro, check `https://about.bnef.com/energy-transition-investment/`

[2]Country profile `https://ourworldindata.org/co2/country/new-zealand`

[3]For license check `https://pixabay.com/de/photos/solar-dach-sonnenenergie-2666770/`

## 1.1. Related Work

PV systems can be split into two categories, on- and off-grid systems. Off-grid systems incorporate the PV module or array which generate direct current (DC), DC-DC converters (batteries), then in order to supply power for household appliances (the electrical load) the DC has to be converted into alternating current (AC) through a DC-AC converter (power inverter), whereas on-grid systems include power transformers instead of batteries, net metering to be connected to the local utility grid. Whenever the PV produced power is more than the current usage, the power is exported. In case of power shortage, power from the utility grid is imported. Several tools for modeling and simulating the behavior of PV systems are available either online such as PV-Watts [9], PVGIS [47], PV-Online, PV*SOl [56] or offline such as PhotoVoltaic systems (PVsyst) [38] and System Advisor Model (SAM) [14] and HOMER [11], see Table 1.1 for a comparison.

| Model | Developer | Description | Availability |
|---|---|---|---|
| SAM | NREL, USA | Detailed performance and economic analysis. | Free |
| PV-Watts | NREL, USA | Online performance and cost estimation. | Free |
| PVsyst | ISE, Switzerland | Performance analysis and costs estimation. | Chargeable |
| HOMER | NREL, USA | Optimization and sensitivity analysis. | Chargeable |
| PV*SOL | Valentine Software, Germany | Performance and economic analysis. | Chargeable |

Table 1.1: Comparison of related tools.

In the following, the related work for each sub-system is discussed.

**Photovoltaic cell models** PV systems are characterized by their current-voltage curve and their maximum power point (MPP) which are dependent on electrical parts on the cell and module level as well as on the electrical load. There exists ample literature for modeling PV systems such as the single-diode model (SDM) which considers a series resistance, a shunt resistance and a linear independent current source connected in parallel to a diode, thus assuming that one lumped diode describes the characteristics of the PV system as developed by De Soto et al. [6]. There exists as well a double-diode model (DDM) that takes into account the loss resulting form the recombination at the depletion region of the P-N junction as explained by Sah et al. [52]. A three-diode model (TDM) additionally takes into consideration the electrical characteristics of the multi-crystalline solar cells and the leakage current through peripheries as presented by Nishioka et al. [41] and Khanna et al. [59]. Work done in [4] approached the PV modeling through Neural Networks. This approach becomes viable when an abundance of data is available.

While both DDM and TDM provide certain advantages, the cost of adding more diodes increases the computational complexity of the simulation. The SDM strikes a good balance between complexity and accuracy, which is one of the probable reasons why commercial tools such as PVsyst also uses the SDM [51] or free but advanced tools such as SAM [58].

The SDM developed by De Soto et al.[6] is a five parameter model based on data provided by manufacturers as well as semi-empirical correlation equations for the prediction of the energy production given certain cell parameters and operating conditions. Tian et al. [58] proposed a modified model for the current-voltage curve to account for parallel and series connections in a PV array. While the SDM is relatively fast when compared to other models, the optimization step adds another layer of computational complexity pushing the need for a yet faster model. A simple efficiency model as used in PV-Watts and other online PV modeling tools provides a good approximation.

**Battery models** Sometimes a battery storage is installed along PV modules. Estimating the lifetime of the battery is critical to correctly estimate the overall costs of such a system. If the battery has to be replaced too many times throughout the assessment period, it could be more expensive to invest in batteries. The lifetime of any other commodity depends on time. This is called calendar lifetime. The battery's lifetime is however also dependent on the frequency of charges and how deep each discharge is (depth of discharge). Therefore, there is an upper limit for the number of cycles of charging and discharging the battery before the battery reaches its lifetime end, mostly before its calendar lifetime. Approaches to predict a li-ion battery's behavior include electro-chemical models [20] based on physics to predict when to recharge the battery to avoid overcharge or undercharge, which also shorten the battery's lifetime. Such models provide reasonable fidelity but their need for very detailed input and computational complexity make them unsuitable for this application.

Models that are used for this application include capacity models as described in [7]. The power extracted or inserted into such models correlates to the charge current to the battery and the state-of-charge (SOC) of the battery. Applying different values of current to the battery changes how much the battery discharges or charges e.g. by changing polarity. To ensure a maximum benefit of the generated power, management systems coupled with the batteries use storage dispatch strategies such as variants peak shaving strategy [27]. An empirical approach to estimate the lifetime and minimize the cost of battery storage done by [10] can be integrated in this work. The efficiency of a roof mount PV system, that is how much of solar power is transformed into electrical power, is not only governed by its electrical components and its geographical location that determines the level of solar irradiation and temperature over the year, but also by the roof tilt, on which it is to be mounted, its orientation and its available area, the area of the roof that is not subject to constant shadow, caused by other neighbouring buildings or trees, or incompatible surface such as a chimney [60].

**Cadaster** An initiative from the Landesamt für Natur, Umwelt und Verbraucherschutz (LANUV) of the Nordrhein-Westfalen (NRW) has made a solar cadastre dataset for the buildings' roofs of the state including orientation, tilt and area. The solar cadastre is based on high resolution laser scanner data which were transformed into a digital map of surfaces. By intersecting this with a map of buildings, resulting in a list of subsurface of the buildings with their tilt, orientation and area. Additionally, unsuitable surface elements such as chimneys, dorms and woody plants were recognized along with the percentage of shadowing on the surfaces [32]. Thus, a good approximation of the available area on the roofs has been made available.

**Irradiance** Using these pieces of information, the incident radiation, the radiation on the tilted solar panel, can be calculated using the sum of direct and diffuse irradiance. The literature has an abundance of models to estimate the diffuse irradiance on a tilted surface. Isotropic or semi-isotropic models assume that the sky radiates with the same intensity from all directions except for the direction of the solar disk. Such models include Duffie [22], Liu and Jordan [34] and Koronakis [25]. Anisotropic models rely on anisotropy indices that describe how solar irradiance changes in different directions. Such models include Klucher [24], Hay and Davis [19] and Perez [44].

**Optimization** To work out the optimal size of a PV system, the total power of the PV system and the capacity of the battery have to be chosen to satisfy the electrical load. One method is to make simplified calculations based on monthly averages of meteorological data as done by Barra et al. [29]. Another method is to use stochastic features of the data such distributions and correlations of the actual data as presented by Balouktsis et al. [3]. When considering an on-grid system, the goal is usually to reduce the overall cost of electricity. Optimization for such systems required on hourly or even sub-hourly measured values averaged over around a 10-years period of meteorological data and load curve taken by an average citizen to carry out the simulations. This method is used by the majority of PV tools nowadays such as PV-Watts and SAM [9, 51].

## 1.2. Contribution

While SAM and PVsyst provide financial modeling, many of the aforementioned variables have to be modeled manually, which renders these tools suitable for engineers but not easily accessible by the average stakeholder, a homeowner. Other easily accessible tools such as PV-Watts or PVGIS are, on the other hand, intuitive and user-friendly, but do not account for financial modeling. Moreover they do not deliver an optimal design, a design that minimizes the overall costs of electricity [28].

In this work, a tool is developed to simulate and search for a techno-economic optimal design of a grid-connected PV-Battery open rack (fixed) systems. The Sun's apparent position is calculated for any time of year and meteorological information for the region as well as cadastral information for the rooftop of the target building are retrieved automatically. The average load curve is assumed as given by the federal association of the energy and water industry (BDEW) for a residential and a commercial profile.

The simulation of PV panels is done using both an electrical model (SDM) and a simple efficiency model. The simulation of a lithium-ion battery is implemented using a simple round-trip efficiency model. The battery's lifetime is estimated using a statistical method.

The financial model implemented in this work accounts for the present and future costs of the PV-Battery system, the costs paid to grid and revenues from feeding (exporting) the grid an excess of energy. Furthermore, the effect of the deviation of various financial parameters is discussed to provide an overview of how these affect the optimal design of the system.

Finally, the optimization process is, initially, approached by different optimization methods and then a relatively fast heuristic approach is introduced that suits this application. The optimization pipeline, while allows for a financially unconstrained optimization, a financial limit on the equity is also possible.

## 1.3. Outline

Section 2 goes over the available data that shape the basis of this work. It provides an overview of the available meteorological and cadastral data as well as describes the used algorithms. Section 3 describes the methods used to simulate the PV systems and to calculate the annual energy yield. Then the methods of finding an optimal size of the PV roof panel are described in Section 4. Section 5 presents various study cases. Finally, Section 6 provides a summary and discusses further work.

# 2. Input Data

The output of a PV rooftop changes as many physical variables change. Some of which are independent of the PV system (mainly meteorological data such as solar irradiance, the PV panel orientation with respect to the Sun) or dependent on it which are mainly the electrical specifications given by the manufacturer, such as the Maximum Power Point (MPP). This section goes over the independent data, see Table 2.1.

## 2.1. Meteorological Data

In this section, data given by several meteorological services are compared and the relevant information are then discussed.

| Features | Units | Relevance | DWD | MeteoNorm | NREL |
|---|---|---|---|---|---|
| Air temperature | °C | • | ✓ | ✓ | ✓ |
| Air pressure | hPa | • | ✓ | ✓ | ✓ |
| Cloud cover | octa | | ✓ | ✓ | |
| Mass mixing ratio (absolute humidity) | g/kg | | ✓ | ✓ | |
| Relative humidity | % | | ✓ | ✓ | ✓ |
| Precipitation | mm or cm | | | ✓ | ✓ |
| Dew point temperature | °C | | | ✓ | ✓ |
| Wind direction | degree | | ✓ | ✓ | ✓ |
| Wind Speed | m/sec | • | ✓ | ✓ | ✓ |
| Extraterrestrial horizontal radiation | $W/m^2$ | | | ✓ | |
| Direct normal irradiance | $W/m^2$ | | | ✓ | ✓ |
| Direct horizontal irradiance | $W/m^2$ | • | ✓ | ✓ | |
| Diffuse horizontal irradiance | $W/m^2$ | • | ✓ | ✓ | ✓ |
| Global horizontal irradiance | $W/m^2$ | | | ✓ | ✓ |
| Clear-sky direct normal irradiance | $W/m^2$ | | | | ✓ |
| Clear-sky diffuse horizontal irradiance | $W/m^2$ | | | ✓ | ✓ |
| Clear-sky global horizontal irradiance | $W/m^2$ | | | ✓ | ✓ |
| Solar zenith or altitude | degree | • | | ✓ | ✓ |
| Solar azimuth | degree | • | | ✓ | |
| Incoming infrared radiation | $W/m^2$ | | ✓ | ✓ | |
| Outgoing infrared radiation | $W/m^2$ | | ✓ | ✓ | |
| Ultraviolet radiation | $W/m^2$ | | | ✓ | |
| Photosynthetic active radiation | $W/m^2$ | | | ✓ | |
| Surface Albedo | | | | ✓ | ✓ |
| Illuminance[1] | lux | | | ✓ | |
| Covered area | | | Germany | World | World |
| Interval | min | | 60 | 60 | 60, 30, 15 |
| License | | | free | chargeable | free |

Table 2.1: Features provided by different meteorological datasets. Relevant data to this work are marked with a bullet. In the following, either DNI or direct horizontal irradiance is used.

The data used in this work is the Test Reference Years (TRY) given by the Deutscher

[1]Values for direct, diffuse and global illuminance.

Wetterdienst (DWD) which provides hourly data for each variable over the course of an average year for the period of 1995-1995 (8760 hours). It provides information about the temperature measured 5m above ground and an hourly average of Diffuse and Direct Horizontal Irradiance. The position of the Sun can be calculated given a time of year as done in this work (see Section 2.2).
The Direct Normal Irradiance (DNI) is the amount of solar radiation per unit area measured on a perpendicular surface to the sun while the Direct Horizontal Irradiance is measured on a horizontal surface. So both can be calculated interchangeably given the solar altitude angle (see Section 3.1). The Global Horizontal Irradiance (GHI) is sum of direct and diffuse horizontal irradiance. Consequently, the data given by the DWD covers the requirements of the meteorological data for this work.
The data is provided for each square kilometer (tile) in Germany. However, since this work deals with residential areas, only the data from the closest tile to each ZIP code in Germany is extracted resulting in 8178 distinctive tiles.

## 2.2. Sun Position

The algorithm to calculate the Sun's position in this thesis is the SPA algorithm is explained in [50]. The algorithm is based on the book *The Astronomical Algorithms* by Jean Meeus [37], which is based on the Variations Sèculaires des Orbites Planètaires Theory which is developed by Bretagnon and Francou. The advantage of this algorithm is its great accuracy to calculate the Sun's altitude and azimuth angles in the period from the year -2000 to 6000 with uncertainties of $\pm 0.0003°$.

The calculations rely on a large set of (>2350) fixed parameters for Earth written as period tables.

**Earth periodic terms** used in the calculation of Earth's longitude and latitude angles in the heliocentric model, i.e. position of Earth with respect to the center of the Sun.

**Nutation periodic terms** Since the Earth's orbit is affected by the swaying motion of Earth because of the Moon, the longitude and obliquity of Earth needs correction from a model, where a planet has no moon.

In this section, the algorithm's equation, which are dependent on these parameters are not listed but can be accessed directly in the paper [50].

**Julian day** the Julian day $d_{\text{julian}}$ is calculated, which is the number of days since the beginning of the Julian Period, Jan 1 of the year -4712 at 12 in Greenwich civil time. The mean sidereal time at Greenwich $v_0$ calculated given the Julian day $d_{\text{julian}}$ and some fixed parameters.

**Earth and Sun Position** The Earth's heliocentric longitude $\lambda_{\oplus,\text{helio}}$ and latitude $\phi_{\oplus,\text{helio}}$ angles and the radius of the Earth's orbit $R_\oplus$ in Astronomical Units (AU) are calculated given the Julian day $d_{\text{julian}}$ and Earth periodic terms.

The Sun's longitude $\lambda_{\odot,\text{geo}}$ and latitude $\phi_{\odot,\text{geo}}$ angles are then calculated in the geocentric model, i.e. the Sun position with respect to the Earth's center.

$$\begin{aligned} \lambda_{\odot,\text{geo}} &= \lambda_{\oplus,\text{helio}} + 180^\circ \\ \phi_{\odot,\text{geo}} &= -\phi_{\oplus,\text{helio}} \end{aligned} \tag{2.1}$$

Then, the nutation in Sun's longitude $\Delta\lambda_{\odot,\text{geo}}$ and in the obliquity of the ecliptic $\Delta\varepsilon$ are calculated using the mean anomaly of the Sun, the mean anomaly of the Moon, the mean elongation of the Moon from the Sun. These are calculated using the nutation periodic terms and other fixed parameters.

The true obliquity of the ecliptic $\varepsilon$ is calculated by first calculating the mean obliquity of the ecliptic $\varepsilon_0$ using fixed parameters and the Julian day $d_{\text{julian}}$ and the by

$$\varepsilon = \frac{\varepsilon_0}{3600} + \Delta\varepsilon \tag{2.2}$$

The Sun's geocentric longitude without the correction for aberration $\lambda'_\odot$ and the apparent sidereal time at Greenwich $v$ are calculated as

$$\begin{aligned} \lambda'_\odot &= \lambda_{\odot,\text{geo}} + \Delta\lambda_{\odot,\text{geo}} \\ v &= v_0 + \Delta\lambda_{\odot,\text{geo}} \cdot \cos(\varepsilon) \end{aligned} \tag{2.3}$$

To correct for aberration, the Sun's apparent longitude $\lambda_\odot$ is calculated as

$$\lambda_\odot = \lambda'_\odot - \frac{20.4898}{3600 \cdot R_\oplus} \tag{2.4}$$

Then, the Sun's geocentric right ascension $\alpha_{\odot,\text{geo}}$ and declination $\delta_{\odot,\text{geo}}$ angles are calculated

$$\begin{aligned} \alpha_{\odot,\text{geo}} &= \operatorname{atan2}\left(\frac{\sin\lambda_\odot \cdot \cos\varepsilon - \tan\phi_{\odot,\text{geo}} \cdot \sin\varepsilon}{\cos\lambda_\odot}\right) \\ \delta_{\odot,\text{geo}} &= \arcsin\Big(\sin\phi_{\odot,\text{geo}} \cdot \cos\varepsilon + \cos\phi_{\odot,\text{geo}} \sin\varepsilon \cdot \sin\lambda_\odot\Big) \end{aligned} \tag{2.5}$$

The observer's geocentric hour angle $\theta_{\text{HRA, geo}}$ is calculated as

$$\theta_{\text{HRA, geo}} = v + \lambda - \alpha_{\odot,\text{geo}} \tag{2.6}$$

where $\lambda$ is the observer's geographical longitude angle.

**Topocentric Model** After calculating the Sun's geocentric right ascension $\alpha_{\odot,\text{geo}}$ and declination $\delta_{\odot,\text{geo}}$ angles, they need to be transformed into a topocentric model, i.e. the Sun's position angles are calculated with respect to the observer at the Earth's surface e.g. the PV panel (see Figure 2.1).

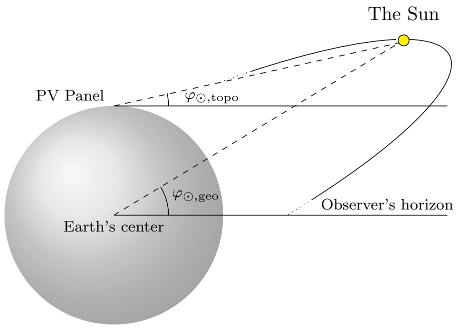


Figure 2.1: The Sun's geocentric and topocentric altitude $\varphi_{\odot,\text{geo}}$ and $\varphi_{\odot,\text{topo}}$ respectively.

Calculation of the Sun's topocentric right ascension $\alpha_{\odot,\text{topo}}$ is calculated in the following steps

(a) The equatorial parallax in the sun right ascension

$$\zeta = \frac{8.794}{3600 \cdot R_\oplus} \tag{2.7}$$

(b) the angle $\theta_u$

$$\theta_u = \arctan\Big((1 - f_\oplus) \cdot \tan\phi\Big) \tag{2.8}$$

where $\phi$ is the observer's latitude angle, $f_\oplus = 0.33581\%$ is the Earth's flattening ratio.

(c) The term $x$ is to correct for the Observer's elevation is calculated by

$$x = \cos\theta_u + \frac{E}{r_{\oplus,\text{equatorial}}} \cdot \cos\phi \tag{2.9}$$

where $r_{\oplus,\text{equatorial}} = 6378140\text{m}$ is the Earth's equatorial radius, and $E$ is the observer's distance to the center of Earth in meters.

(d) The parallax in the Sun's right ascension can now be calculated by

$$\Delta\alpha_\odot = \text{atan2}\Big(\frac{-x \cdot \sin\zeta \cdot \theta_{\text{HRA, geo}}}{\cos\delta_{\odot,\text{geo}} - x \cdot \sin\zeta \cdot \cos\theta_{\text{HRA, geo}}}\Big) \tag{2.10}$$

(e) The Sun's topocentric right ascension $\alpha_{\odot,\text{topo}}$ is then given as

$$\alpha_{\odot,\text{topo}} = \alpha_{\odot,\text{geo}} + \Delta\alpha_\odot \tag{2.11}$$

The topocentric local hour angle $\theta_{\text{HRA, topo}}$ can be calculated as

$$\theta_{\text{HRA, topo}} = \theta_{\text{HRA, geo}} + \Delta\alpha_\odot \tag{2.12}$$

And the Sun's topocentric declination $\delta_{\odot,\text{topo}}$ as

$$\delta_{\odot,\text{topo}} = \text{atan2}\Big(\frac{(\sin\delta_{\odot,\text{geo}} - y\cdot\sin\zeta)\cdot\cos\Delta\alpha_{\odot}}{\cos\delta_{\odot,\text{geo}} - x\cdot\sin\zeta\cdot\cos\theta_{\text{HRA, geo}}}\Big) \tag{2.13}$$

where $y$ is a term to correct for the observer's elevation, similar to the term $x$ in Equation (2.9) and is calculated as follows

$$y = \sin\theta_u + \frac{E}{r_{\oplus,\text{equatorial}}}\cdot\sin\phi \tag{2.14}$$

The Sun's topocentric altitude angle without correction for atmospheric refraction $\varphi'_{\odot}$ is calculated as

$$\varphi'_{\odot} = \arcsin\left(\sin\phi\cdot\sin\delta_{\odot,\text{topo}} + \cos\phi\cdot\cos\delta_{\odot,\text{topo}}\cdot\cos\theta_{\text{HRA, topo}}\right) \tag{2.15}$$

To correct for atmospheric refraction, the difference is calculated as

$$\Delta\varphi_{\odot} = \frac{p_{\text{ambient}}}{1010}\cdot\frac{283}{273.15 + T_{\text{ambient}}}\cdot\frac{1.02}{60\cdot\tan\left(\varphi'_{\odot} + \frac{10.3}{\varphi'_{\odot}+5.11}\right)} \tag{2.16}$$

where $p_{\text{ambient}}$ and $T_{\text{ambient}}$ are ambient pressure in hPa and the ambient temperature in Celsius degrees respectively. Finally the Sun's topocentric altitude $\varphi_{\odot}$ and azimuth $\gamma_{\odot}$ after correction for atmospheric refraction are given as

$$\begin{aligned} \varphi_{\odot} &= \varphi'_{\odot} + \Delta\varphi_{\odot} \\ \gamma_{\odot} &= \text{atan2}\left(\frac{\sin\theta_{\text{HRA, topo}}}{\cos\theta_{\text{HRA, topo}}\cdot\sin\phi - \tan\delta_{\odot,\text{topo}}\cdot\cos\phi}\right) + 180^{\circ} \end{aligned} \tag{2.17}$$

Hence, with a given time, geographical longitude $\lambda$ and latitude $\phi$ angles, as well as ambient pressure $p_{\text{ambient}}$ and temperature $T_{\text{ambient}}$ the Sun's position can be calculated with a high precision.

## 2.3. Cadastral Data

When a stakeholder considers investing in installing rooftop mount solar panels, it is important to know the orientation and the inclination of the building's rooftop, since that has a huge impact on the irradiation received by the solar panels. For this purpose, the calculation of these angles is done automatically by the user's address input. The state office for nature, environment and consumer protection of the NRW state (LANUV) has done a fascinating work by recording Laser Detection and Ranging (LIDAR) data of all buildings in the state of NRW and intersecting it with the a two dimensional map of the cities. This resulted in a number of surfaces of rooftops for each city in the NRW[1] with a precision of half meter.

| Parameter | Description |
|---|---|
| geb_id | The ID of the building, the surface belongs to. |
| richtung | The orientation of the surface where south is 180° and west is 270°. |
| neigung | The tilt angle of the surface. |
| gemeinde_gn | Name of the city, municipality, etc. |

Table 2.2: Features of the surfaces provided by the LANUV cadaster that are used in this thesis.

**Data structure** The data is available in GIS format and can be viewed as a list of surfaces. Each surfaces has relevant information such as the surface tilt and orientation

- City name
  - lat_50.68255_50.69893.json
  - ...
  - lat_50.83287_50.85486.json
    - Building 1
    - ...
    - Building $k \leq 1000$
      - geb_id
      - bounds
      - lon
      - lat
      - surfaces
        - surface 1
        - ...
        - surface $l$

Figure 2.2: The structure of cadaster data after processing.

[1]Data licence Germany attribution Version 2.0 - `https://www.opengeodata.nrw.de/produkte/umwelt_klima/klima/solarkataster/photovoltaik/`

The surfaces have been grouped by the building they belong to. The position of the shapes (polygons) is provided in European Terrestrial Reference System 1989 (ETRS98) coordinates, thus measured in meters. The bounds, i.e. the borders of the surfaces defining the building, have been calculated and converted into World Geodetic System of 1984 (WGS84) coordinates. The center of the building is stored as longitude and latitude angles in WGS84 coordinates. The buildings have been then sorted in an ascending order and every one thousand building has been stored in a json file that has the minimum and the maximum latitude of the buildings it contains in its name as in Figure 2.2.
Each building contains the building's ID, bounds, and the list of the surfaces that belong to the building. The list of surfaces has not been processed and includes all information as provided by LANUV cadaster, especially the parameters in Table 2.2 as well as the geographical shapes (in ETRS98 coordinates) as in Figure 2.3. Each surface contains a multiple of polygons. The first polygon is the shape of the surface, and the following polygons are obstacles and unusable areas.

**Search** Once a longitude and a latitude of a building is given along a city's name, the algorithm checks if the dataset of the corresponding city exists, then it iterates through the JSON files available and parses their names into a latitude range, if the latitude of the corresponding building is inside the latitude range of one of the JSON files, both the latitude and the longitude given are checked if they are in the bounds of any of the 1000 buildings in the JSON file. If the given coordinates are found, then the building object is returned.

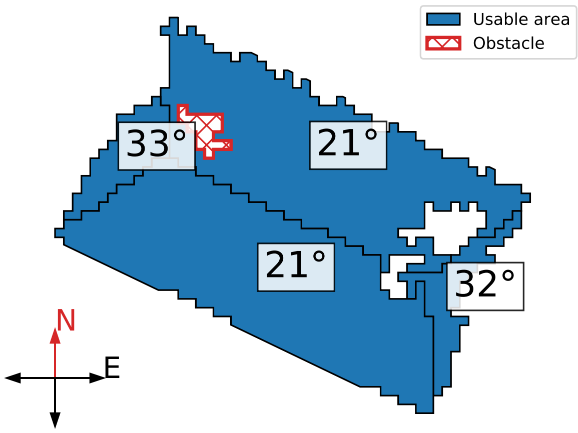


Figure 2.3: An example of a random building provided in the cadaster with the inclination of each of the surfaces of its rooftop.

One of the advantages of this dataset, is that structures that make an obstacle for the PV panels such as chimney are recognized and removed from the surfaces. Shadows are cut from the surfaces of the rooftop.

**Maximum number of panels** Assuming the all the modules are installed in parallel to the azimuth (orientation) of the surface either horizontally or vertically (see Figure 2.4), the maximum number of modules that fit in each surface can be estimated using a simple fitting algorithm. First the surfaces are smoothed out by averaging neighboring nodes with a fixed critical distance, then for each surface with a slope in the range of 15° to 45° the algorithm iteratively checks whether for the current location an available slot on the surface exist, i.e. if the slot is completely inside the surface and does not intersect with any obstacle. See Figure 2.4. Surfaces with tilt angles from 0° to 5° are considered flat surfaces and surfaces with a tilt angle from 5° to less than 15° is very expensive to construct because of static reasons.

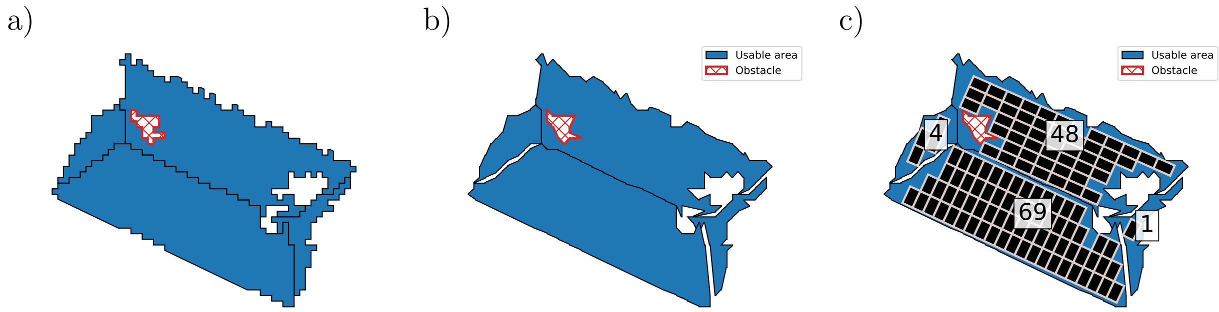


Figure 2.4: a) Raw data from the stored cadaster dataset, here (LANUV). b) the surfaces of the building after smoothing. c) The maximum number of slots for PV panels on each surface fit without intersecting with obstacles.

After this step is done, the simulation process sorts the surfaces by their mean annual incidence irradiance and fills the given number of PV panels starting the surface with the hgiher irradiance until it is completely filled, then moves to the next surface. Note that this algorithm is only used for approximation of the maximum panels that fit with an irregular shape, but it might underestimate the maximum number of panels that fit in the surface. Implementing an algorithm with high accuracy needs higher computational complexity making them not suited for this application. Thus, a professional examination on the spot is required.

## 2.4. Load profile

The load curve can be defined as the power requirement of a stakeholder in every time step, e.g. hour. The scale and fluctuations of the load curve has big a effect on the energetic and financial output of the system as will be demonstrated later sections, see Figure 3.38 for a comparison. Thus, it is key to simulate how the load changes over time in order to correctly predict the PV system's output. In this work, both residential as well as commercial buildings are accounted for.

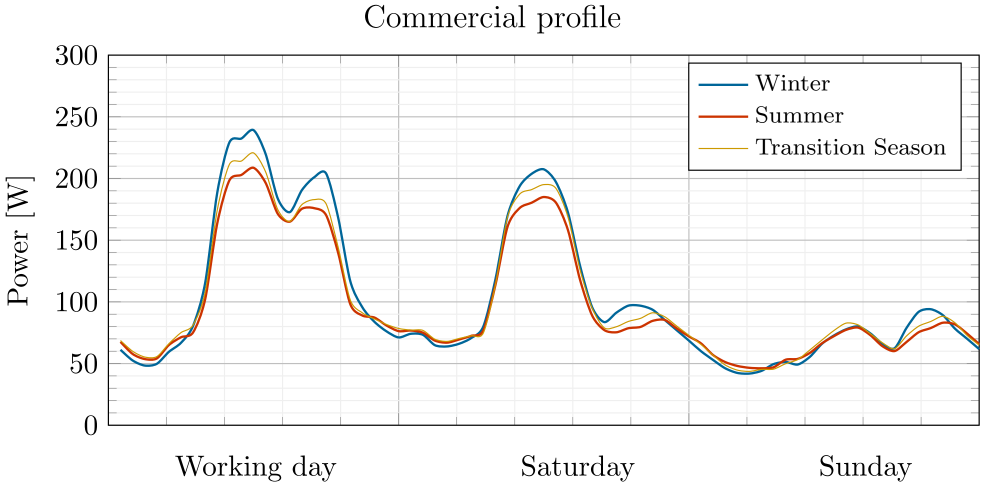


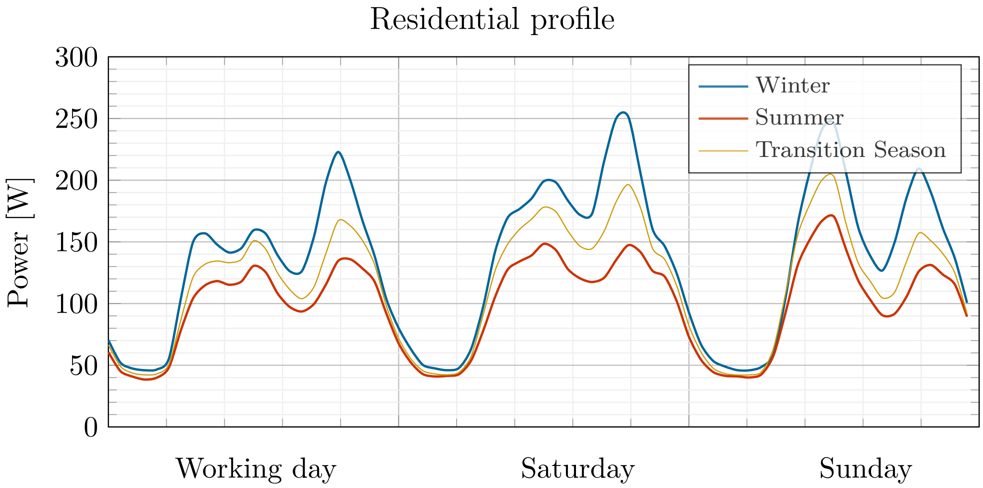


Figure 2.5: An hourly-based load profile for general trade (g0) above and household (h0) below on different days and in different seasons normalized by 1000 kWh per year [17].

**Commercial load curve** Commercial buildings show a regular and stable consumption over the course of a season. It differs for the most part on the day of the week. On working days more energy is consumed than on Sundays (see Figure 2.5). The load profile given by the federal association of the energy and water industry (BDEW) is processed here into an hourly distribution for general trade buildings (g0) for a normalized annual consumption of 1000 kWh per year. The load curve be then scaled according to the total area of the building and its class. For example offices show a tendency to consume 55 kWh/m$^2$ on average while food retailers consume 230 kWh/m$^2$ (see Table 2.3).

| Commercial | Annual Energy Consumption [kWh/m$^2$] | Commercial | Annual Energy Consumption [kWh/m$^2$] |
|---|---|---|---|
| Bakery | 500 | Pharmacy | 135 |
| Food Retailer | 230 | Barber | 130 |
| Gastronomy | 230 | Dental practice | 75 |
| Butchery | 190 | Office | 55 |
| Non-food retailer | 150 | Medical Practice | 42 |

Table 2.3: Average annual energy consumption per m$^2$ of commercials by profession[1].

The reasons for this wide diversity in commercials' load come down to what each of them uses. For example 82% of energy usage of bakeries comes from the backing process and fridges. Food retailers consume 59 kWh/m$^2$ a year of their total annual load for illumination. Offices on the other hand only need 27.5 kWh/m$^2$ for illumination. For businesses that close on Saturday, a Sunday consumption is assumed instead.
The approximations per area gives a good hint for the average production, but there is a considerable deviation for subjective reasons.

**Residential load curve** Residential buildings on the other hand show a gradual transition from one season to another. The load peaks to its highest on December 30 in winter where it reaches 0.36% of the annual consumption and drops by 60% to its lowest on July 18 in summer, as can be seen in Figure 2.6.

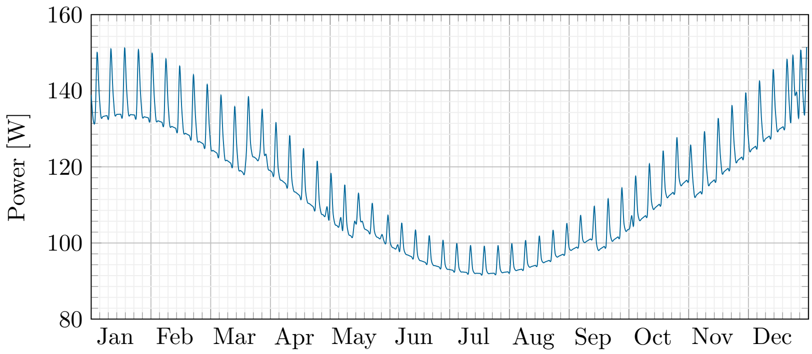


Figure 2.6: An hourly-based load profile for residential buildings (h0) normalized by 1000 kWh per year, peaking on the weekends and dropping on working days while showing a transitional tendency between seasons throughout the year [17].

[1]For details, check `https://evh.de/gewerbekunden/energie-sparen/energieberatung/energiespartipps`

It is also important to note that the residential data in Figure 2.5 are data extracted and averaged from the same data in Figure 2.6 which explains the deviation between seasons as opposed to the relatively steady power usage of commercial buildings. Scaling of residential buildings' load is based on the number of people living in the household and on two characteristics of the building. *Houses*, for example, consume more energy than *apartments* do for the same number of residents. Another relevant characteristic is whether warm water is heated using electricity or gas.

| | **Annual Energy Consumption [kWh]** | |
|---|---|---|
| **Number of residents** | Apartment | House |
| 1 | 2000 | 2900 |
| 2 | 3000 | 3800 |
| 3 | 4000 | 4800 |
| 4 | 4500 | 5500 |
| 5+ | 5200 | 6800 |

Table 2.4: Average energy consumption of residential buildings by number of people in the household in year 2021/22 assuming warm water is heated with electricity [5].

Consequently, the evaluation of the load at the $h$-hour of the year can be described as

$$P_{\text{load}}(h) = P_{\text{load, ref}}(h) \cdot E_{\text{load}}/1000 \text{ kWh} \tag{2.18}$$

Where $P_{\text{load, ref}}(h)$ is the normalized probability for the $h$-hour according to Figure 2.5 for commercial buildings and Figure 2.6 for residential buildings.
The Annual load is evaluated as follows:

$$E_{\text{load}} = \begin{cases} \text{Annual load per m}^2 \times \text{Area} & \text{for commercial buildings} \\ \text{Annual load per residents} & \text{for residential buildings} \end{cases} \tag{2.19}$$

annual load per residents is taken from Federal Ministry for Environment, Nature Conservation and Nuclear Safety (BMUV) [5] (see Table 2.4) and the annual energy consumption per $\text{m}^2$ is taken from data provided by SWH. EVH (see Table 2.3). Here winter, summer and transitional seasons are defined according to Table 2.5.

| **Season** | **Period** | |
|---|---|---|
| Winter | November 1st | March 20th |
| Spring (transitional) | March 21st | May 14th |
| Summer | May 15th | September 14th |
| Fall (transitional) | September 15th | October 31st |

Table 2.5: Definition of seasons as given by the BDEW [17].

# 3. Simulation of a Photovoltaic System

In this section, the simulation of a PV system is presented. First the calculation of incident radiation in Section 3.1 which follows from the calculation of the Sun's position in Section 2.2 Section 3.2 explains in depth the simulation of PV cells and derives the Single Diode Model (SDM) and then the simple efficiency model. The calculation of the annual energy output is presented in Section 3.2.3. The simple model of simulating the energy storage is then presented in Section 3.3. The presented models are validated in Section 3.4. Finally the financial model and the battery's lifetime model are presented in Section 3.5.

## 3.1. Incident Radiation

Before solar beams hit the surface of PV panel, a fair amount of them diffract and diffuse in the atmosphere resulting in two types of solar radiation on Earth, the direct radiation and the diffuse radiation. As mentioned in Section 2.1 the solar radiation given by the DWD dataset is measured on a horizontal surface. Occasionally, the direct normal irradiance (DNI) $I_{\text{direct, N}}$ is given, which is measured on a normal surface i.e. perpendicular to solar beams. The relationship between the DNI and the direct horizontal irradiance $I_{\text{direct, H}}$ is given by

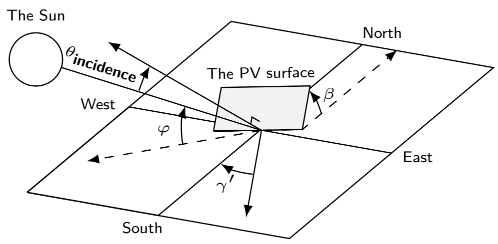


Figure 3.1: The angle of incidence $\theta_{\text{incidence}}$, the altitude of the Sun $\varphi$, the PV surface inclination $\beta$ and the azimuth of the PV surface $\gamma$.

$$I_{\text{direct, H}} = I_{\text{direct, N}} \cdot \sin(\varphi_\odot) \tag{3.1}$$

where $\varphi_\odot$ is the altitude of the Sun, see Equation (2.17). The global (total) horizontal irradiance is the sum of both types of radiation

$$I_{\text{global, H}} = I_{\text{direct, H}} + I_{\text{diffuse, H}} \tag{3.2}$$

Solar panels are usually not mounted horizontally rather on tilted rooftop with a given orientation (azimuth). Therefore, the angle of incidence has to be calculated in order to evaluate the solar radiation coming to the solar panel. The angle of incidence $\theta_{\text{incidence}}$ can be calculated as follows [22]

$$\cos\theta_{\text{incidence}} = \cos\varphi_\odot \cdot \sin\beta \cdot \cos(\gamma_\odot - \gamma) + \sin\varphi_\odot \cdot \cos\beta \tag{3.3}$$

where $\beta$ is the inclination (tilt) of the panel, $\gamma$ is the azimuth of the panel, where North is origin and west is positive (see Figure 3.1).

After calculating the angle of incidence $\theta_{\text{incidence}}$, the solar direct radiation on the tilted PV panel can be calculated geometrically as follows

$$I_{\text{direct, T}} = I_{\text{direct, H}} \cdot \frac{\cos\theta_{\text{incidence}}}{\sin\varphi_{\odot}} \tag{3.4}$$

As regards to diffuse radiation on a tilted surface, several models exist to predict it. Here the isotropic sky model by Duffie [22] is used

$$I_{\text{diffuse, T}} = I_{\text{diffuse, H}} \cdot \frac{1+\cos\beta}{2} \tag{3.5}$$

As the direct and diffuse beams hit the Earth's surface, some of them reflect and reach the PV panel as well. The radiations reflected from the ground can be described as

$$I_{\text{reflected, T}} = r_{\text{albedo}} \cdot I_{\text{global, H}} \cdot \frac{1-\cos\beta}{2} \tag{3.6}$$

where $r_{\text{albedo}}$ is the reflectance of the surface (albedo). The value of albedo depends on the material. Snow for example has a reflectance of 80% and fresh asphalt has a reflectance of 4%.
Therefore, the *global incident irradiance* $\mathcal{I}$ on the PV surface is

$$\mathcal{I} = I_{\text{direct, T}} + I_{\text{diffuse, T}} + I_{\text{reflected, T}} \tag{3.7}$$

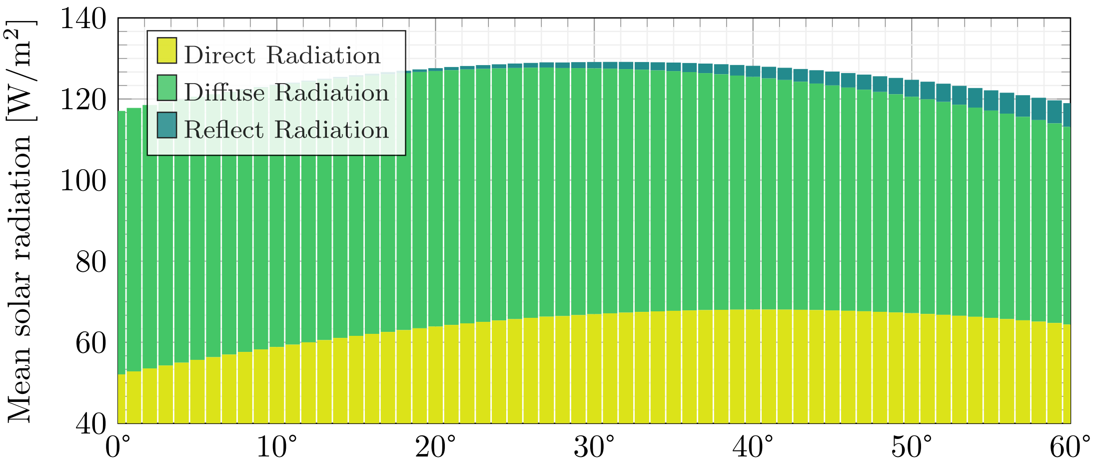


Figure 3.2: Share of the compoentns of the incident radiation averaged over a year on a panel oriented to the South $\gamma = 180°$ by various inclination angles in Aachen, Germany (50°46'16.1"N 6°03'05.4"E) based on the DWD dataset. Albedo is assumed to be constant $r_{\text{albedo}}$ =20%.

A wise choice of the inclination and orientation angles is critical for optimum insolation. The optimal azimuth in the northern hemisphere is true South, while the inclination angle differs from place to another. For example in Aachen it is around 31° in this model, see Figure 3.2.

## 3.2. Photovoltaic Model

Solar cells are semiconductor devices that transform portions of the incident radiation into electricity. Most solar cells are made of mono-crystalline silicon, which have better efficiency than poly-crystalline silicon [30] and are cheaper to produce than other more efficient materials such as Gallium Arsenide [21]. Semiconductors are materials with electrical conductivity that varies depending on their temperature. Their conductivity is better with lower temperatures. Silicon conductivity can be changed by doping silicon crystal (of the order of $10^{-6}$) with atoms that have an electron more on their valence shell, namely five valence electrons (pentavalent atoms) such as phosphorus to create a slightly negatively charged region (n-region) and with trivalent atoms such as boron to create a slightly positively charged region (p-region). When n-region and p-region are joined in the same crystal together, a depletion region, also called a junction, is created in between, as electrons from the n-region recombine with atoms that have a deficiency of electrons in their valence shell (holes) in the p-region region. This forms an electric field in the depletion region which causes electrons to move only in one direction, from the p-region to the n-region (see Figure 3.3).

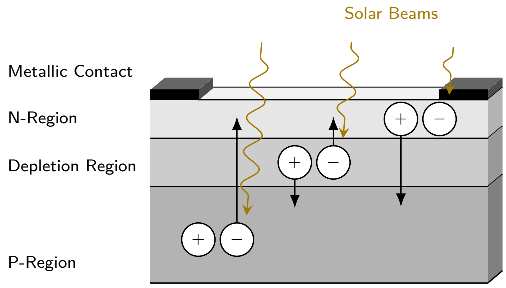

Figure 3.3: A cross section of a single junction photovoltaic solar cell.

**Power generation** Both regions become in the valence band, a state where electrons cannot be in a free state and hence move freely away from the atom. The energy needed to allow the electrons to move from the valence band to the conduction band is called the energy gap $E_g$ which decreases as temperature rises, see Equation (3.9). Incidence radiation is electromagnetic radiation which can be considered as discrete energy units (photons). The energy of a photon is given by

$$E_{\text{photon}} = h \cdot f_{\text{photon}} \tag{3.8}$$

where $h$ is the Planck's constant and $f_{\text{photon}}$ is the frequency of the photon. Photons with energy higher than the energy gap interact with electrons of an atom and bring them to the free state (photons are absorbed) in the p- and n-regions as well as in the depletion region. A photon with this energy can still only liberate one electron, the rest of its energy is lost to the cell as heat [39].

The electric field in the depletion region separates some of the liberated electrons before they recombine. By connecting the p-region and the n-region in a circuit, liberated electrons travel from the n-region through the circuit to the p-region and recombine with holes, this flow of electrons is called photocurrent $I_{\text{ph}}$. The band gap depends on the material the cell is made out of as well as its temperature. R. Pässler

[48] has given an approximation for the energy gap for semiconductors in $e$V as

$$E_g(T) = E_g(0) - \frac{\alpha \cdot T_{\text{phonon}}}{2} \cdot \left( \sqrt[p]{1 + (\frac{2T}{T_{\text{phonon}}})^p} - 1 \right) \tag{3.9}$$

where $t$ is given in kelvin unless otherwise mentioned, $E_g(0)$ is the band gap at absolute zero, $\alpha$ and $p$ are parameters, $t_{\text{phonon}}$ is approximately the average phonon temperature. Analogous to photons, a phonon is the quantized energy of vibration in the crystal lattice. For example, of a mono-crystalline lattice. The parameters of different semiconductor materials are given in Table 3.1. This approximation fits well below 80° Celsius [53] which is enough for civil purposes

| **Semiconductor** | $E_g(298.15)$ [$e$V] | $E_g(0)$ [$e$V] | $\alpha$ | $T_{\textbf{phonon}}$ | $p$ |
|---|---|---|---|---|---|
| Silicon | 1.124 | 1.17 | 0.318 | 406 | 2.33 |
| Cadmium Telluride | 1.528 | 1.606 | 0.310 | 108 | 1.97 |
| Gallium Arsenide | 1.427 | 1.519 | 0.472 | 230 | 2.44 |

Table 3.1: Physical parameters of different semiconductor materials used in PV systems [48]. Values of energy gap at 25° is calculated by the given approximation.

**Energy losses** In an ideal solar cell, the current generated by the solar cell is proportional to the incident radiation. Practically, this is not the case. Incident radiation contains a wide spectrum of wavelengths, but only those with higher energies than the energy gap of the electrons $E_{\text{photon}} > E_g(t)$ are absorbed. For silicon, this is equivalent to 1.1 $\mu$m at 25°C. This puts a theoretical limit to the efficiency of the single junction PV systems, for silicon this is 27%, for Cadmium Telluride it is 27.5% of total incident radiation [54, 39].

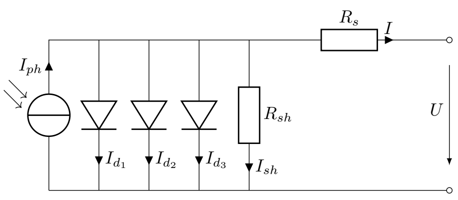


Figure 3.4: An equivalent circuit diagram based on Three-Diode Model of a solar cell.

The current generated by the solar cell in ideal conditions is called photocurrent $I_{\text{ph}}$. The output current of the solar cell $I$ is never equal to $I_{\text{ph}}$ due to electrical losses. When electrons are liberated in the p- and n-regions, many of them recombine with holes (recombination) before they travel through the circuit. Also a diffusion current is generated where electrons travel from n-region to the p-region, despite the barrier created in the depletion region, this loss of current is denoted by $I_{\text{d}_1}$. Additionally, the recombination process is not limited to the p- and n-regions but also occurs in the depletion region [52]. The loss of current due to this reason is denoted by $I_{\text{d}_2}$. Current could also be lost due to recombination in defect regions and through peripheries [41, 59] which is denoted by $I_{\text{d}_3}$.

Since we are looking at the system in temperatures considerably higher than absolute zero, losses take places in the form of two types resistance as well. The first happens because of resistance in the way of the electrons in the p- and n-regions and in the metallic contacts, this can be presented by a resistor in series and it is referred to as $R_\mathrm{s}$. The second type of resistance happens as electrons are shunted across the depletion region, resulting in additional current leakage. This is referred to as $R_\mathrm{sh}$ and the leaked current as $I_\mathrm{sh}$. Figure 3.4 is an equivalent circuit diagram for the solar cell with the aforementioned current leakages and resistances.

### 3.2.1. Single-Diode Model

Despite the fact, that the model with three diodes provides accurate approximations, it is computationally exhaustive which makes it unsuitable for the purposes of this work. Therefore, two assumptions are made to simplify this model. The first is that the solar cells do not contain defect regions. Thus, $I_{d_3}$ is removed. The second is that current leakage in the depletion region is negligible for the estimation of annual energy yield, thus, removing $I_{d_2}$ also. The resulting model is called the Single-Diode Model (SDM). Since only one diode is used. $I_d$ is used instead of $I_{d_1}$ for simplicity. The equivalent circuit diagram of the SDM can be seen in Figure 3.5. This model, while delivers decent results [22] it only requires data usually given by the manufacturer. It can also be extended into PV modules [36] and a PV arrays [58].

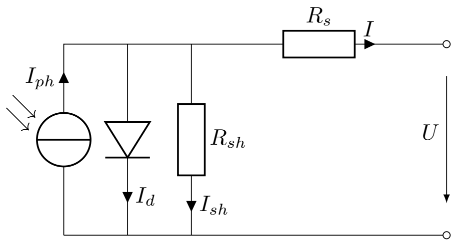


Figure 3.5: An equivalent circuit diagram for the Single-Diode Model of a solar cell.

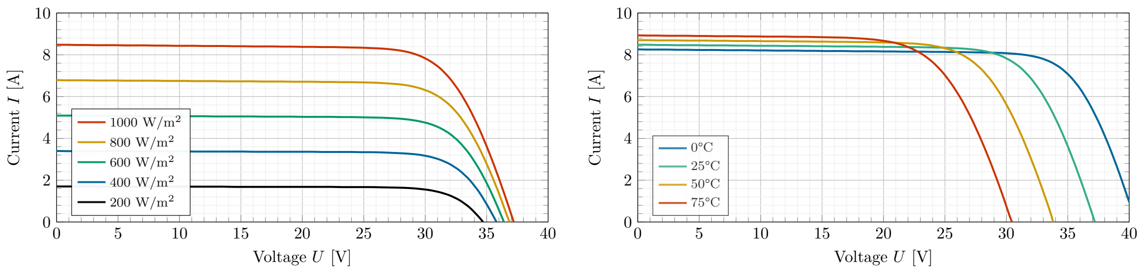


Figure 3.6: I-U curve by incident radiation at cell temperature 25°C on the left and by cell temperature at an irradiance of 1000 W/m$^2$ on the right. The data is produced by a simulation performed using this work for the module by BP solar model PB3325T.

When the load is not connected to the module, an open-circuit voltage $U_\mathrm{oc}$ is produced, but no current flows. If the module is short-circuited, no voltage is produced, but the short-circuit current $I_{\mathrm{sc}}$ flows. In both cases, no power is delivered by the module. However, when the load is connected to the module, a certain voltage is produced and some current will flow. The power delivered to the load, which is the product of the voltage and current, can be evaluated using a current-voltage curve (I-U curve) which changes according to cell temperature and incident radiation (see Figure 3.6).

The maximum power point (MPP) is when power delivered by the module at a given temperature and radiation is on its maximum. It is near the knee of the I-U curve. Since the generated power changes with the load demand, MPP tracking devices are used to adjust the load so that the delivered power always close to MPP. Such devices are based on MPP tracking (MPPT) algorithms to predict the optimal load demand and adjusts the load accordingly. This is possible, since the house appliances are not directly connected to the PV module in a DC-current rather through an a DC-AC inverter. To estimate the MPP delivered by the PV cell, reproducing I-U curve given cell temperature and incident radiation is key.

**Testing Conditions** Manufacturers usually provide relevant information by testing the PV cells in the Standard Reference Conditions (SRC) and the Nominal Operation Cell Temperature (NOCT). These conditions are listed in Table 3.2.

| Parameters | SRC | NOCT |
|---|---|---|
| Ambient temperature | | 20°C |
| Cell temperature | 25°C | |
| Incident radiation | 1000 W/m$^2$ | 800 W/m$^2$ |
| Air mass | 1.5 | 1.5 |

Table 3.2: Parameters in different testing conditions of solar cells. The cell temperature is NOCT varies by each module.

**Cell temperature** Estimating cell temperature, also called operating temperature is an important part of modeling a PV cell. It can be approximated through ambient temperature $t_{\mathrm{ambient}}$, incident radiation $\mathcal{I}$ and wind speed $v_{\mathrm{wind}}$ as given by Sandia [14]

$$T_{\mathrm{cell}} = T_{\mathrm{ambient}} + \Big(\exp(a + b \cdot v_{\mathrm{wind}}) + \frac{dt}{1000}\Big) \cdot \mathcal{I} \tag{3.10}$$

where $a, b, dt$ are construction parameters. In this application it is considered $a = -3.56$, $b = -0.075$ and $dt = 3$ °C. If the wind speed is not available, a model by [36] can used

$$T_{\mathrm{cell}} = T_{\mathrm{ambient}} + \Big(\frac{T_{\mathrm{NOCT}} - 20°C}{0.8}\Big) \cdot \mathcal{I} \tag{3.11}$$

**Derivation of output current** According to Kirchhoff's law, the output current can be calculated given the photocurrent $I_{\mathrm{ph}}$, the diode (leakage) current $I_{\mathrm{d}}$ and the shunt current $I_{\mathrm{sh}}$

$$I = I_{\mathrm{ph}} - I_{\mathrm{d}} - I_{\mathrm{sh}} \tag{3.12}$$

The photocurrent $I_{\text{ph}}$ changes linearly with the incident irradiation $\mathcal{I}$, see Equation (3.7), as well as with cell temperature. $I_d$ is the considered leakage current, modeled by a diode, from which the model inherits its non-linear characteristics. The shunt current $I_{sh}$ can be written as

$$I_{\text{sh}} = \frac{U + R_{\text{s}} \cdot I}{R_{\text{sh}}} \tag{3.13}$$

Current flowing through the diode is temperature dependent and is given by the equation

$$I_{\text{d}} = I_0 \cdot \left( e^{\frac{U_d}{nU_T}} - 1 \right) \tag{3.14}$$

Where $I_0$ is the reverse saturation current. $U_d$ is the voltage across the diode. $n$ is an ideality factor. $U_T$ is the volt equivalent of temperature and is given by

$$U_T = \frac{k \cdot T_{\text{cell}}}{q} \tag{3.15}$$

where $T_{\text{cell}}$ is the diode's temperature in Kelvin. $k$ is the Boltzmann constant and $q$ is the elementary charge of an electron. By substituting $U_d$ with $U - R_s \cdot I$ and using Equation (3.15), Equation (3.14) becomes

$$I_d = I_0 \cdot \Big( \exp\big(\frac{q \cdot (U + R_s \cdot I)}{n \cdot k \cdot T_{\text{cell}}}\big) - 1 \Big) \tag{3.16}$$

The ideality factor $n$ corresponds to various mechanisms responsible for moving the electrons across the depletion region. Here we assume that it only relates to the material of the semiconductor used and does not change with temperature or incident radiation. Its value is between 1 and 2. When $n$ is close to 1, it can be interpreted that current the leakage is mainly due to diffusion. When it approaches 2, current is leaked primarily in the recombination process in the depletion region, for silicon cells it is usually close to 1.3 [49, 58].
Now substituting Equation (3.13) and Equation (3.16) in Equation (3.12) yields

$$I = I_{\text{ph}} - I_0 \cdot \Big( \exp\big(\frac{q \cdot (U + R_s \cdot I)}{n \cdot k \cdot T_{\text{cell}}}\big) - 1 \Big) - \frac{U + R_s \cdot I}{R_{sh}} \tag{3.17}$$

**Photovoltaic array** The SDM can be applied to PV modules and array. A PV module is a group of PV cells connected in series. PV arrays are a group of PV modules connected in series and in parallel. If $N_{c,\text{module}}$ represents the number of cells in series in a module and $N_{\text{modules, series}}$ represents number of modules connected in an array in series, then we define

$$N_s = N_{c,\text{module}} \cdot N_{\text{modules, series}} \tag{3.18}$$

If we have $N_{\text{p}}$ modules connected in parallel, then the number of modules is

$$N_{\text{modules}} = N_{\text{p}} \cdot N_{\text{modules, series}} \tag{3.19}$$

and Equation (3.17) becomes [58]

$$I = N_p \cdot I_{\text{ph}} - N_p \cdot I_0 \cdot \Big( \exp\big(\frac{q \cdot (U + \frac{N_s}{Np} R_s \cdot I)}{N_s \cdot n \cdot k \cdot T_{\text{cell}}}\big) - 1 \Big) - \frac{U + \frac{N_s}{Np} R_s \cdot I}{\frac{N_s}{Np} R_{sh}} \tag{3.20}$$

where $I$ and $U$ are the current and the voltage of the array respectively.

The reverse saturation current $I_0$ changes non-linearly with temperature. The reverse saturation current at SRC temperature $T_{\text{ref}}$ is denoted $I_{0,\text{ref}}$. With this reference, it can be calculated at any cell temperature $T_{\text{cell}}$ [39]

$$I_0(T_{\text{cell}}) = I_{0,\text{ref}} \cdot (\frac{T_{\text{cell}}}{T_{\text{ref}}})^3 \cdot \exp\Big(\frac{q \cdot E_g(T_{\text{ref}})}{k \cdot T_{\text{ref}}} - \frac{q \cdot E_g(T_{\text{cell}})}{k \cdot T_{\text{cell}}}\Big) \tag{3.21}$$

The energy gap of electrons (see Equation 3.9) is multiplied with the elementary charge $q$ to convert its unit from [eV] into Coulombs.

The photocurrent $I_{\text{ph}}$ depends on both the incident radiation $\mathcal{I}$ and the cell temperature $T_{\text{cell}}$

$$I_{\text{ph}}(T_{\text{cell}}, \mathcal{I}) = I_{\text{ph, ref}} \cdot \frac{\mathcal{I}}{\mathcal{I}_{\text{ref}}} \cdot \big(1 + \mu_{I_{\text{sc}}}(T_{\text{cell}} - T_{\text{ref}})\big) \tag{3.22}$$

where $I_{\text{ph, ref}}$ is the photocurrent at SRC temperature $T_{\text{ref}}$ and $\mathcal{I}_{\text{ref}}$ is SRC incident radiation. The parameter $\mu_{I_{\text{sc}}}$ is the relative short-circuit current temperature coefficient.

The shunt resistance $R_{\text{sh}}$ is mainly dependent on incident irradiation and can be viewed as independent of temperature [18]

$$R_{\text{sh}}(\mathcal{I}) = R_{\text{sh, ref}} \cdot \frac{\mathcal{I}_{\text{ref}}}{\mathcal{I}} \tag{3.23}$$

where $R_{\text{sh, ref}}$ is the shunt resistance in SRC. The series resistance $R_{\text{s}}$ on the other hand is independent of both temperature and incident radiation, thus

$$R_{\text{s}} = R_{\text{s, ref}} \tag{3.24}$$

Previous equations contained different parameters, unfortunately many of them are not provided by the manufacturer. Table 3.3 contains parameters need for I-U curve approximation and demonstrates which are typically provided by the manufacturer.

| Parameters | Symbol | Availability |
|---|---|---|
| Maximum Power Point in SRC | $P_{\text{max, ref}}$ | ✓ |
| Efficiency | $\eta_{\text{PV}}$ | ✓ |
| Relative power temperature coefficient | $\mu_{\text{P}}$ | ✓ |
| Short-circuit current in SRC | $I_{\text{sc, ref}}$ | ✓ |
| Open-circuit voltage in SRC | $U_{\text{oc, ref}}$ | ✓ |
| Current at MPP in SRC | $I_{\text{mpp, ref}}$ | ✓ |
| Voltage at MPP in SRC | $U_{\text{mpp, ref}}$ | ✓ |
| Relative short-circuit current temperature coefficient | $\mu_{I_{\text{sc}}}$ | ✓ |
| Relative open-circuit voltage temperature coefficient | $\mu_{U_{\text{oc}}}$ | ✓ |
| Series resistance in SRC | $R_{\text{s, ref}}$ | |
| Shunt resistance in SRC | $R_{\text{sh, ref}}$ | |
| Reverse saturation current in SRC | $I_{\text{0, ref}}$ | |
| Photocurrent in SRC | $I_{\text{ph, ref}}$ | |
| Ideality factor | $n$ | |

Table 3.3: Availability of required parameters to approximate the I-U curve of a solar cell in different temperatures and radiation. As well as demonstrating which are usually provided by the manufacturer.

When absolute temperature coefficients are provided, the relative coefficients can be calculated by

$$\mu_{I_{\text{sc}}} = \frac{\mu'_{I_{\text{sc}}}}{I_{\text{sc, ref}}}, \qquad \mu_{V_{\text{oc}}} = \frac{\mu'_{V_{\text{oc}}}}{V_{\text{oc, ref}}} \tag{3.25}$$

where $\mu'_{I_{\text{sc}}}$ and $\mu'_{V_{\text{oc}}}$ are the absolute temperature coefficients for short-circuit current and open-circuit voltage respectively.

**Parameters Estimation** On these grounds, it is critical to estimate the five unknown parameters. The model presented by DeSoto et al. provides five equations which can be simultaneously solved to estimate the parameters.

- *The first equation* is derived from Equation (3.20) in open-circuit conditions in SRC, as the current $I$ becomes zero, and the voltage provided becomes $V_{\text{oc}}$, thus

$$N_p \cdot I_{\text{ph, ref}} - N_p \cdot I_{\text{0, ref}} \cdot \Big(\exp\big(\frac{q \cdot U_{\text{oc, ref}}}{N_s \cdot n \cdot k \cdot T_{\text{ref}}}\big) - 1\Big) - \frac{U_{\text{oc, ref}}}{\frac{N_s}{N_p} R_{\text{sh, ref}}} = 0 \tag{3.26}$$

- *The second equation* is also derived from Equation (3.20) in short-circuit conditions in SRC, as the voltage $U$ becomes zero and the current becomes $I_{\text{sc, ref}}$

$$I_{\text{sc, ref}} = N_p \cdot I_{\text{0, ref}} - N_p \cdot I_{\text{0, ref}} \cdot \Big(\exp\big(\frac{q \cdot I_{\text{sc, ref}} R_{\text{sc, ref}}}{N_s \cdot n \cdot k \cdot T_{\text{ref}}}\big) - 1\Big) - \frac{I_{\text{sc, ref}} \cdot \frac{N_s}{N_p} R_{\text{s, ref}}}{\frac{N_s}{N_p} R_{\text{sh, ref}}} \tag{3.27}$$

- *The third equation* is derived by substituting the voltage and current given by the manufacturer at MPP in SRC in Equation (3.20), which yields

$$\begin{aligned}I_{\text{mpp, ref}} = {} & N_{\text{p}} \cdot I_{\text{ph, ref}} \\ & - N_p \cdot I_{0,\text{ ref}} \left( \exp\left( \frac{q(U_{\text{mpp, ref}} + I_{\text{mpp, ref}} \cdot \frac{N_s}{N_p} R_{\text{s, ref}})}{N_s \cdot n \cdot k \cdot T_{\text{ref}}} \right) - 1 \right) \\ & - \frac{U_{\text{mpp, ref}} + I_{\text{mpp, ref}} \cdot \frac{N_s}{N_p} R_{\text{s, ref}}}{\frac{N_s}{N_p} R_{\text{sh, ref}}}\end{aligned} \tag{3.28}$$

Since power is the product of current $I$ and voltage $U$ and its maximum MPP in SRC is when $U = U_{\text{mpp, ref}}$ and $I = I_{\text{mpp, ref}}$ then the derivative of the power function $P$ with respect to voltage is zero at MPP

$$\left. \frac{\partial P_{\text{ref}}}{\partial U_{\text{ref}}} \right|_{P = U_{\text{mpp, ref}} \cdot I_{\text{mpp, ref}}} = 0 \tag{3.29}$$

- *The fourth equation* is

$$\frac{I_{\text{mpp, ref}}}{U_{\text{mpp, ref}}} = \frac{\frac{q \cdot N_p \cdot I_{0,\text{ ref}}}{N_s \cdot nkT_{\text{ref}}} \cdot \exp\left( \frac{q\left(U_{\text{mpp, ref}} + I_{\text{mpp, ref}} \frac{N_s}{N_p} R_{\text{s, ref}}\right)}{N_s \cdot n \cdot k \cdot T_{\text{ref}}} \right) + \frac{1}{\frac{N_s}{N_p} R_{\text{sh, ref}}}}{1 + \frac{q \cdot I_{0,\text{ ref}} R_{\text{s, ref}}}{nkT_{\text{ref}}} \cdot \exp\left( \frac{q\left(U_{\text{mpp, ref}} + I_{\text{mpp, ref}} \frac{N_s}{N_p} R_{\text{s, ref}}\right)}{N_s \cdot n \cdot k \cdot T_{\text{ref}}} \right) + \frac{R_{\text{s, ref}}}{R_{\text{sh, ref}}}} \tag{3.30}$$

- *The fifth equation* ensures that the relative open-circuit voltage temperature coefficient $\mu_{U_{\text{oc}}}$ given by the manufacturer (see Table 3.3) is approximated well by the model

$$\mu_{U_{\text{oc}}} \cdot U_{\text{oc, ref}} = \frac{\partial U_{\text{oc}}}{\partial t_{\text{cell}}} \approx \frac{U_{\text{oc}}(t_{\text{cell}}) - U_{\text{oc, ref}}}{T_{\text{cell}} - T_{\text{ref}}} \tag{3.31}$$

After some algebraic rearrangement we get

$$U_{\text{oc}}(T_{\text{cell}}) = U_{\text{oc, ref}} \cdot \left(1 + \mu_{U_{\text{oc}}}(T_{\text{cell}} - T_{\text{ref}})\right) \tag{3.32}$$

By using Equation (3.32) in Equation (3.20) in SRC, fifth equation becomes

$$N_p \cdot I_{\text{ph}}(T_{\text{cell}}, \mathcal{I}_{\text{ref}}) - N_p \cdot I_0(T_{\text{cell}}) \left( \exp\left( \frac{q \cdot U_{\text{oc}}(T_{\text{cell}})}{N_s \cdot n \cdot k \cdot T_{\text{cell}}} \right) - 1 \right) - \frac{U_{\text{oc}}(T_{\text{cell}})}{\frac{N_s}{N_p} R_{\text{sh, ref}}} = 0 \tag{3.33}$$

Where $I_{\text{ph}}(t_{\text{cell}}, \mathcal{I}_{\text{ref}})$, $I_0(t_{\text{cell}})$, and $U_{\text{oc}}(t_{\text{cell}})$ are evaluated using Equation (3.22), Equation (3.21) and Equation (3.32) respectively. While the cell temperature $t_{\text{cell}}$ can be freely chosen, it is recommended to be $t_{\text{ref}} \pm 10$ Kelvin [6].

By simultaneously solving equations (3.26), (3.27), (3.28), (3.30) and (3.33), the five unknown required parameters (see Table 3.3) can be estimated. After the parameters are estimated, the I-U curve can be approximated by solving Equation (3.20).

With that in mind, the current $I_{\text{mpp}}$ and voltage $U_{\text{mpp}}$ at MPP can be estimated at any operating temperature $T_{\text{cell}}$ and incident radiation $\mathcal{I}$ by simultaneously solving the following equations:

$$I_{\text{mpp}} = N_p \cdot I_{\text{ph}}(T_{\text{cell}}, \mathcal{I}) - N_p \cdot I_0(T_{\text{cell}}) \left( \exp\left( \frac{q(U_{\text{mpp}} + I_{\text{mpp}} \frac{N_s}{N_p} R_s)}{N_s \cdot n \cdot k \cdot T_{\text{cell}}} \right) - 1 \right) - \frac{U_{\text{mpp}} + I_{\text{mpp}} \frac{N_s}{N_p} R_s}{\frac{N_s}{N_p} R_{\text{sh}}(\mathcal{I})} \tag{3.34}$$

and

$$\frac{I_{\text{mpp}}}{U_{\text{mpp}}} = \frac{\frac{q \cdot N_p}{N_s \cdot n \cdot k \cdot T_{\text{cell}}} \cdot I_0(T) \cdot \exp\left( \frac{q\left(U_{\text{mpp}} + I_{\text{mpp}} \frac{N_s}{N_p} R_s\right)}{N_s \cdot n \cdot k \cdot T_{\text{cell}}} \right) + \frac{1}{\frac{N_s}{N_p} R_{\text{sh}}(\mathcal{I})}}{1 + \frac{q R_s}{n \cdot k \cdot T_{\text{cell}}} \cdot I_0(T_{\text{cell}}) \cdot \exp\left( \frac{q\left(U_{\text{mpp}} + I_{\text{mpp}} \frac{N_s}{N_p} R_s\right)}{N_s \cdot n \cdot k \cdot T_{\text{cell}}} \right) + \frac{R_s}{R_{\text{sh}}(\mathcal{I})}} \tag{3.35}$$

where $R_{\text{sh}}(\mathcal{I})$ is evaluated as in Equation (3.23). Finally the output power point MPP is

$$P_{\max} = I_{\text{mpp}} \cdot U_{\text{mpp}} \tag{3.36}$$

**Results** The five equations were first solved using the non-linear `least_squares` algorithm from python library `scipy` for different modules to estimate their missing parameters (see Table 3.4).

| **Module** | **Semiconductor** | $R_{\text{s, ref}}$ [m$\Omega$] | $R_{\text{sh, ref}}$ [$\Omega$] | $I_{\text{0, ref}}$ [nA] | $I_{\text{ph, ref}}$ [A] | $n$ |
|---|---|---|---|---|---|---|
| KD210GX-LP | mono-crystalline silicon | 5.929 | 2.066 | 0.348 | 8.605 | 1.001 |
| PB3-215 | poly-crystalline silicon | 6.390 | 1.543 | 0.400 | 8.138 | 1.000 |
| PB3-220 | poly-crystalline silicon | 7.028 | 2.693 | 0.388 | 8.225 | 1.000 |
| PB3-225 | poly-crystalline silicon | 6.455 | 2.698 | 0.393 | 8.323 | 1.000 |
| PB3-235 | poly-crystalline silicon | 6.026 | 3.485 | 0.351 | 8.495 | 1.010 |

Table 3.4: Results of the estimated five parameters using the single-diode model with five equations.

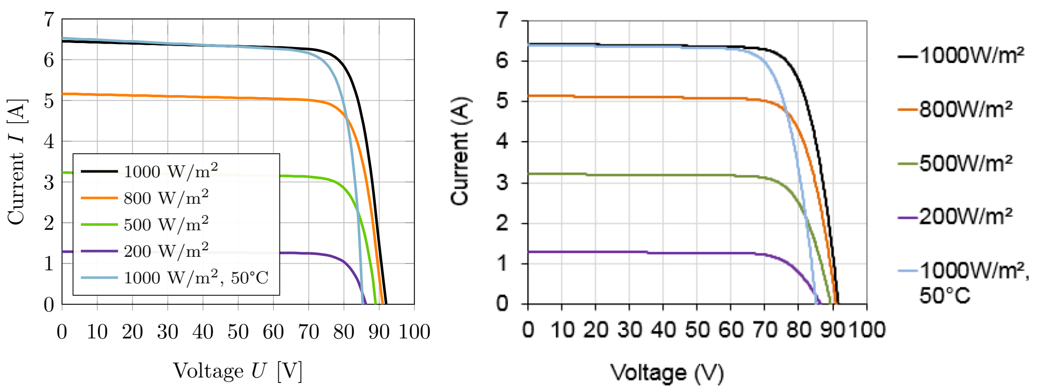


Figure 3.7: Comparison of I-V curves by dependence on incident radiation at temperature 25°C and in 1 kW/m$^2$ at 50°C in blue for module SPR-X22-470-COM . This model's prediction on the left, data-sheet[1]on the right. Raw data was not available to calculate the MSE

Some manufacturers provide more information about the module in NOCT (see Table 3.2), we can use these information to test the model's predictions. The data-sheets for the modules in Table 3.4 provide parameters in NOCT, and a single-diode model implemented by [58] have shared their results. Thus, we can compare the results of this work to them.

| **Module** | **model** | **SRC** | | | | | **NOCT** | | | | |
|---|---|---|---|---|---|---|---|---|---|---|---|
| | | $P_{\max}$ | $V_{\mathrm{mpp}}$ | $I_{\mathrm{mpp}}$ | $V_{\mathrm{oc}}$ | $I_{\mathrm{sc}}$ | $P_{\max}$ | $V_{\mathrm{mpp}}$ | $I_{\mathrm{mpp}}$ | $V_{\mathrm{oc}}$ | $I_{\mathrm{sc}}$ |
| PB3-215 | data-sheet | 215.0 | 29.10 | 7.40 | 36.50 | 8.10 | 154.8 | 25.90 | 5.92 | 33.20 | 6.56 |
| | this work | 215.2 | 29.17 | 7.38 | 36.51 | 8.10 | 156.9 | 26.32 | 5.96 | 33.19 | 6.58 |
| | [58] | 215.3 | 29.10 | 7.40 | 36.50 | 8.10 | 156.6 | 26.21 | 5.98 | 33.20 | 6.63 |
| PB3-220 | data-sheet | 220.0 | 28.90 | 7.60 | 36.60 | 8.20 | 158.0 | 25.70 | 6.08 | 33.30 | 6.64 |
| | this work | 219.5 | 28.96 | 7.58 | 36.61 | 8.20 | 160.0 | 26.18 | 6.11 | 33.29 | 6.66 |
| | [58] | 219.6 | 28.90 | 7.60 | 36.60 | 8.20 | 160.3 | 26.07 | 6.15 | 33.30 | 6.71 |
| PB3-225 | data-sheet | 225.0 | 29.10 | 7.70 | 36.60 | 8.30 | 162.0 | 25.90 | 6.16 | 33.30 | 6.72 |
| | this work | 224.0 | 29.16 | 7.68 | 36.61 | 8.30 | 163.0 | 26.33 | 6.19 | 33.29 | 6.74 |
| | [58] | 224.1 | 29.10 | 7.70 | 36.60 | 8.30 | 163.3 | 26.23 | 6.23 | 33.30 | 6.79 |
| PB3-235 | data-sheet | 235.1 | 29.80 | 7.89 | 37.20 | 8.48 | 169.2 | 26.50 | 6.31 | 33.80 | 6.87 |
| | this work | 235.1 | 29.80 | 7.89 | 37.20 | 8.48 | 172.7 | 26.93 | 6.41 | 33.87 | 6.94 |
| | [58] | 235.1 | 29.80 | 7.89 | 37.20 | 8.48 | 171.3 | 26.84 | 6.38 | 33.85 | 6.94 |
| KD210GX-LP | data-sheet | 210.0 | 26.60 | 7.90 | 33.20 | 8.58 | 148.0 | 23.50 | 6.32 | 29.90 | 6.98 |
| | this work | 210.1 | 26.60 | 7.90 | 33.20 | 8.58 | 151.5 | 23.80 | 6.37 | 29.98 | 6.97 |
| | [58] | 210.1 | 26.60 | 7.90 | 33.20 | 8.58 | 149.9 | 23.72 | 6.32 | 29.90 | 6.98 |

Table 3.5: Validation of the model results with the data-sheet and a model by Tian et al.[58]

As can be seen in Table 3.5 the estimation of MPP is quite accurate in SRC and NTC. However in Germany and more accurately in Aachen only barely a week gets more irradiance than 800W/m$^2$, in fact around 76% of the year get irradiance less than 400W/m$^2$ when the sun is up. Thus, it is important to consider the low irradiance conditions (see Table 3.6). Figure 3.7 compares the I-U-curves of the module SPR-X22-470-COM as estimated by this model and as given by the data-sheet.

| **Module** | **model** | **SRC** | | | **NOCT** | | | **Low Irradiance** | | |
|---|---|---|---|---|---|---|---|---|---|---|
| | | $P_{\max}$ | $V_{\mathrm{mpp}}$ | $I_{\mathrm{mpp}}$ | $P_{\max}$ | $V_{\mathrm{mpp}}$ | $I_{\mathrm{mpp}}$ | $P_{\max}$ | $V_{\mathrm{mpp}}$ | $I_{\mathrm{mpp}}$ |
| SPR-X21-470-COM | data-sheet | 470.0 | 77.60 | 6.06 | 356.0 | 73.00 | 4.88 | 90.6 | 74.40 | 1.22 |
| | this work | 470.4 | 78.31 | 6.01 | 381.2 | 74.07 | 5.15 | 90.5 | 75.20 | 1.20 |
| SPR-X20-445-COM | data-sheet | 445.0 | 76.50 | 5.82 | 337.0 | 71.90 | 4.68 | 85.6 | 73.00 | 1.17 |
| | this work | 446.8 | 78.24 | 5.71 | 362.5 | 73.74 | 4.92 | 84.7 | 74.02 | 1.14 |
| SPR-E19-410-COM | data-sheet | 410.0 | 72.90 | 5.62 | 311.0 | 68.70 | 4.53 | 78.7 | 69.4 | 1.14 |
| | this work* | 411.2 | 74.80 | 5.50 | 329.1 | 69.91 | 4.71 | 76.7 | 69.75 | 1.10 |

Table 3.6: Comparison the model results with the data-sheet of different modules in low irradiance. Low Irradiance is 200 W/m$^2$ at operating temperature of 25°C.

[1] `https://us.sunpower.com/sites/default/files/sp-x-and-e-series-residential-solar-panels-supplementary-technical-spec_0.pdf`

### 3.2.2. Simple Efficiency Model

The SDM introduced earlier makes many analytical information for the PV module accessible and provides relatively accurate results. However every calculation point needs an optimization which hurdles it from being fast enough to be included in another optimization algorithm in online applications.

If the MPP is considered as a function of cell temperature $t_{\text{cell}}$ and irradiance $\mathcal{I}$, it becomes evident that a linear approximation is a possible solution for a faster approximation (see Figure 3.8).

Equation 3.22 shows a linear relationship between photocurrent $I_{\text{ph}}$ and both irradiance and cell temperature. It could be assumed that the diode current and the series resistance are negligible $I_{\text{d}} \to 0, R_{\text{s}} \to 0$ as well as that the shunt resistance is big $R_{\text{sh}} \to \infty$. Thus, Equation (3.12) becomes

$$I \approx I_{\text{ph}} \tag{3.37}$$

In this case, Equation (3.36) can be written analogous to Equation (3.22) as

$$P_{\max} = N_{\text{modules}} \cdot P_{\text{max, ref}} \cdot \frac{\mathcal{I}}{\mathcal{I}_{\text{ref}}} \cdot (1 + \mu_P (T_{\text{cell}} - T_{\text{ref}})) \tag{3.38}$$

where $\mathcal{I}_{\text{ref}}$ and $t_{\text{ref}}$ are the irradiance and cell temperature as given in Table 3.2. $P_{\text{max, ref}}$ is the maximum power in SRC and $\mu_{\text{P}}$ is the power temperature coefficients.

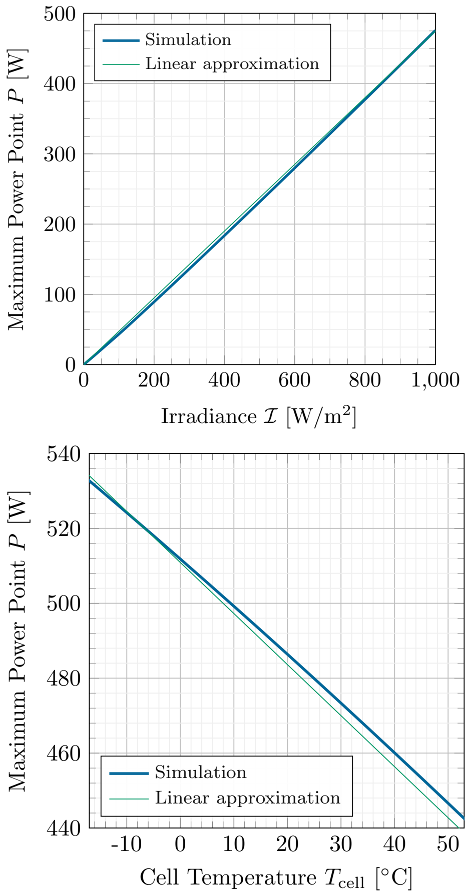


Figure 3.8: Comparison between SDM simulation and linear approximation of MPP for SPR-X22-470-COM.

Sometimes, only the efficiency of the module per unit area in SRC $\eta_{\text{PV}}$ is given, in this case, the area of the module $A_{\text{module}}$ is required. The approximation of the maximum power becomes

$$P_{\text{max, ref}} = \eta_{\text{PV}} \cdot A_{\text{module}} \cdot \mathcal{I}_{\text{ref}} \tag{3.39}$$

The simplicity of this model allows for embedding it in many online applications such as in the online optimization algorithm in this work.

### 3.2.3. Annual Energy Output

When a PV module is connected directly to the house appliances through an inverter, there will be an excess of energy (energy surplus) during peak hours if the load is not high enough and this excess of energy reduces the system's efficiency in an off-grid system. A reduction of profitability is dependent on the grid feed-in tariff for on-grid system. Figure 3.9 illustrates this concept. Excess of power during peak hours is colored in blue and power deficit is colored in red. From midnight until around 5 am, the load is at minimum. Hence, there is a relative balance of power because the panels do not produce power in these hours either. During daytime there is an excess of power which is lost and in evening a deficiency of power becomes clear.

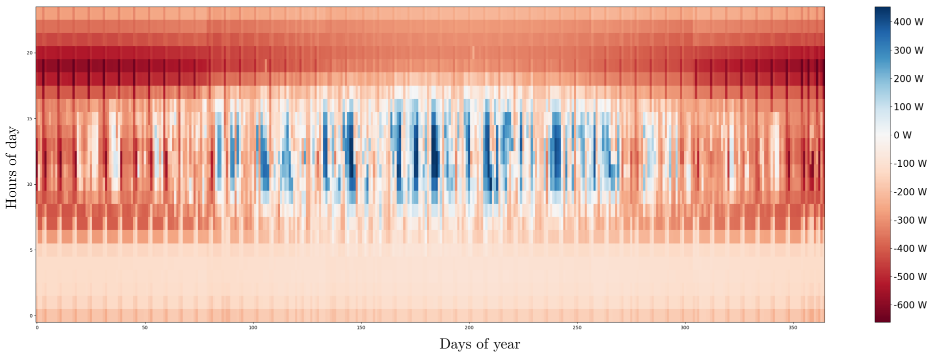


Figure 3.9: The power balance between generated power by PV modules and the load. The data was simulated by the efficiency model for the typical load of one person living in a house with two AE335HM6-60 modules by AE SOLAR.

The power balance is calculated as follows

$$P_{\text{balance}}(t) = P_{\text{AC}}(t) - P_{\text{load}}(t) \tag{3.40}$$

where $P_{\text{load}}(h)$ is the energy consumed by the load at the $t$-th hour of year given by the corresponding load profile, see Equation (2.18) and $P_{\text{AC}}(t)$ is the AC power output calculated with a simple inverter efficiency model

$$P_{\text{AC}}(t) = \eta_{\text{inverter}} \cdot P_{\text{PV}}(t) \tag{3.41}$$

where $\eta_{\text{inverter}}$ is the efficiency of the DC-AC inverter and $P_{\text{DC}}(t)$ is the maximum power point of the PV system, that is the power that can be produced by the PV array at that hour of year under the given meteorological conditions

$$P_{\text{DC}}(t) = P_{\max}(\mathcal{I}_t, T_{\text{cell},t}) \tag{3.42}$$

where $\mathcal{I}_h$ and $t_{\text{cell, h}}$ are the incidence radiation and cell temperature at the $h$-th hour. The cell temperature is calculated as given by Equation (3.10). $P_{\max}$ can be calculated either by Equation (3.38) or Equation (3.36).

The annual energy output is defined as the amount of energy generated the PV array. In case of the simulation in Figure (3.9) for example, the annual energy output is 778.65kWh. Only 643.43kWh were actually used by the load and the rest is an excess of energy which is exported to the local grid or stored in a battery if present.

In this respect, the annual output energy can be defined as the energy that can be produced by the PV system considering only the meteorological and electric constraints as

$$E_{\text{DC, annual}} = \sum_{h=1}^{8760} P_{\text{DC}}(t) \tag{3.43}$$

and the annual energy output AC can be expressed as

$$E_{\text{AC, annual}} = \sum_{t=1}^{8760} P_{\text{AC}}(t) \tag{3.44}$$

Moreover, the energy output that is delivered to the load is described by

$$E_{\text{PV}\to\text{Load}} = E_{\text{AC, annual}} - \left( \sum_{t=1}^{8760} P_{\text{balance}}(t)\Big|_{\geq 0} \right) \tag{3.45}$$

which is the difference between the energy output AC produced by the PV array and the energy surplus (see Figure 3.10).

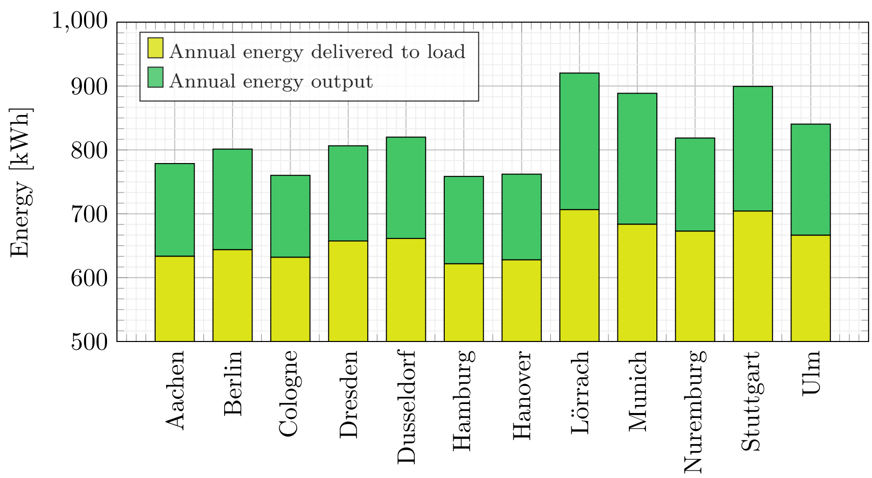


Figure 3.10: Comparison between annual energy output and annual energy output delivered to the load in different cities in Germany. The data was simulated by the simple efficiency model for the typical load of one person living in a house with a 120W MPP module.

Simulation of commercial buildings can be seen in Figure (3.11).

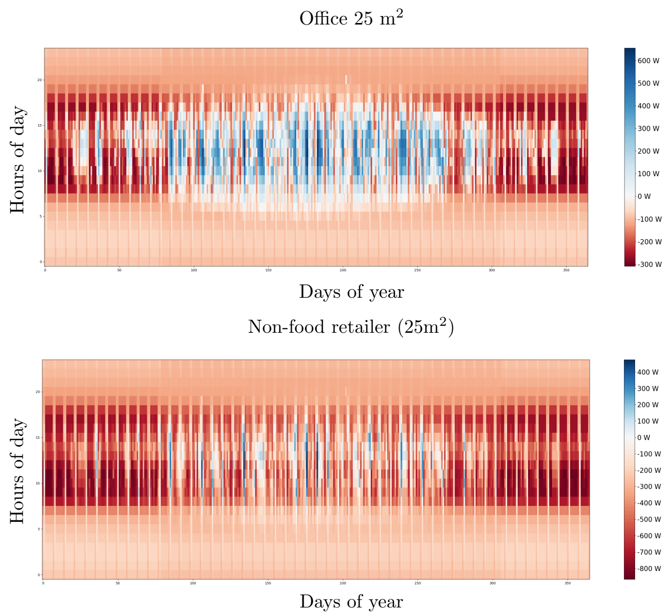


Figure 3.11: The energy balance between generated energy by the PV system and the load for the typical load of commercial buildings (g0) for an office (left) and a non-food retailer (right) of area 25m$^2$ with a 120W MPP module.

See Figure 3.12 an overview of the data flow in the system.

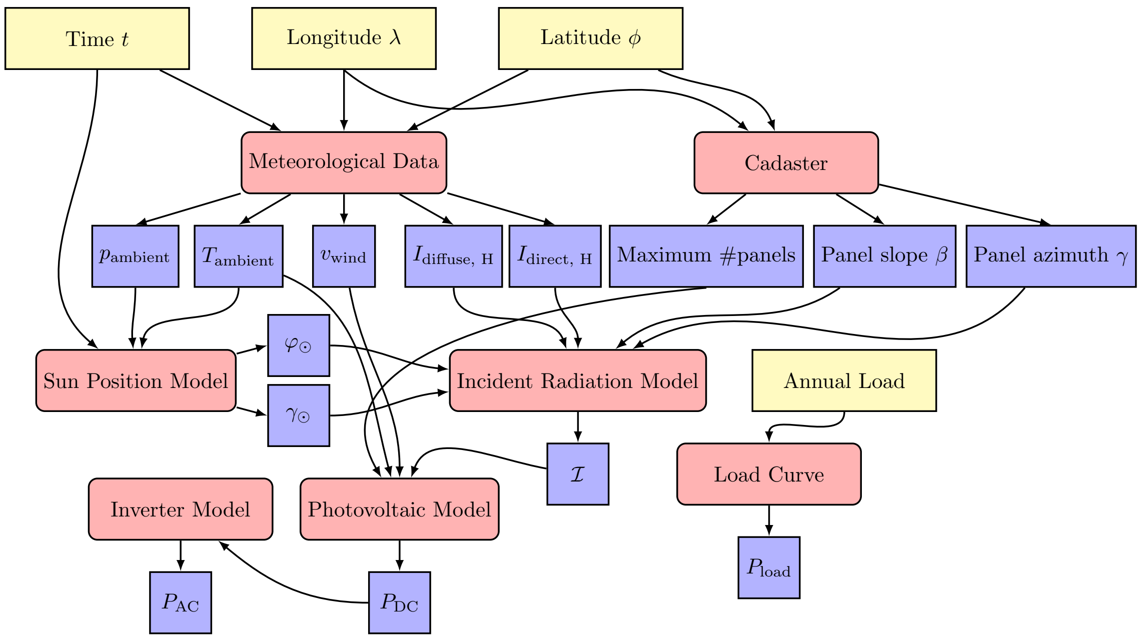


Figure 3.12: Overview of the data flow in the system for every time step and for each rooftop's surface.

## 3.3. Battery Storage Model

Energy generated during the day can be stored in a battery for later use. Batteries store energy by transforming electric energy from and into chemical energy. The prominent types of battery used with PV systems is the Lithium-Ion Battery, as it allows for storing large quantities of electrical energy. It has recently become more popular because of the decrease in its costs and light weight [13]. Other alternatives are the lead-acid and nickel-cadmium batteries.

Storing electro-chemical energy in a lithium-ion battery is a based on an important attribute of lithium atoms (Li). Lithium atoms have only one electron on their covalent bond. When a lithium atom is in a free state, it becomes conductive and loses the electron instantly (*non-equiliberium state*). However, when they are a part of metal oxide molecule such as ($LiCoO_2$) they become stable (*equilibrium state*) and require more energy to get in the free state.

A typical lithium-ion battery has three main parts, the cathode which is a metal oxide such as ($LiCoO_2$), the anode which is carbon such as graphite ($LiC_6$) and in between theere is an electrolyte, which is typically ethylene carbonate ($(CH_2O)_2CO$). Since ethylene carbonate is an insulator, electrons do not flow through it, whereas lithium ions ($Li^+$) can.

**Charging process** Applying an external voltage between the cathode and the anode results in a voltage difference between the anode and the cathode. This forces lithium atoms to leave the metal oxide in the anode to form lithium ions ($Li^+$) and electrons ($e^-$). The formed lithium ions ($Li^+$) pass through the electrolyte to the cathode. The electrons ($e^-$), on the other hand, move through the external circuit to the cathode. Hence pushing the lithium ions to non-equilibrium state. After removing the external circuit, some lithium ions reach the equilibrium state by passing through to the cathode leaving electrons behind in the anode. This creates a voltage difference stopping more lithium ions to recombine with the metal oxide in the cathode. This process is called charging.

**Discharging process** When an external load is connected, electrons have to pass through it to compensate for the voltage difference caused in the charging process. As this happens, more lithium-ions pass through to the cathode and keep the voltage steady. This keeps going on until there are no more lithium-ions in the anode. This process is called discharging. Each charging process followed by a discharge process is called a *cycle*.

**Capacity** The amount of energy that can be delivered by battery is called the available capacity. When the current withdrawn from the battery is nominal, the capacity becomes nominal $C_{\text{bat,nom}}$ which both are given by the manufacturer. However the nominal capacity decreases with time due to decreasing of the battery's calendar lifetime and by the number of cycles elapsed (degradation). By the end of its lifetime the capacity reaches 80%.

**Battery's lifetime** The battery's lifetime can be affected by its calendar lifetime $N_{\text{bat,time}}$ which can be assumed to be 20 years as well as by the number of full cycles elapsed (see Figure 3.13). Several regression models approximate the lifetime of the lithium-ion battery such as . A comparison of tthe models by [35], [10], [62] and by Battery university[1] can be seen in Figure 3.13. An approximation of the number of full cycles of lithium-ion batteries as given by [35]

$$N_{\text{bat, cyc}} = \beta_0 \cdot \text{DOD}^{-\beta_1} \cdot \exp\big(\beta_2 \cdot (1 - \text{DOD})\big) \tag{3.46}$$

where DOD is the depth of discharge and $\beta_0, \beta_1$ and $\beta_2$ are parameters.

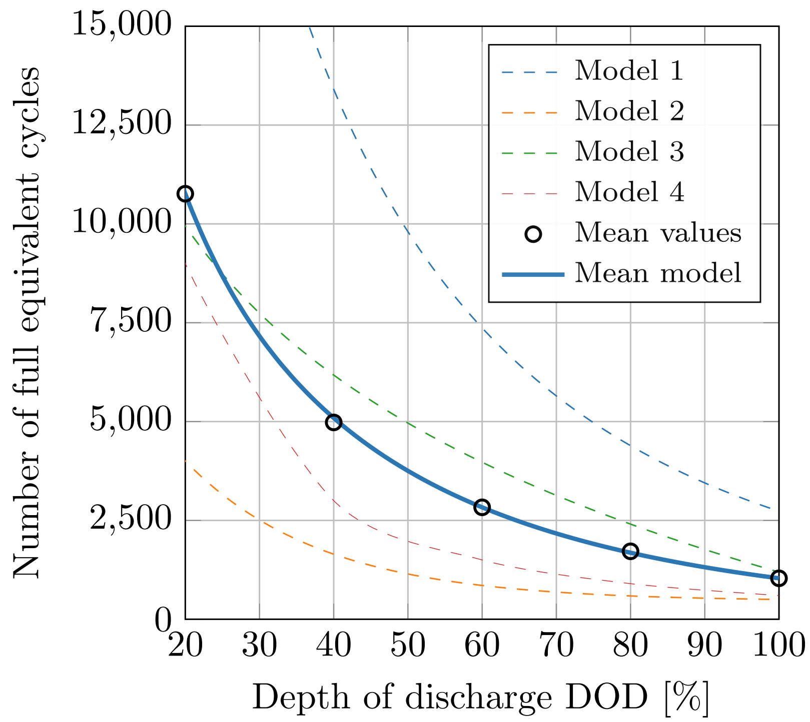


Figure 3.13: Cycle life of a Li-ion battery by Model 1 [35], Model2 [10], Model 3 [62] and by Battery university[1] and a mean model.

By averaging the values of the aforementioned models we get the following parameters $\beta_0 = 1036, \beta_1 = 0.5618$ and $\beta_2 = 1.7957$ for a mean regression model. This, gives an MSE of 0.02%. This curve gives 3753 cycles at 50% DOD. Using a battery storage in a PV system reduces the energy surplus and allows for maximum use of PV potential.

[1]https://batteryuniversity.com/article/bu-808-how-to-prolong-lithium-based-batteries

**Topologies** Battery Energy Storage Systems (BESS) can be coupled with a PV system in different topologies. The AC-coupled BESS is connected to the household load via a bidirectional inverter which controls the energy flow from and into the BESS. Another inverter is connected to the PV system for tracking the MPP. While allowing for a flexible installation, the efficiency of this model is not optimum because of high number of conversion stages. This is usually used for large-scale utilities. A common way for household systems is DC-coupling. The number of conversion is reduced by sharing the same inverter. The PV system and the BESS are connected to each other by DC-DC converters. In the following, a DC coupled BESS is assumed.

The power discharged from or stored in batteries correlates to the charge current applied to the battery and to the state-of-charge (SOC) of the battery. Applying different values of current to the battery changes how much the battery discharges or charges e.g. by changing polarity. To ensure a maximum benefit of the generated power, a management system is usually coupled with the battery system. This uses storage dispatch strategies such as variants peak shaving strategy.

**Modeling** A simple model to simulate the battery along with grid export and import meters would be to store the energy and extract it using a simple round-trip efficiency equation. The battery storage is charged

$$E_{\text{BESS}}(t) = E_{\text{BESS}}(t-1) + \min\left\{P_{\text{balance}} \cdot \eta_{BESS}, \quad \text{SOC}_{\text{max}} \cdot C_{\text{nom}} - E_{\text{BESS}}(t-1)\right\} \tag{3.47}$$

if the following criteria are met

$$P_{\text{balance}} > 0 \qquad \text{and} \qquad E_{\text{BESS}}(t-1) < \text{SOC}_{\text{max}} \cdot C_{\text{nom}} \tag{3.48}$$

where $E_{\text{BESS}}(t)$ is the energy stored in the battery at the $h$-th hour of year, $\text{SOC}_{\text{max}}$ is a user-specified maximum state of charge and $\eta_{BESS}$ is the round-trip efficiency of the battery.

Similarly, the battery is discharged

$$E_{\text{BESS}}(t) = E_{\text{BESS}}(t-1) - \min\left\{-P_{\text{balance}}, \quad E_{\text{BESS}}(t-1) - \text{SOC}_{\text{min}} \cdot C_{\text{nom}}\right\} \tag{3.49}$$

if the following criteria are met

$$P_{\text{balance}} < 0 \qquad \text{and} \qquad E_{\text{BESS}}(t-1) > \text{SOC}_{\text{min}} \cdot C_{\text{nom}} \tag{3.50}$$

where $\text{SOC}_{\text{min}}$ is a specified minimum state of charge. The energy delivered to the load by the battery $E_{\text{BESS}\rightarrow\text{Load}}$ can be calculated by monitoring the energy flowing out of the BESS when discharging.

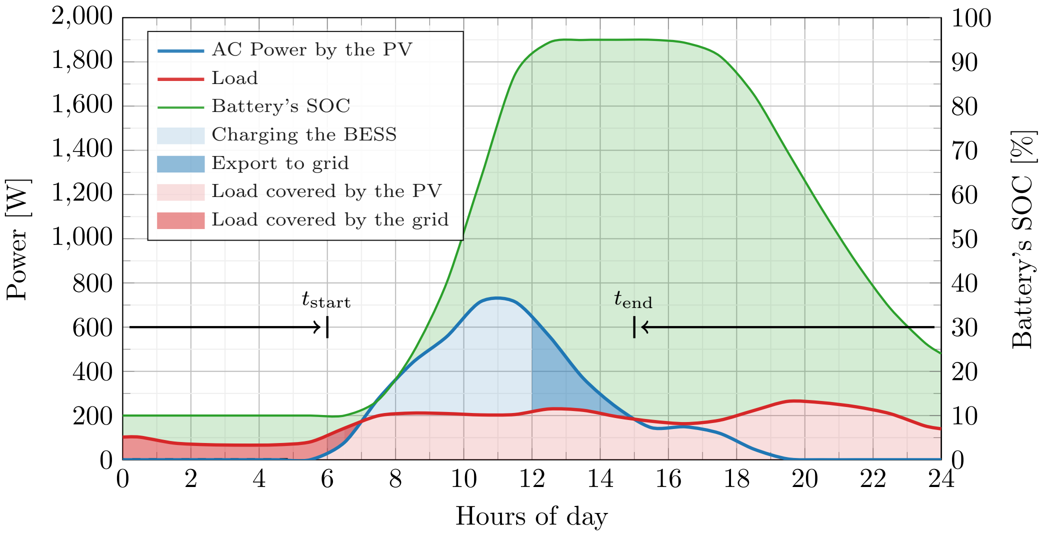


Figure 3.14: Power balance across the system through the hours of day. The load profile here is scaled to 1500kWh and six PV modules with peak of 300W each. The battery capacity is 2kWh with 10% minimum SOC and 95% maximum SOC.

Additional criteria for discharging is used to prevent two cycles a day. This is to maximize the lifetime of the battery. Therefore, discharging is only allowed outside the charging hours

$$\begin{aligned} t_{\text{start}} &= \min(t) \text{ such that } P_{\text{balance}}(t-1) < 0 \text{ and } P_{\text{balance}}(t) > 0 \\ t_{\text{end}} &= \max(t) \text{ such that } P_{\text{balance}}(t) > 0 \text{ and } P_{\text{balance}}(t+1) < 0 \end{aligned} \tag{3.51}$$

where $t$ is the hour of day.

## 3.4. Model Validation

In this section, the model is validated in a standalone installation, i.e. no BESS is installed. Then the model is validated with a coupled BESS.

### 3.4.1. Photovoltaic Model

To validate the model presented, the results given by the model and different other tools are compared.

**SAM tools** The System Advisor Model (SAM) is an open-source tool developed by the NREL to simulate renewable energy systems. It allows the simulation of a photovoltaic system with custom weather data and load profile. Thus, the tool is well suited to compare the model in this work with. The exact same weather data and load profile are used for both models. Furthermore it provides several simulation models. For the validation of standalone PV system, the PVWatts-Standalone and the PV-Standalone models are compared. The PVWatts-Standalone is the model used in the online tool PVWatts. The Detailed PV-Standalone is a detailed model which includes electrical models for different parts of the system. The DWD dataset was converted into NSRDB format which SAM can read. The year was set to 2008. This is relevant to the calculation of the Sun's position in SAM which in turn affects the panels output.

**PV*SOL** PV*SOL is a simulation tool with an online version, the premium version is chargeable. In this section, the results are compared to the online version of PV*SOL which unfortunately does not allow for uploading custom weather data or load profile. It has its own weather data for a given location and it has its own load profile which can be re-scaled. Hence the comparison here will be bit less fair.

Table 3.7 provides the settings that were used for the tools in this validation step.

| Parameter | Symbol | Value |
|---|---|---|
| MPP | $P_{\text{max, ref}}$ | 0.3 kW |
| Temperature power coefficient | $\mu_{\text{P}}$ | -0.351% |
| Cell temperature in NOCT | $T_{\text{NOCT}}$ | 41°% |
| Region | | Aachen, Germany (50°46'16.1"N 6°03'05.4"E) |
| Number of modules | $N_{\text{modules}}$ | 6 |
| Efficiency | $\eta_{\text{PV}}$ | 19.9% |
| Module area | $A_{\text{module}}$ | 1.5075 m$^2$ |
| Annual load energy | $E_{\text{load}}$ | 1500 kWh |
| Inverter efficiency | $\eta_{\text{inverter}}$ | 99% |
| Albedo | $r_{\text{albedo}}$ | 20% |
| Panels azimuth | $\gamma$ | 205° |
| Panels tilt | $\beta$ | 21° |

Table 3.7: System Design and simulation settings for validation.

The simulation profile for SAM was set as *Photovoltaic, PVWatts/Detailed PV Model, Distributed Residential Owner*. The losses out of soiling, shading or wiring where disabled. The hourly values were interpreted to be half an hour ahead (+0.5) only for validation purposes, since SAM does not allow this to be changed, as opposed of half an hour behind (-0.5) to match the DWD dataset.

**Results** Figure 3.15 provides a visualization of the simulated energy output given by this work and SAM tool by NREL.

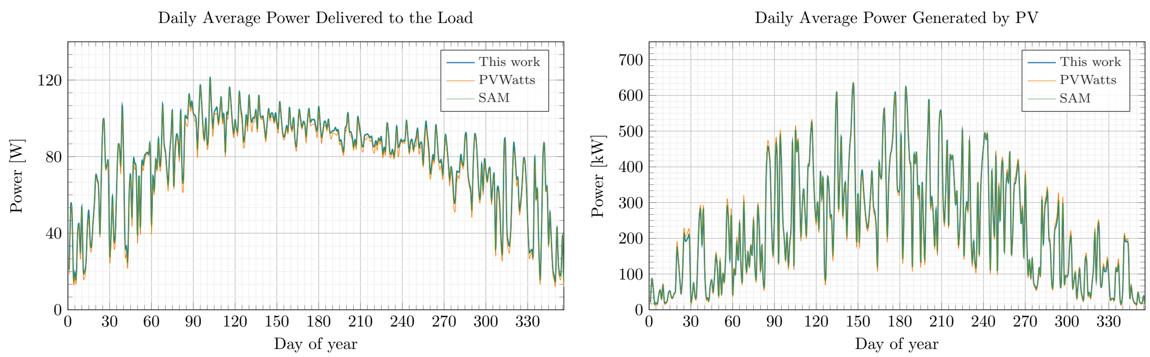


Figure 3.15: Comparison of the power output AC and the energy delivered to the load as a result of the simulation by this work, SAM PVWatts, and SAM detailed model.

For the annual values see Table 3.8.

| Parameter | PV*SOL | PVWatts | SAM Detailed | This work |
|---|---|---|---|---|
| DC output | - | 1970.00 kWh | 1975.83 kWh | 1975.88 kWh |
| AC output | 1765 kWh | 1950.32 kWh | 1956.07 kWh | 1956.12 kWh |
| AC output delivered to load | 417 kWh | 660.48 kWh | 679.27 kWh | 679.28 kWh |
| Energy surplus | 1348 kWh | 1289.84 kWh | 1276.77 kWh | 1276.84 kWh |

Table 3.8: Comparison of annual results by different simulation tools and this work. The data gathered in SAM is from the sum of hourly data of the following tables AC inverter output power, electricity from system to load, and Electricity to grid.

In the following, only SAM's Detailed PV-Standalone model is compared.

**Error Analysis** Since the difference in Watt units is dependent on the system's maximum power, the error percentage is calculated as

$$\text{Error}(t) = \frac{P_{\text{ref}}(t) - P_{\text{Thesis}}(t)}{P_{\text{ref}}(t)} \tag{3.52}$$

Using different models for the calculation of any part of the system might result in a considerable error as will be demonstrated in the following sections.

**Incident radiation** The DC output of the system $P_{\max}$ is proportional to the incident radiation. Figure 3.16 shows an overview of the error between the model implemented in this work and SAM tools.

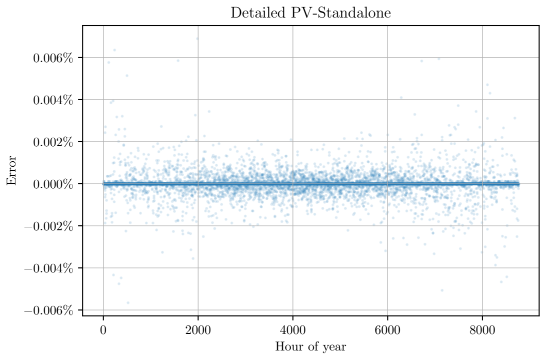


Figure 3.16: The error of incident radiation between SAM tools and this work.

The DC output is also slightly affected by the cell temperature. Figure 3.17 demonstrates the errors in cell temperature.

**Cell temperature** Both the model in this work as well as SAM's Detailed PV-Standalone model implement Sandia cell temperature model, which is dependent on incident radiation, ambient temperature and wind speed. Since the last two come directly from the same meteorological data, the error in cell temperature between the Detailed PV-Model and the model in this work, comes mainly from the error in the incident radiation.

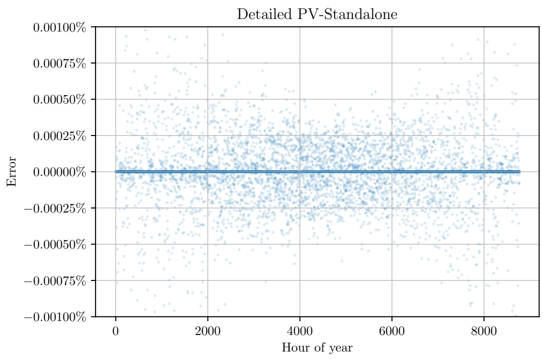


Figure 3.17: The error of cell temperature between SAM tools and this thesis.

**DC power** Figure 3.18 shows how the DC output is affected by the different models since all models used for comparison here implement the same simple efficiency model, see Equation (3.38). SAM, additionally, supports much advanced models, such as the SDM demonstrated in Section 3.2.1.

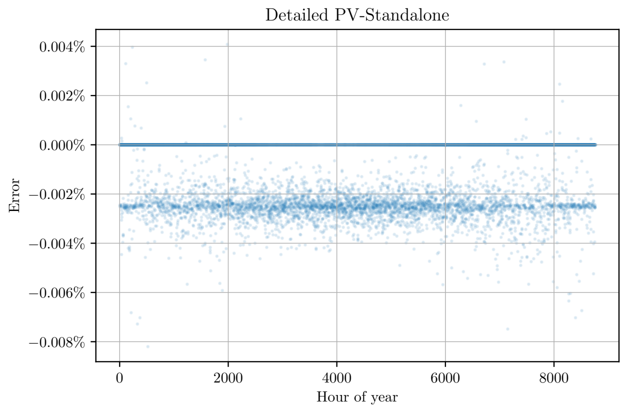


Figure 3.18: The error of DC output between SAM tools and this work.

Figure 3.18 suggests that the model implemented in the thesis and SAM's Detailed PV-Standalone model agree to a good accuracy in terms of DC power generated from solar irradiation.

**AC power** The implementation of the inverter in SAM Detailed PV-Standalone is based on an empirical model by Sandia [14] while the model in this work assumes an AC output always proportional to DC, see Equation (3.41) as does PVWatts-detailed model. Figure 3.19 demonstrates the resulting error of AC output. However, a greater deviation in the error happens when using the full capabilities of the inverter model in SAM, such as wiring losses. Note that AC losses here happen only because of the inverter's efficiency and not other independent losses.

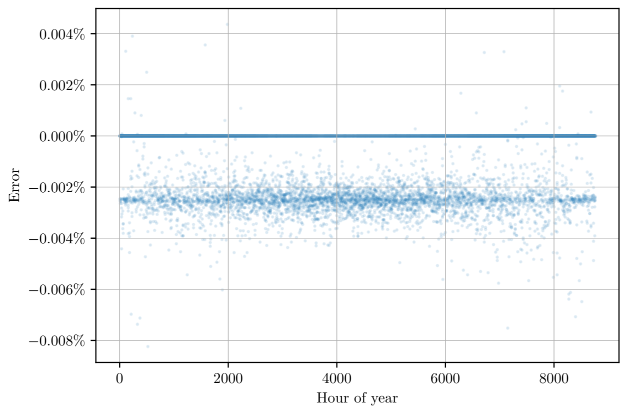


Figure 3.19: The error of AC output between SAM tools and this work.

The error of the electricity delivered to load can be seen in Figure 3.20. The models agree to a good degree when the AC output power is higher than the load, as the system delivers exactly the power required by the load profile. Whereas, when the

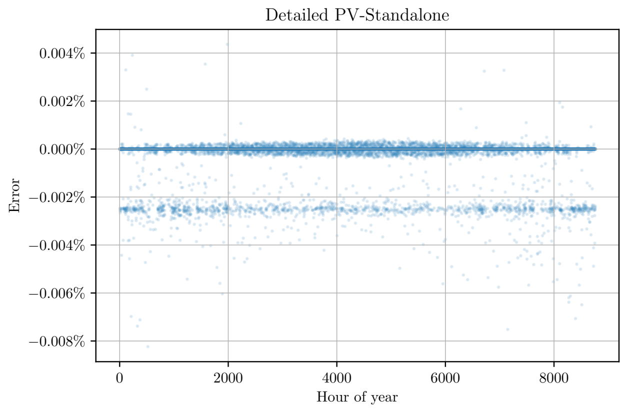


Figure 3.20: The error of electricity delivered to load between SAM tools and this work.

load is higher than AC output power, the error becomes affected directly by the error in the AC output.

**Power balance** Even though the error in power balance is low when compared to SAM's Detailed PV-Standalone model, some peaks appear. Peaks greater than 1% error occur in 6 hours out of 8760 hours in a year. Peaks greater than 0.1% occur in 46 hours out of 8760 hours in a year.

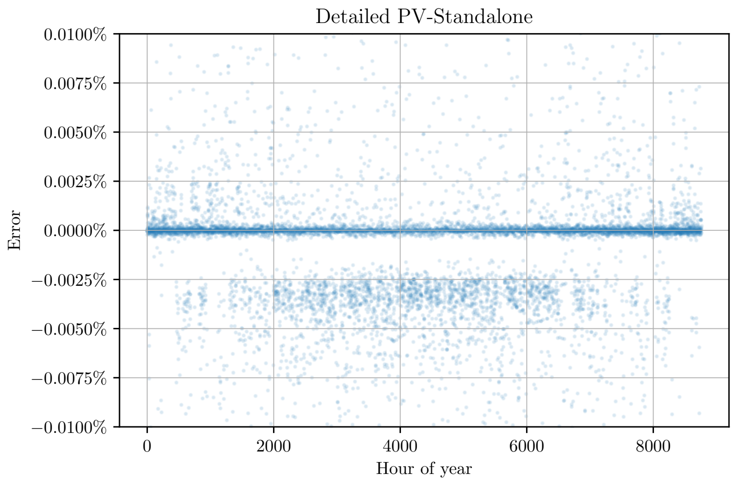


Figure 3.21: The error of power balance between SAM tools and this work.

See Table 3.9 for comparison of MAE and max error between this work and SAM's Detailed PV-Standalone model.

| Variable | MAE | Maximum Error |
|---|---|---|
| Sun azimuth | 0.00011% | -0.00089% |
| Sun altitude | 0.00013% | 0.12738% |
| Angle of incidence | 0.00003% | 0.00049% |
| Direct incident radiation | 0.00216% | -0.36072% |
| Diffuse incident radiation | 0.00005% | 0.00049% |
| Global incident radiation | 0.00023% | -0.00689% |
| Cell temperature | 0.00011% | 0.04073% |
| DC output power | 0.00128% | -0.00820% |
| AC output power | 0.00128% | -0.00823% |
| AC power delivered to load | 0.00049% | -0.00823% |
| AC power surplus | 0.00314% | -0.76583%∗ |
| Power balance | 0.00470% | -0.76583%∗ |

Table 3.9: Comparison of MAE and maximum error between SAM tools and the model in this work by changing the implementation of different parts of this work. ∗ Power values less than 0.5W are excluded from the MAE and maxium error (8 hours out of 8760 hours of a year), since different inverter models are used, a larger deviation is expected, but does not have a big impact on the system as a whole.

Since AC power surplus is just the positive values of the power balance, the maximum error is also large because of the aforementioned reason. When excluding the power values less than a Watt, the maximum error for both variables is 0.5431To understand how different sub-models of the system affect the DC output, the same criteria are kept and only one sub-model is changed in Table 3.10 and compare the resulting error.

| Model | MAE | Maximum Error |
|---|---|---|
| Base model | **0.00128%** | **-0.00820%** |
| Sun position with Almanac [40] | 0.61887% | -3104.73% |
| Cell temperature by [36] | 0.08897% | 1.91071% |

Table 3.10: Comparison of MAE and maximum error of the DC output between SAM tools and the model in this work by changing the implementation of different parts of this work.

As can be seen in Table 3.10, different sub-systems result in a much larger error. Using a different Sun's position algorithm result in an error larger by two orders of magnitude and a different model for cell temperature results by an error 70 times larger. Hence, the Almanac algorithm for the calculation of the Sun's position is not used, rather the NREL's SPA algorithm introduced in Section 2.2.

### 3.4.2. Battery-Coupled Model

The validation in this section is done using only SAM tools, since the free version of PV*SOL does not provide a battery-coupled system to simulate. PVWatts does not provide corresponding dispatching strategy. The SAM model used here is *Energy Storage, Detailed-PV Battery, Distributed Residential Owner*. The same settings are used for PV as in Table 3.7. The battery parameters are as shown in Table 3.11. Note that the dispatching strategy for the validation allows for multiple cycles a day. Whereas the model does not allow this normally. In the following, some comparisons would also be made for the dispatching strategy in this work, which only allows for a maximum of one cycle a day to increase the lifetime of the battery.

| Parameter | Symbol | Value |
|---|---|---|
| Capacity | $C_{\text{nom}}$ | 2 kWh |
| Round-trip efficiency | $\eta_{\text{BESS}}$ | 94.5% |
| Coupling | | DC-Coupling |
| DC-DC conversion efficiency* | | 99% |
| Inverter efficiency cutoff* | | 100% |
| Minimum SOC | $\text{SOC}_{\text{min}}$ | 10% |
| Maximum SOC | $\text{SOC}_{\text{max}}$ | 95% |
| Storage Dispatch* | | Input grid power target (zero) |

Table 3.11: BESS design parameters.
* Some variables are only available in SAM but are default in the architecture design of this work.

A monthly distribution of energy delivered to the load by the battery can be seen in Figure 3.22.

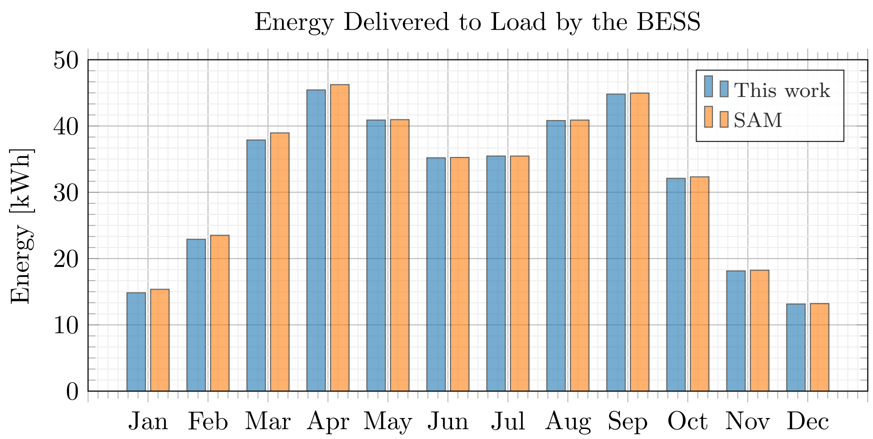


Figure 3.22: Comparison of monthly energy delivered by the BESS to the load.

The model for the battery storage implemented in this work is different from the electrical model implemented in SAM's Detailed PV-Battery model. Hence, the error is not as low as the standalone model. The dispatching strategy also plays an important role on when and how much the battery delivers energy to the load. A slightly different strategy algorithm could, therefore, counts for a considerable error. Thus, in this section of validation. The dispatching strategy is approximated to the input grid power target zero strategy that SAM's Detailed PV-Battery provides. For a reference only, the error is also computed with the dispatching strategy of one cycle a day provided in this work.

Figure 3.23 demonstrates the error in the state-of-charge of the battery throughout the year.

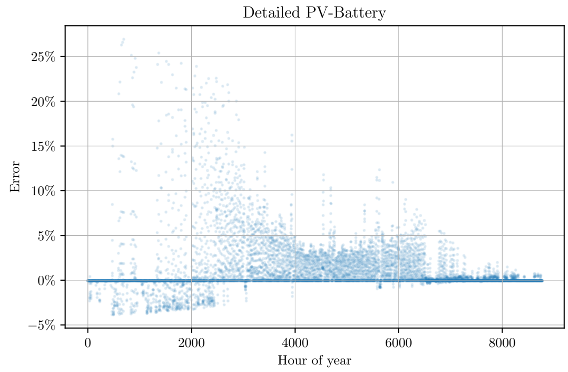


Figure 3.23: The error of the battery state of charge.

Table 3.12 provides an overview of the errors of the different variables for the model. The rest of the values are identical to Table 3.9. An increase in the error of AC power delivered to the load by the PV is noticeable. With SAM's Detailed PV-Battery model 0.09%, in comparison the error was 0.0005% with SAM's Detailed PV-Standalone model.

| Variable | More Than One Cycle A Day | | One Cycle A Day | |
|---|---|---|---|---|
| | MAE | Maximum Error | MAE | Maximum Error |
| DC output power | 0.00128% | -0.00820% | 0.00128% | -0.00820% |
| AC power delivered to load by the PV | 0.09181% | -100.000% | 0.09181% | -100.000% |
| AC power delivered to load by the BESS | 0.85859% | -100.000% | 7.87411% | -1500.59% |
| Battery SOC | 1.45011% | -26.9059% | 5.46148% | -180.469% |

Table 3.12: Overview of MAE and maximum error of different variables between SAM's Detailed PV-Battery and the model in this work under the same dispatching strategy and under the assumption of one cycle a day (SAM still assumes more than a cycle a day).

A comparison of the state-of-charge level of the BESS can be found in Figure 3.24.

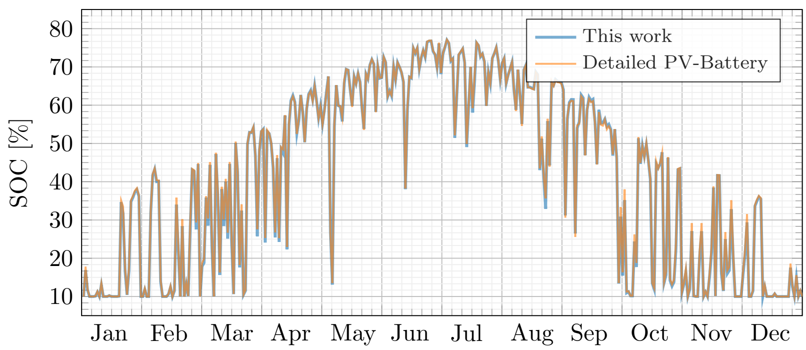


Figure 3.24: Comparison of average state-of-charge of the BESS throughout the year.

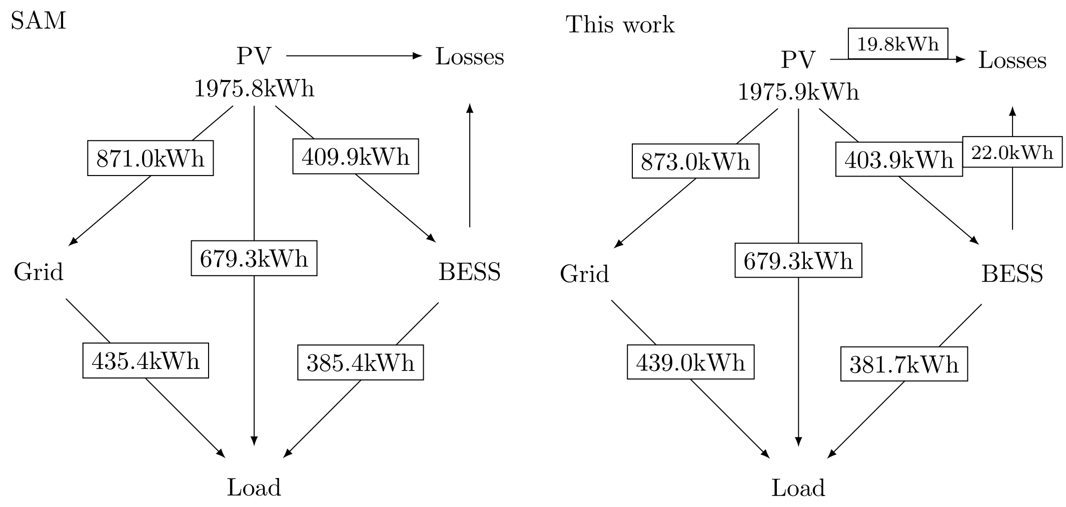


Figure 3.25: Comparison of annual energy flow through the system by SAM detailed model and this work.

See Figure 3.25 for a comparison of annual values of energies. SAM detailed model has an electrical evaluation of the inverter and the battery. Therefore, the losses are evaluated in many steps and more complicated to be shown on the figure above.

**Use case 2** For a wider overview, some of the previous parameters are changed as shown in Table 3.13, the rest of the parameters are as previous use case. The values are chosen as they demonstrate a bigger difference in the annual values than other values.

| Parameter | Symbol | Value |
|---|---|---|
| Capacity | $C_{\text{nom}}$ | 4 kWh |
| Number of modules | $N_{\text{modules}}$ | 10 |
| Annual load energy | $E_{\text{load}}$ | 4500 kWh |

Table 3.13: Design parameters used for use case 2.

Table 3.14 shows a comparison of error for different different simulation variables for use case 2.

| Variable | MAE | Maximum Error |
|---|---|---|
| DC output power | 0.00128% | -0.00836% |
| AC power delivered to load by the PV | 0.00069% | -0.00872% |
| AC power delivered to load by the BESS | 1.33577% | 100.000% |
| Battery SOC | 0.91163% | 23.31867% |

Table 3.14: Overview of MAE and maximum error of different variables between SAM's Detailed PV-Battery and the model in this work.

Figure 3.26 compares the annual energy flow of the system by SAM's Detailed PV-Battery model and the model in this work for this use case.

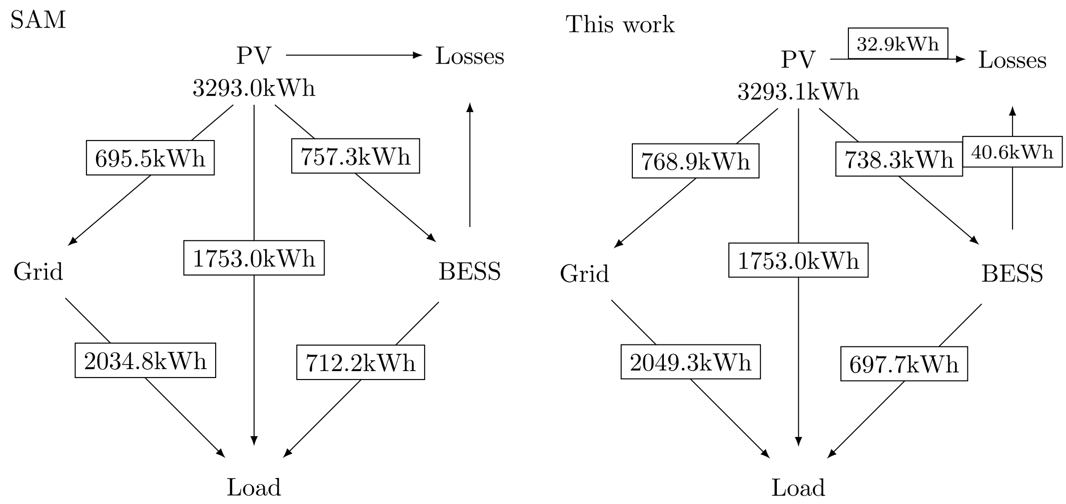


Figure 3.26: Comparison of annual energy flow through the system by SAM's Detailed PV-Battery model and this work for use case 2.

The annual AC output of SAM's PV-Battery model is 3205.8 kWh whereas the model in this work has an AC output of 3260.2 kWh meanwhile the DC output of both systems is roughly the same. Hence, an error emerges from the electrical model in SAM's Detailed PV-Battery model and the simple efficiency model in this work. Inverter's efficiency is usually dependent on both temperature and the PV DC output. By comparing Figure 3.26 and 3.14, it can be deduced that this error has no effect on the AC power delivered to the load. However, this together with the error emerging from the electrical model of the battery in SAM's Detailed PV-Battery, the annual energy delivered to the load by the BESS is affected. As result the annual energy exported to the grid is affected as well.

## 3.5. Financial Model

When designing a PV system, the decrease of expenditure on electricity is of an eminent importance for the stakeholder. Thus, the main factors considered here are the buying and selling rates from the grid, the cost of producing solar energy and the cost of energy storage. The calculation of costs for producing solar energy is presented in Section 3.5.2 and for storing energy considering degradation and lifetime is presented in Section 3.5.3. Both of the costs are then incorporated together to calculate the total costs compared with the costs of the local grid in Section 3.5.1.

### 3.5.1. Levelized Cost of Electricity

The levelized cost of electricity (LCOE) is the total cost paid for one kWh of electricity, whether it is imported from the grid or produced on site. A reduction in the mean cost of electricity follows from revenues by exporting to the grid. This, however, is supported in Germany for only 20 years. The LCOE is given as [61]

$$c_{\text{LCOE}} = \frac{C_{\text{import}} - C_{\text{feed-in}} + C_{\text{BESS}} + C_{\text{PV}}}{E_{\text{load}}} \tag{3.53}$$

where $C_{\text{import}}$ are the annual costs paid to grid for importing electricity, $C_{\text{feed-in}}$ are the annual revenues from exporting to the grid, $C_{\text{BESS}}$ are the annual costs for energy storage, and $C_{\text{PV}}$ are the annual costs for producing solar energy. The annual costs of energy imported from the grid is given by

$$C_{\text{import}} = c_{\text{grid}} \cdot \left( \underbrace{E_{\text{load}} - E_{\text{PV}\rightarrow\text{Load, BESS}}}_{\text{Energy imported from grid}} \right) \tag{3.54}$$

where $E_{\text{PV}\rightarrow\text{Load, BESS}}$ is the annual energy delivered to the load and to the BESS by the PV and the cost of a kWh charged by the grid $c_{\text{grid}}$. The annual revenues by exporting energy to the grid is given by

$$C_{\text{feed-in}} = c_{\text{feed-in}} \left( \underbrace{E_{\text{AC, annual}} - E_{\text{PV}\rightarrow\text{Load, BESS}}}_{\text{Energy exported to grid}} \right) \tag{3.55}$$

where $c_{\text{feed-in}}$ is the feed-in tariff rate, i.e. the revenue of one kWh exported to the grid. The annual costs of storing energy can be described as

$$C_{\text{BESS}} = c_{\text{LCOE, BESS}} \cdot E_{\text{PV}\rightarrow\text{BESS}} \tag{3.56}$$

where $c_{\text{LCOE, BESS}}$ is the levelized cost of stored energy. The annual costs of producing solar energy

$$C_{\text{PV}} = c_{\text{LCOE, PV}} \cdot E_{\text{AC, annual}} \tag{3.57}$$

where $c_{\text{LCOE, PV}}$ is the levelized cost of solar energy. The energy consumed by the load from the PV and the BESS is

$$E_{\text{PV}\rightarrow\text{Load, BESS}} = E_{\text{PV}\rightarrow\text{Load}} + \underbrace{E_{\text{PV}\rightarrow\text{BESS}}}_{=E_{\text{BESS}\rightarrow\text{Load}}/\eta_{\text{bat}}} \tag{3.58}$$

Both the electricity and feed-in rates are given by the government and are discussed in Section 3.5.4. The calculations of $c_{\text{LCOE, PV}}$ and $c_{\text{LCOE, BESS}}$ follow in Section 3.5.2 and Section 3.5.3 respectively.

### 3.5.2. Levelized Cost of Solar Energy

The levelized cost of solar energy is defined as the ratio of the overall cost of the system with respect to its lifetime output [31]

$$c_{\text{LCOE, PV}} = \frac{C_{\text{system}}}{E_{\text{AC, lifetime}}} \tag{3.59}$$

where $C_{\text{system}}$ is the costs for purchasing and maintaining the system, $E_{\text{AC, lifetime}}$ is the lifetime energy output of the system. If the value of the energy output is level over its lifetime then it could be calculated by simply multiplying the annual energy output $E_{\text{AC, annual}}$ with the lifetime of the system $N_{\text{PV, years}}$ in years. Conversely, the money that is present now has more value than the money received in a month, since the money now can be invested and make profit immediately. The value of the output energy of the system decreases over time. This decrease is measured by the discount rate $r_{\text{dr, PV, real}}$ (real). If the inflation rate $r_{\text{inflation}}$ is considered, the nominal discount rate $r_{\text{dr, PV}}$ can be given as [55]

$$r_{\text{dr, PV}} = (1 + r_{\text{dr, PV, real}}) \cdot (1 + r_{\text{inflation}}) - 1 \tag{3.60}$$

Accounting for these is key to correct evaluation of the cost of energy. To account for that in terms of the value of output energy, the annual output energy is divided by the capital recovery factor (CRF), which is given as [55]

$$r_{\text{CRF, PV}} = \frac{r_{\text{dr, PV}} \cdot (1 + r_{\text{dr, PV}})^{N_{\text{PV, years}}}}{(1 + r_{\text{dr, PV}})^{N_{\text{PV, years}}} - 1} \tag{3.61}$$

hence

$$E_{\text{AC, lifetime}} = \frac{E_{\text{AC, annual}}}{r_{\text{CRF, PV}}} \tag{3.62}$$

The cost of the PV system can be split up in equity $C_{\text{equity, PV}}$ that is paid now as well as follow-on investments for operation and maintenance $C_{\text{O\&M}}$ that are paid annually

$$C_{\text{system}} = C_{\text{equity, PV}} + C_{\text{O\&M, NPV}} \tag{3.63}$$

since future value of money changes, calculation of the net present value (NPV) of the O&M costs is required. The NPV coefficient is derived from [55]

$$\alpha_{\text{NPV}} = \sum_{n=1}^{N_{\text{PV, years}}} \frac{(1 + r_{\text{inflation}})^{n-1}}{(1 + r_{\text{dr, PV}})^{n}} \tag{3.64}$$

and equity is described here as

$$C_{\text{equity, PV}} = C_{\text{module}} \cdot N_{\text{modules}} + C_{\text{additional}} \tag{3.65}$$

where $C_{\text{module}}$ is the cost of one module and $N_{\text{modules}}$ are the number of purchased modules and $C_{\text{additional}}$ are additional costs that includes installation and inverter costs, and installation fees. Additional costs are relative to the installed modules, see Table A.1. Now by putting it together Equation (3.59) becomes

$$c_{\text{LCOE, PV}} = \frac{C_{\text{equity, PV}} + C_{\text{O\&M}} \cdot \alpha_{\text{NPV}}}{E_{\text{AC, annual}}} \cdot r_{\text{CRF, PV}} \tag{3.66}$$

Here it is assumed that the real discount rate for a PV system is $r_{\text{dr, PV, real}}$ is 4% [15] and the lifetime of a PV system $N_{\text{PV, years}}$ to be 25 years.

### 3.5.3. Levelized Cost of Stored Energy

To financially optimize the battery's capacity, an analysis of energy balance is emitted first after being converted to days, see Equation (3.40) and Figure 3.9 as described in [10] as opposed to previously in hours since one cycle per day of the BESS is considered here. Once this is done, a distribution of $N_{\text{E}}$ surplus energy classes is calculated as follows

$$E_{\text{surplus},i} = \frac{E_{\text{surplus, max}}}{N_{\text{E}}} \cdot i \tag{3.67}$$

where $E_{\text{surplus},i}$ is the floor energy of the $i$-th class and $E_{\text{surplus, max}}$ is the maximum energy surplus, see Figure 3.27.

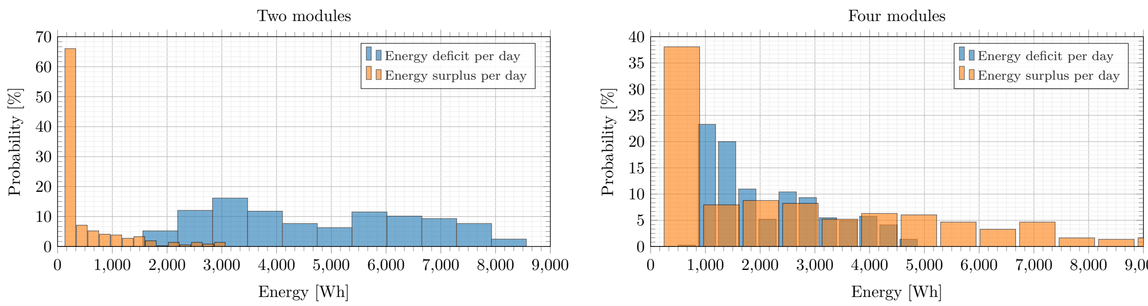


Figure 3.27: Energy surplus and energy deficit distributions with one resident and different number of $60\text{W}_\text{p}$ modules.

Estimation of the battery's lifetime is key to determining its optimal capacity. As discussed in Section 3.3 the depth of discharge (DOD) is an important variable to consider. The DOD of $i$-th class is given as

$$\text{DOD}_i = \min\left\{\frac{E_{\text{surplus},i}}{C_{\text{nom}}}, \quad 1\right\} \tag{3.68}$$

An estimation of the battery's lifetime can be calculated considering the analysis energy balance and both the calendar lifetime $N_{\text{BESS, cal}}$ and the number of cycles $N_{\text{BESS, cyc}}$ as follows

$$N_{\text{BESS, days}} = \sum_{i=1}^{N_{\text{E}}} p_{\text{surplus, i}} \cdot \min\left\{N_{\text{BESS, cyc}_i}, N_{\text{BESS, cal}}\right\} \tag{3.69}$$

where $p_{\text{surplus, i}}$ is the probability of the $i$-th class of energy surplus and $N_{\text{BESS, cyc}_i}$ is the equivalent number of full cycles for the $i$-th class calculated using equations (3.46) and (3.68). It is noted that here $N_{\text{BESS, cyc}_i}$ and $N_{\text{BESS, cal}}$ are given in days.
The lifetime of the battery in years is given as

$$N_{\text{BESS, years}} = \frac{N_{\text{BESS, days}}}{365.25} \tag{3.70}$$

and the lifetime energy stored by the battery is given by

$$E_{\text{BESS, lifetime}} = \frac{E_{\text{PV}\rightarrow\text{BESS}}}{r_{\text{CRF, BESS}}} \tag{3.71}$$

where $E_{\text{PV}\rightarrow\text{BESS}}$ is the annual energy stored in the battery, $r_{\text{CRF, BESS}}$ is the cost recovery factor of the battery, calculated analogously to Equation (3.61) considering the lifetime of the battery $N_{\text{BESS, years}}$ and the real discount rate of the battery $r_{\text{dr, BESS, real}}$ which can be assumed to be about 3% for residential use [33]. Note, that this excludes the inflation rate $r_{\text{inflation}}$. Finally, the levelized cost of stored energy is the ratio between the lifetime costs of the battery with respect to its lifetime output and is given by [45]

$$c_{\text{LCOE, BESS}} = \frac{c_{\text{BESS}} \cdot C_{\text{nom}}}{E_{\text{BESS, lifetime}}} \tag{3.72}$$

where $c_{\text{BESS}}$ is the cost of one kWh of a lithium-ion battery.

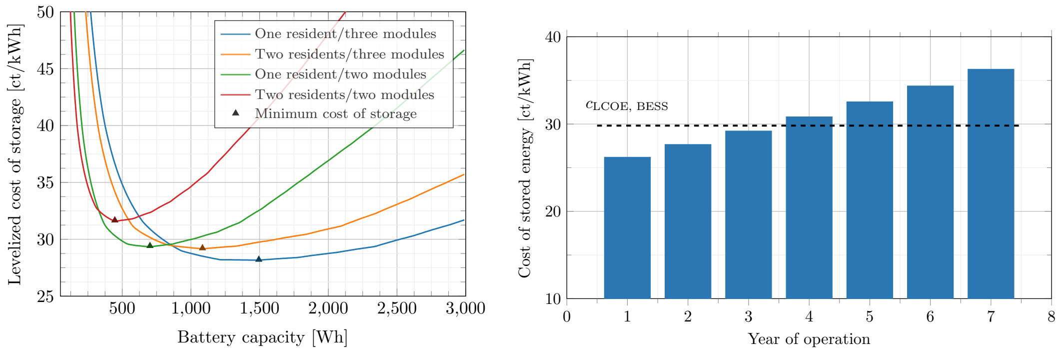


Figure 3.28: On the left, the cost of storage by profile using 60W$_\text{p}$ modules and their optimal capacity, i.e. with minimum levelized cost of stored energy. On the right, the cost of stored energy by year of operation with an expected lifetime of 7 years.

The equity of the whole system can be now calculated as

$$C_{\text{equity}} = \underbrace{C_{\text{equity, BESS}}}_{=c_{\text{BESS}} \cdot C_{\text{nom}}} + C_{\text{equity, PV}} \tag{3.73}$$

See Figure 3.28 (b) for the increasing of cost of storage in dependency of the battery's age. The results follow from the model simulated in Section 3.4.2 assuming an inflation rate of $r_{\text{inflation}}$=2.6%, see Table A.1.

### 3.5.4. Financial Parameters

In this section, the values for four financial parameters are discussed for the simulation of an "average year" within the analysis period.

**Electricity retail rate by year** The current electricity retail price in Aachen as of September 2021 is $c_{\text{grid, today}}$ =31.09 ct/kWh, see Table A.1. With a $r_{\text{grid, annually}}$ =2% of annual increase rate[61] the average price over 25 years would be $c_{\text{grid}}$ =39.82 ct/kWh which is calculated as follows

$$c_{\text{grid}} = \frac{1}{N_{\text{analysis}}} \cdot \sum_{n=0}^{N_{\text{analysis}}-1} c_{\text{grid, today}} \cdot (1 + r_{\text{grid, annually}})^n \tag{3.74}$$

where $N_{\text{analysis}}$ is the number of years in the analysis period, $n$ is the $n$-th year of the analysis period.

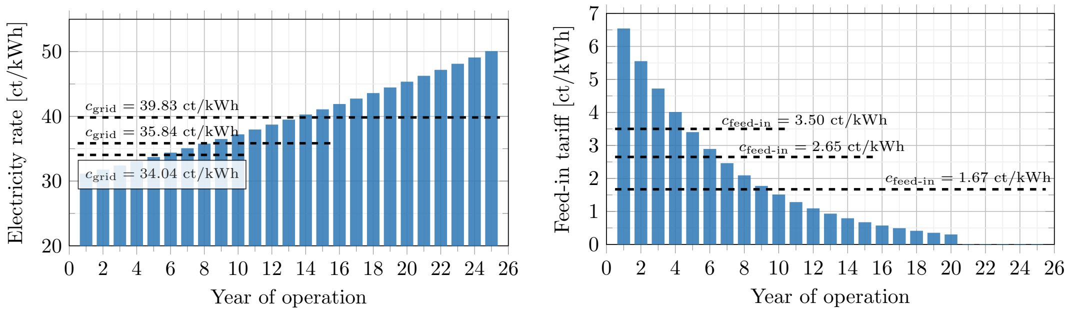


Figure 3.29: Cost of electricity imported from the grid annually and average cost of imported electricity within the scope of 25, 15 and 10 years on the left. Change of feed-in tariff on an annual basis and the average feed-in tariff on the right.

**Feed-in tariff by year** According to the Renewable Energy Sources Act (EEG) in Germany, the feed-in tariffs are only considered for the period of 20 years[1] and exports to grid afterwards are not compensated. Based on historical data, see Table A.1, the current feed-in tariff is $c_{\text{feed-in, today}} = 6.53$ and has been decreasing by fluctuating rates (between 5% and 30%) from 57.40 ct/kWh to 6.53 ct/kWh as of April 2022. Since 2021 January, the have been steadily decreasing by $r_{\text{feed-in, annually}}$ ≈15% annually ($r_{\text{feed-in, monthly}}$ ≈1.457% monthly). We calculate the average feed-in tariff over $N_{\text{analysis}}$ years as follows

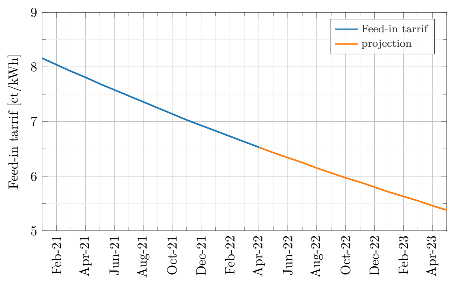


Figure 3.30: Feed-in tariffs in Germany since 2021 and a projection until 2023.

$$c_{\text{feed-in}} = \frac{1}{N_{\text{analysis}}} \cdot \sum_{n=0}^{\min(N_{\text{analysis}},20)-1} c_{\text{feed-in, today}} \cdot (1 - r_{\text{feed-in, annually}})^n \tag{3.75}$$

[1] https://www.bmwi.de/Redaktion/DE/Artikel/Energie/foerderung-der-erneuerbaren-energien.html

Hence, the average feed-in tariff over 25 years is $c_{\text{feed-in}}$ =1.67 ct/kWh, see Figure 3.29. The monthly decease is accounted for in simulation. The feed-in tariff through the months of the first year could be approximated by

$$c_{\text{feed-in}}(m) = c_{\text{feed-in}}(0) \cdot (1 - r_{\text{feed-in, monthly}})^m \tag{3.76}$$

where $m$ is the month of year starting from $m = 0$.

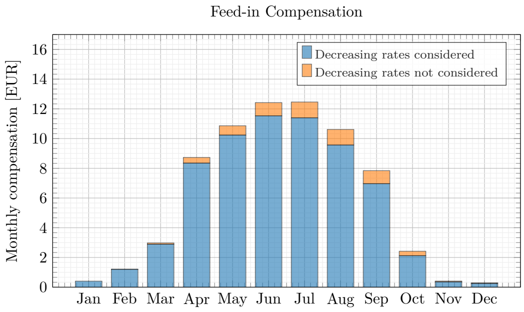


Figure 3.31: Illustration of monthly feed-in compensation by the grid when the decreasing rates of feed-in tariffs are considered and when not.

see Figure 3.31 for a comparison of the monthly compensation calculated for the model simulation in Section 3.4.2. It is also important to note, that the feed-in tariffs apply only if at least $r_{\text{self-consumption, min}}$ ≥30% of the produced energy is consumed locally for each month[1] see Equation (3.81) for the calculation of self-consumption.

**Cost of battery by year** The battery's lifetime is usually much less than PV system's lifetime. As a result, the battery is expected to be replaced several times through the years of operation. If a battery is expected to have a lifetime of 13 years for example, then it has to be replaced twice within an analysis period of 25 years. As the costs of lithium-ion batteries decrease, throughout the years, the average price of the replacement years is considered. The cost of the battery in 2018 was ranging from 800 to 1300 EUR/kWh incl. VAT [12] and it ranges today from 500 to 1200 EUR/kWh incl. VAT [26]. If the cost of a battery today per one kWh $c_{\text{BESS, today}}$ =850 EUR/kWh incl. VAT with an annual decrease rate of $r_{\text{BESS}}$=8% [42], its cost in fourteen years will drop down to 288 EUR/kWh.

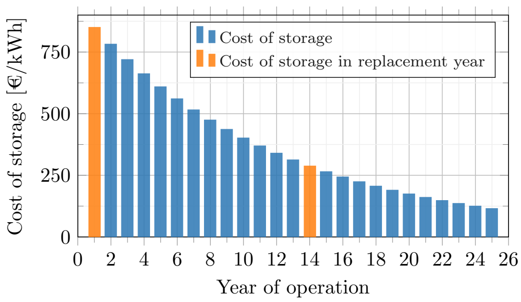


Figure 3.32: Cost of energy storage per kWh by year of operation.

[1] https://www.gesetze-im-internet.de/eeg_2014/__9.html accessed on Apr. 16, 2022

That means the average cost of storage will be 607 EUR/kWh, see Figure 3.32. Hence

$$c'_{\text{BESS, ref}}(N_{\text{BESS, years}}) = \frac{1}{N_{\text{analysis}}} \cdot \sum_{n=0}^{N_{\text{analysis}}-1} c_{\text{BESS, today}} \cdot (1 - r_{\text{BESS}})^{n-(n \text{ fmod } N_{\text{BESS, years}})} \tag{3.77}$$

where fmod is the float modulo operator. The function $c'_{\text{BESS, ref}}$ provides a step-wise curve. To smooth out the curve we define

$$\alpha' = N_{\text{BESS, years}} - \text{ floor}\left(N_{\text{BESS, years}}\right) \tag{3.78}$$

Hence $\alpha'$ is the floating number after the decimal point. Thus, the mean cost of one kWh of a lithium battery is

$$c_{\text{BESS, ref}}(N_{\text{BESS, years}}) = (1 - \alpha') \cdot c'_{\text{BESS, ref}}(N_{\text{BESS, years}}) + \alpha' \cdot c'_{\text{BESS, ref}}(N_{\text{BESS, years}} + 1) \tag{3.79}$$

**Cost of battery by capacity** The cost of lithium-ion battery per kWh $c_{\text{BESS}}$ is also dependent on its nominal capacity $C_{\text{nom}}$. Based on the prices given in Figure 3.33. The decrease in the cost of storage per kWh is approximated with a linear regression model normalized by a reference cost of storage per kWh

$$c_{\text{BESS}} = c_{\text{BESS, ref}} \cdot \left(1.0249406 - 0.024941 \cdot C_{\text{nom}}\right) \tag{3.80}$$

where $C_{\text{nom}}$ is the nominal capacity of the battery in kWh and $c_{\text{BESS, ref}}$ is the reference cost of storage per kWh. See Table 3.15 for different average prices by number of years.

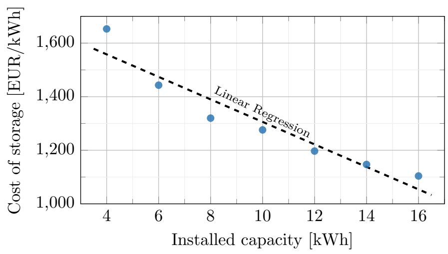


Figure 3.33: Cost of energy storage per kWh by capacity as of 2019[1].

| Parameter | Symbol | Today | 5 years | 10 years | 15 years | 20 years | 25 years |
|---|---|---|---|---|---|---|---|
| Grid rate [ct/kWh] | $c_{\text{grid}}$ | 31.09 | 32.36 | 34.04 | 35.84 | 37.77 | 39.83 |
| Feed-in tariff [ct/kWh] | $c_{\text{feed-in}}$ | 6.53 | 4.84 | 3.50 | 2.65 | 2.09 | 1.67 |

Table 3.15: Levelized values of different parameters by assessment period.

### 3.5.5. Sensitivity Analysis

Assuming financial parameters as shown in Table 3.16, the mean cost of electricity was evaluated by the size of the PV-Battery system as in Figure 3.34 for the scope of 15 and 25 years. For this simulation, the irradiation data for Aachen (50°46'16.1"N 6°03'05.4"E) with PV panels oriented to true south and an inclination of 35° summing up to 1129.8 kWh/m$^2$ annually (see Figure 3.42) were used. The sizes of PV and

[1] https://www.energie-experten.org/erneuerbare-energien/photovoltaik/stromspeicher/preise

Battery are normalized by the annual load i.e. if the annual load is 4500kWh then PV system size of 1 Wp/kWh corresponds to a PV system of maximum power point of 4500Wp in SRC. A battery size of 1 Wh/kWh corresponds to a battery capacity of 4.5 kWh.

| **Parameter** | **Symbol** | **Value** |
|---|---|---|
| Price of PV panels | $C_{\text{module}}/P_{\text{max, ref}}$ | 1400 EUR/kWp |
| Inflation rate | $r_{\text{inflation}}$ | 2.5% |
| Real PV discount rate | $r_{\text{dr, PV, real}}$ | 4% |
| Real Battery discount rate | $r_{\text{dr, BESS, real}}$ | 3% |
| Monthly shrinking rate of feed-in tariff | $r_{\text{feed-in, monthly}}$ | 0% |
| Operation and maintenance costs | $C_{\text{O\&M}}$ | 1% of PV costs |

Table 3.16: Financial parameters used.

The minimum and maximum state of charge of the battery is $\text{SOC}_{\text{min}}$=20% and $\text{SOC}_{\text{max}}$=95%. The battery's round-trip efficiency is considered to be $\eta_{\text{BESS}}$=92%.

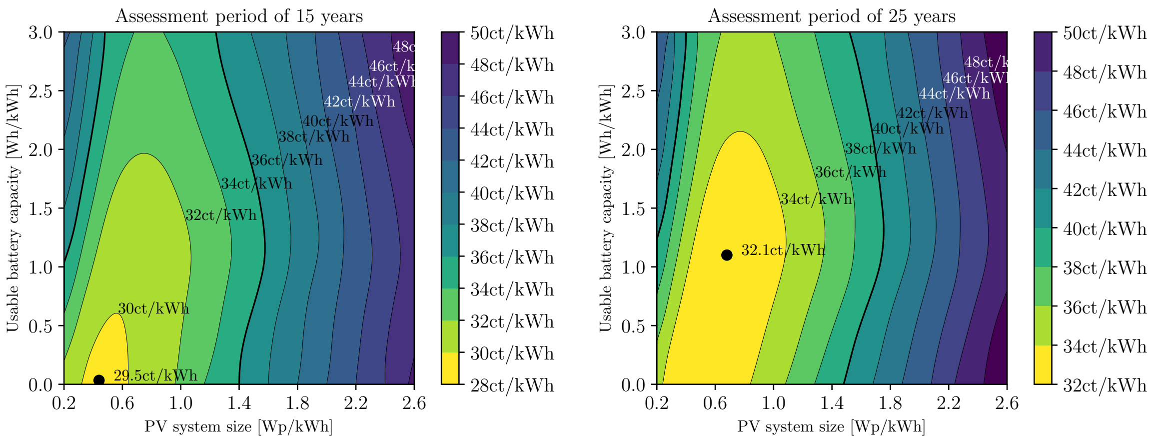


Figure 3.34: Mean cost of electricity by size of system within the scope of 15 years (35.8 ct/kWh limit of profitability) and 25 years (39.8 ct/kWh limit of profitability).
• Minimum levelized cost of electricity.

Figure 3.34 suggests a different size of the system when considering a different scope of years. As the feed-in tariffs tend to decrease, the profitability of exporting excess energy shrinks while it becomes more profitable to store this energy for use at night. In the following, single parameters are changed to see the effect they have on the levelized cost of electricity in a scope of 25 years.

**Lifetime of the battery** To see the difference in the lifetime of the battery, the curve described in Equation (3.46) is scaled to mathch 5000 and 7000 cycles respectively. As can be seen in Figure 3.35 and Figure 3.36, a longer expected cycle life of the battery would results a slightly more profits. This is mainly because of reduction in the number of replacements of the battery.

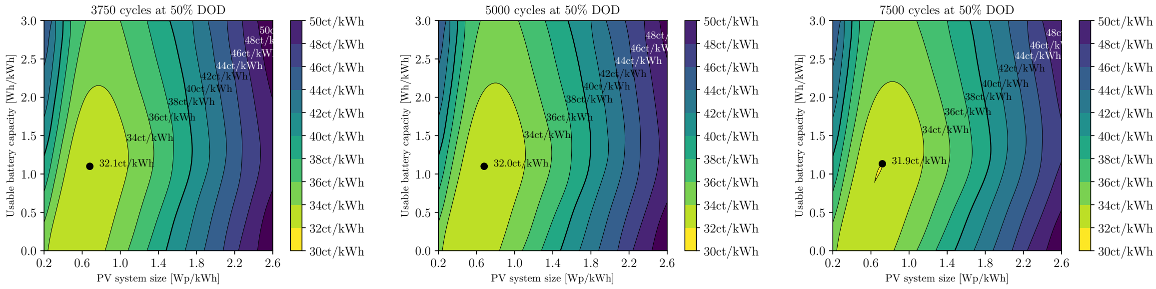


Figure 3.35: Levelized cost of electricity by the cyclic lifetime of the battery.

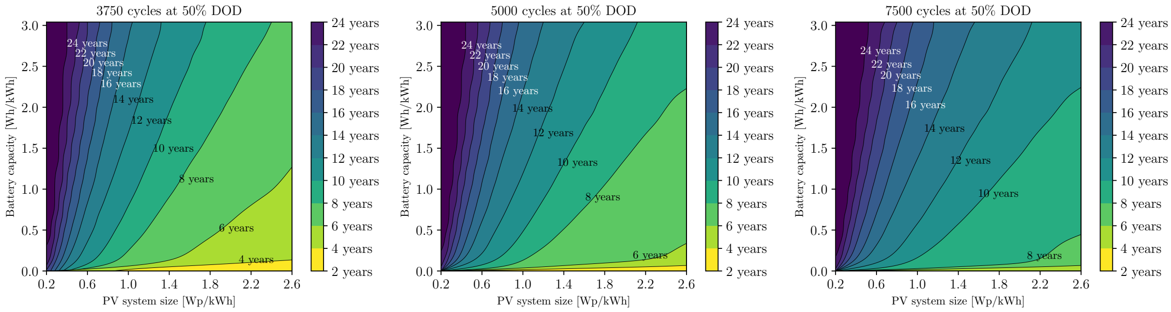


Figure 3.36: Lifetime of the battery by the cyclic lifetime of the battery.

In the following, a cycle life with 3750 cycles at 50% DOD is assumed.

**Shape of load curve** The shape of the load curve have a noticeable impact on the optimum size of the PV system (see Figure 3.37). Despite having the same annual load overall, the difference in the distribution of load throughout the day has a direct effect on how much the battery can charge and discharge and thus on the profitability of the battery.

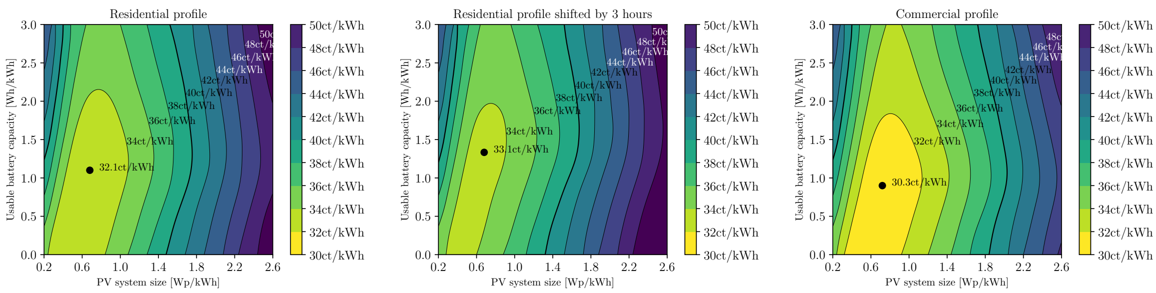


Figure 3.37: Levelized cost of electricity by load curve.

**Inflation rate** The inflation rate, as in Figure 3.38, plays another important role in determining of the PV-Battery system. A higher inflation rate $r_{\text{inflation}}$ than the corresponding increasing rate of electricity rates $c_{\text{grid}}$ means less profitability of the system and thus smaller system size. However, usually high inflation also entails higher electricity rates.

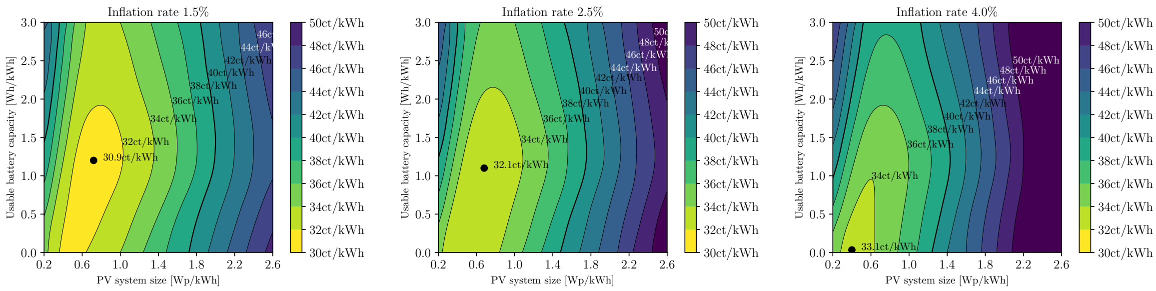


Figure 3.38: Levelized cost of electricity by inflation rate.

In the following, an inflation rate of 2.5% is assumed.

**Mean cost of the battery per kWh** A lower average cost of the battery per kWh is a key factor in have a large battery size. This is also limited by the feed-in tariff. A lower feed-in tariff encourages a bigger size of the battery. (see Figure 3.39)

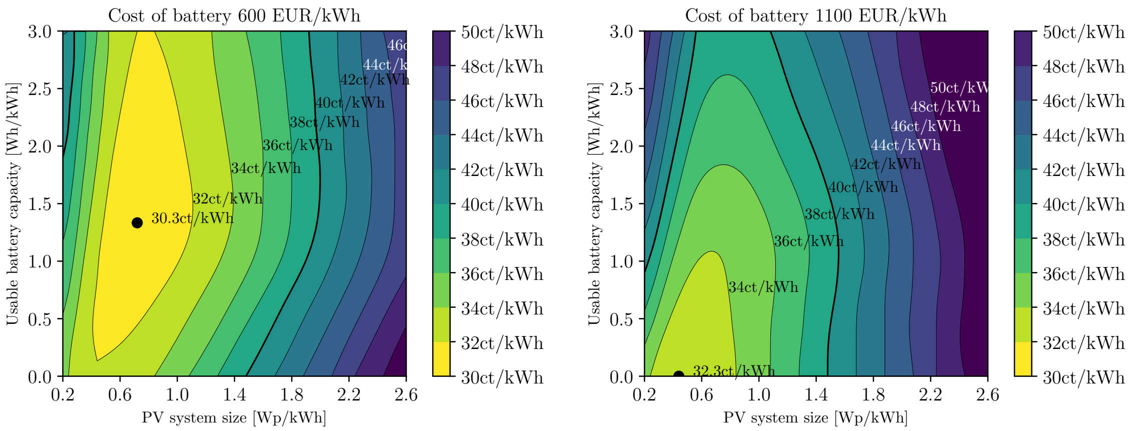


Figure 3.39: Levelized cost of electricity by cost of battery.

In the following a battery cost of 850 EUR/kWh is assumed.

**Feed-in tariff** finally, the average feed-in tariff, while has an impact on the minimum levelized cost of electricity, the impact on the sizing of the system is rather subtle as can be seen in Figure 3.40.

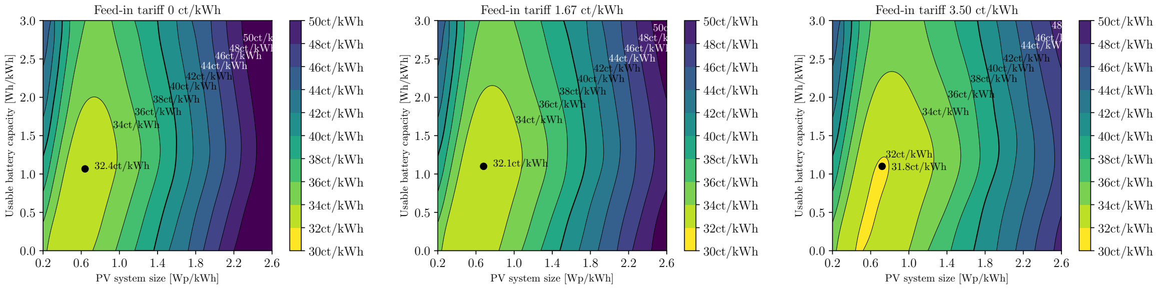


Figure 3.40: Levelized cost of electricity by feed-in tariff.

As can be seen above, along insolation, many financial factors have a vital role in optimizing the size of the system.

**Rule of minimum self-consumption** as mentioned in Section 3.5.4, the feed-in compensation is only applied for a maximum of 70% of the produced energy. A comparison of this limit can be seen in Figure 3.41

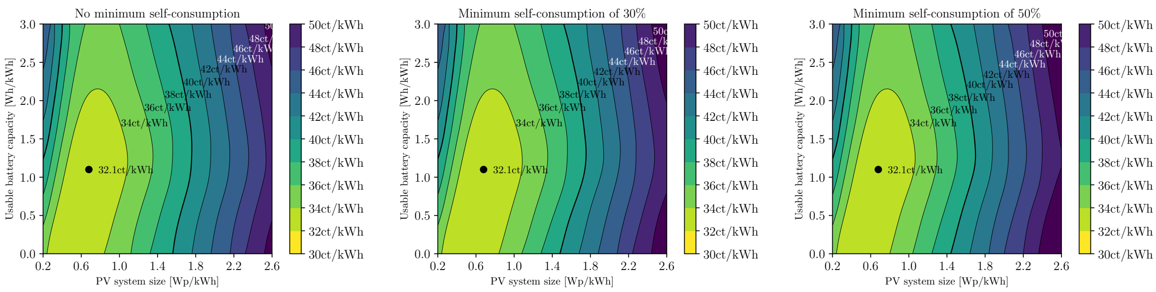


Figure 3.41: Levelized cost of electricity by minimum self-consumption rule.

The difference in system design because of this constraint is not of a great importance as can be seen in Figure 3.41.

**Assessment Criteria** It is important to assess the PV-Battery system in terms of energy to determine its performance. Two assessment criteria are used. Self-sufficiency and self-consumption.

**Self-consumption** is the share of produced energy consumed by the load and can be described as

$$r_{\text{self-consumption}} = \frac{E_{\text{PV}\rightarrow\text{Load}} + E_{\text{PV}\rightarrow\text{BESS}}}{E_{\text{AC, annual}}} \tag{3.81}$$

**Self-sufficiency** is the share of load covered by the produced energy which is described as

$$r_{\text{self-sufficiency}} = \frac{E_{\text{PV}\rightarrow\text{Load}} + E_{\text{BESS}\rightarrow\text{Load}}}{E_{\text{load}}} \tag{3.82}$$

To visualize how both assessment criteria change by PV-Battery size, a simulation is done on the system assuming 85% DOD of the battery.

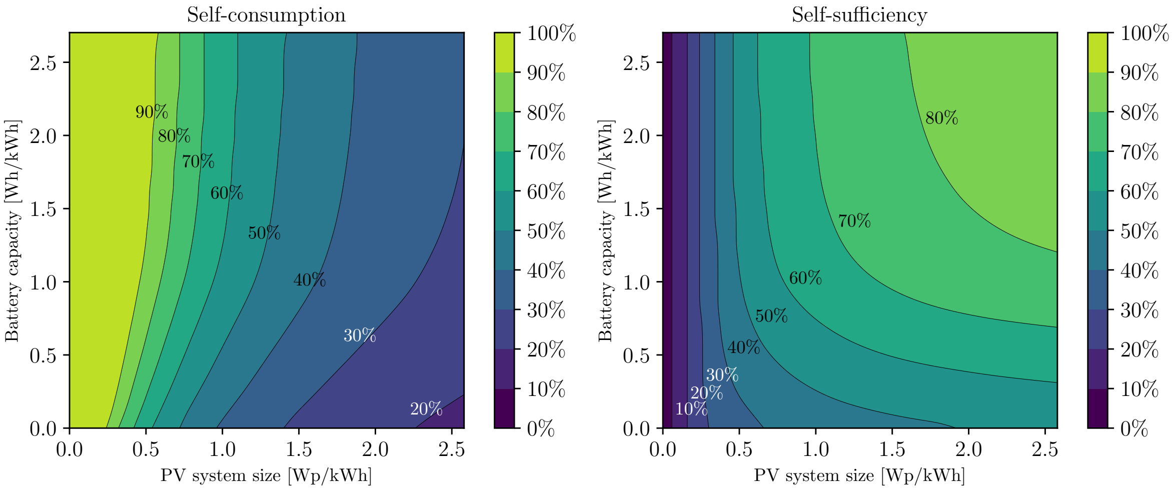


Figure 3.42: Self-consumption and self-efficiency by system size.

Figure 3.42 presents how both criteria change by the system size. It suggests that a system with 1 Wp/kWh achieves 39% self-consumption as well as 43% self-sufficiency without an energy storage. It can also be interpreted that with 1 Wh/kWh storage, the system achieves 58% self-consumption as well as 64% self-sufficiency. While these graphs are normalized to the total load, they still differ by the user profile, i.e. weather profile and the shape of the load curve, in this work, there are two residential and commercial profiles (see Section 2.4 and Figure 3.37).

# 4. Optimization of the Photovoltaic Power Plant

In this section, the methods and procedures for optimizing the PV array size and the battery's capacity to store the maximum amount of energy produced by the PV are discussed.

## 4.1. Objective Function

A design of a rooftop-mount photovoltaic power plant in this scope is a tuple of number of panels $N_{\text{modules}}$ of peak power $P_{\text{max, ref}}$ and a temperature coefficient $\mu_P$ and a lithium-ion battery of capacity $C_{\text{nom}}$.
An optimum design with this respect is a design that minimizes the overall costs of energy either produced by the system or imported from the grid for the lifetime of the system

$$(\hat{N}_{\text{modules}}, \hat{C}_{\text{nom}}) = \underset{(N_{\text{modules}}, C_{\text{nom}})}{\operatorname{argmin}} \Big\{ C_{\text{total, kWh}}(\mathfrak{C}, N_{\text{modules}}, C_{\text{nom}}) \Big\} \tag{4.1}$$

where $\mathfrak{C}$ is the set of the simulation inputs. For simplicity, the function will be written without $\mathfrak{C}$ in the following sections. The total cost of energy (see Equation 3.53) has been chosen as the objective function as it takes into account the following factors

- The lifetime costs of the system, including the lifetime of the battery.
- The ratio of energy the system produces with respect to the total load.
- The electricity rates, the energy deficit that the household has to purchase from the grid, and the energy surplus that the system exports to the grid.

## 4.2. Constraints

Maximizing the profitability of the system is limited by different constraints. The most relevant of which are

**Geometrical Constraints** The maximum output of each PV module is limited by the amount of insolation it receives, which is yet contingent on the climate of the region of interest for comparison see Figure 3.10. Higher ambient temperature play also a fair amount of reducing the overall output of the system. Considering the battery is installed inside the house with roughly constant room temperature throughout the year, the impact of temperature on the battery is neglected. For perspective on the meteorological impact on PV output refer to Figure 3.8.
The amount of insolation is not only limited by the climate of the region, but also dependent on the architecture of the building, i.e. the tilt and orientation of each panel, which is assumed here to be fixed on the roof. Naturally the best orientation for the northern hemisphere is true south and depending on the latitude the optimal tilt of the panel differs, for comparison see Figure 3.2. Another geometrical constraint is the usable roof area, the area on which the PV modules can be installed.

**Load Profile** The behavior of an average individual is not expected to be significantly changed and this is defined by the number of residents in a residential building with their grade of power usage. Whether a separate house or an apartment is considered changes the scale of the hourly load. Additionally if a heat pump is used by electricity this adds to the load, for a short comparison see Tables 2.4 and Table 2.3.

**Storage Capacity** The choice of a battery's capacity comes down to its variable lifetime and energy efficiency. A financial factor is also decisive here. For maximum benefits the battery is assumed to charge during daytime and discharge in the evening. This allows for one cycle a day which is assumed here.

**Optional Financial Constraints** For most stakeholders there is an upper bound to how much of investment they seek to make now. Thus, the initial costs of the overalls system is optionally considered here as a constraint. Note that the initial costs do not include follow-on costs such as battery replacement or costs of operation and maintenance (O&M). If a maximum investment $C_{\text{max, invest}}$ is set, then there is a maximum number of PV panels $N_{\text{modules, max}}$ and a maximum capacity of $C_{\text{bat, max}}$

$$N_{\text{modules, max}} = \frac{C_{\text{max, invest}}}{C_{\text{module}}}, \qquad C_{\text{nom, max}} = \frac{C_{\text{max, invest}}}{c_{\text{BESS, ref}}} \tag{4.2}$$

## 4.3. Optimization Routine

The problem described in Section 4.1 can be approached using different methods. Here a simple heuristic method and Newton's method are explained and then further methods are compared. The target function $c_{\text{LCOE}}(N_{\text{modules}}, C_{\text{nom}})$ is written as $\mathcal{L}(x, y)$ in this section for simplicity.

### 4.3.1. Heuristic Method

As can be seen in section 3.5.5, there is only one optimum. Additionally, the number of panels is always a natural number and the battery's capacity is usually a multiplier of 0.6kWh. Thus, a heuristic method can be used

**Unconstrained optimization** In general, the heuristic method evaluates neighboring "cells" while assuming that the optimum is on the right side of the starting point.

```
input: float x_0, float x_step, float y_step, func f
input: int max_steps, float tol
output:float, float
begin
  x, y ← x_0, 0
  steps ← 1
  while steps ≤ max_steps:
       curr ← f(x, y)
       dx, dy ← 0, 0

       if f(x+step_x, y+step_y) < curr:
           dx, dy ← x_step, y_step

       else:
           if f(x+x_step, y) ≤ curr + tol:     dx ← x_step
           elif f(x−x_step, y) ≤ curr + tol:   dx ← −x_step
           if f(x, y+y_step) < curr + tol:     dy ← y_step

       x, y ← x + dx, y + dy

       if dx = dy = 0:
           break

       steps ← steps + 1
  return x, y
end
```

Figure 4.1: Heuristic search in pseudocode.

As can be seen in Figure 4.1, the algorithm has a flexible movement on the $N_{\text{modules}}$ axis (x-axis), but can only increase the $C_{\text{nom}}$ if it is more profitable with a given tolerance. The algorithm is tested with different resolutions (x and y steps) for this use case and the number of iterations needed are compared.

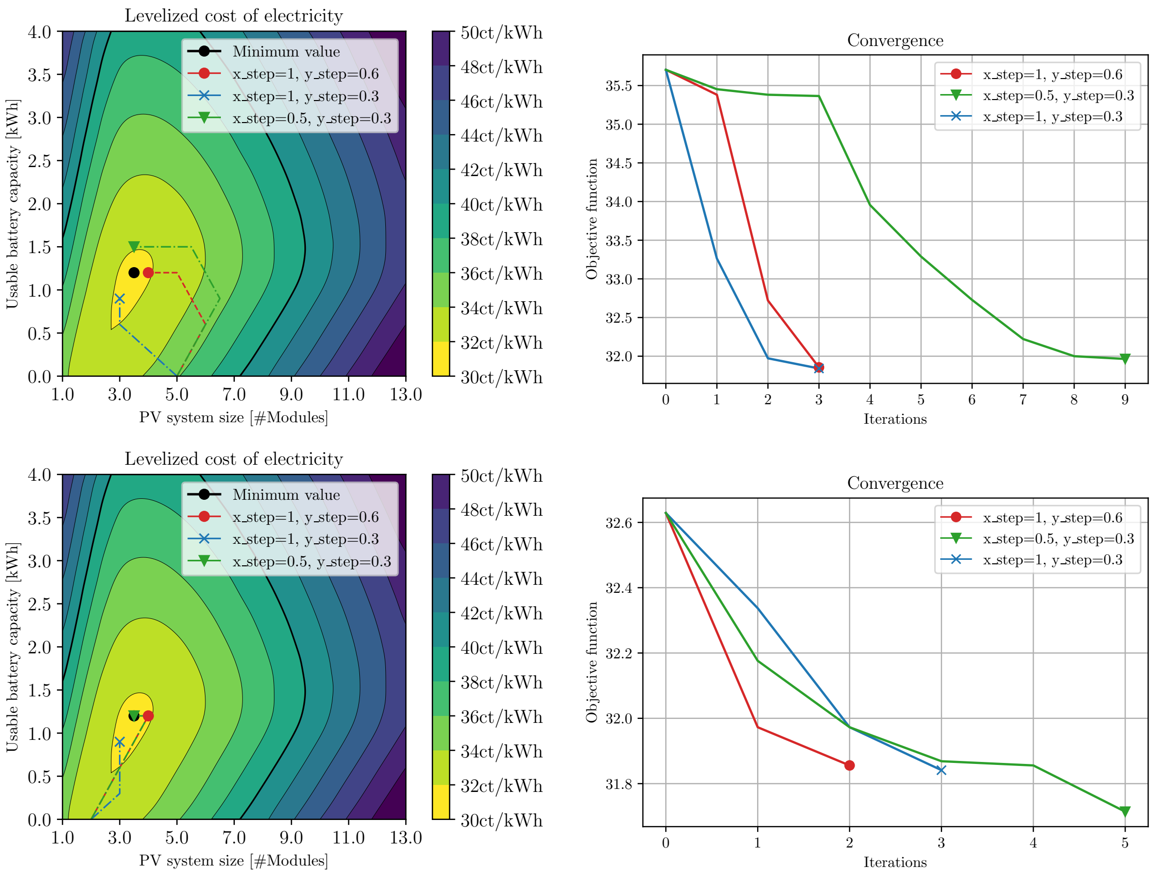


Figure 4.2: Optimization procedure using heuristic method with different resolutions and starting points.

It is evident from Figure 4.2 that a good resolution is needed for this method to work properly. Also a starting point where it is more likely that the optimum is on right saves more time, hence a small number of panels. The case of resolution where `x_step`=0.5 and `y_step`=0.6 with a starting point in `x_0`=5 is a good example where the algorithm takes longer time. A good starting point is, therefore, `x_0`=2.

**Constrained optimization** If the maximum amount of investment is less than the value that purchases two PV modules, then, clearly one PV module is the optimal design. Otherwise the starting point of `x_0`=2 is within the search space as defined in Equation (4.8). Therefore, a detection whether the optimal design violates the constraints is possible once the algorithm surpasses financial constrain line.
If that is the case, analogously to Section 4.3.2, the algorithm optimizes only along the financial constraint line. The financial constraint line can be defined by the number of modules as

$$C_{\text{nom}}(N_{\text{modules}}) = \frac{1}{c_{\text{BESS}}} \cdot \Big(C_{\text{max, invest}} - C_{\text{module}} \cdot N_{\text{modules}}\Big) \tag{4.3}$$

Note that the capacity here is not necessarily a multiplier of `y_step`. The subtraction of the modulo of the result with `y_step` gives the maximum capacity that is a multiplier of `y_step` and does not violate the financial constraints.

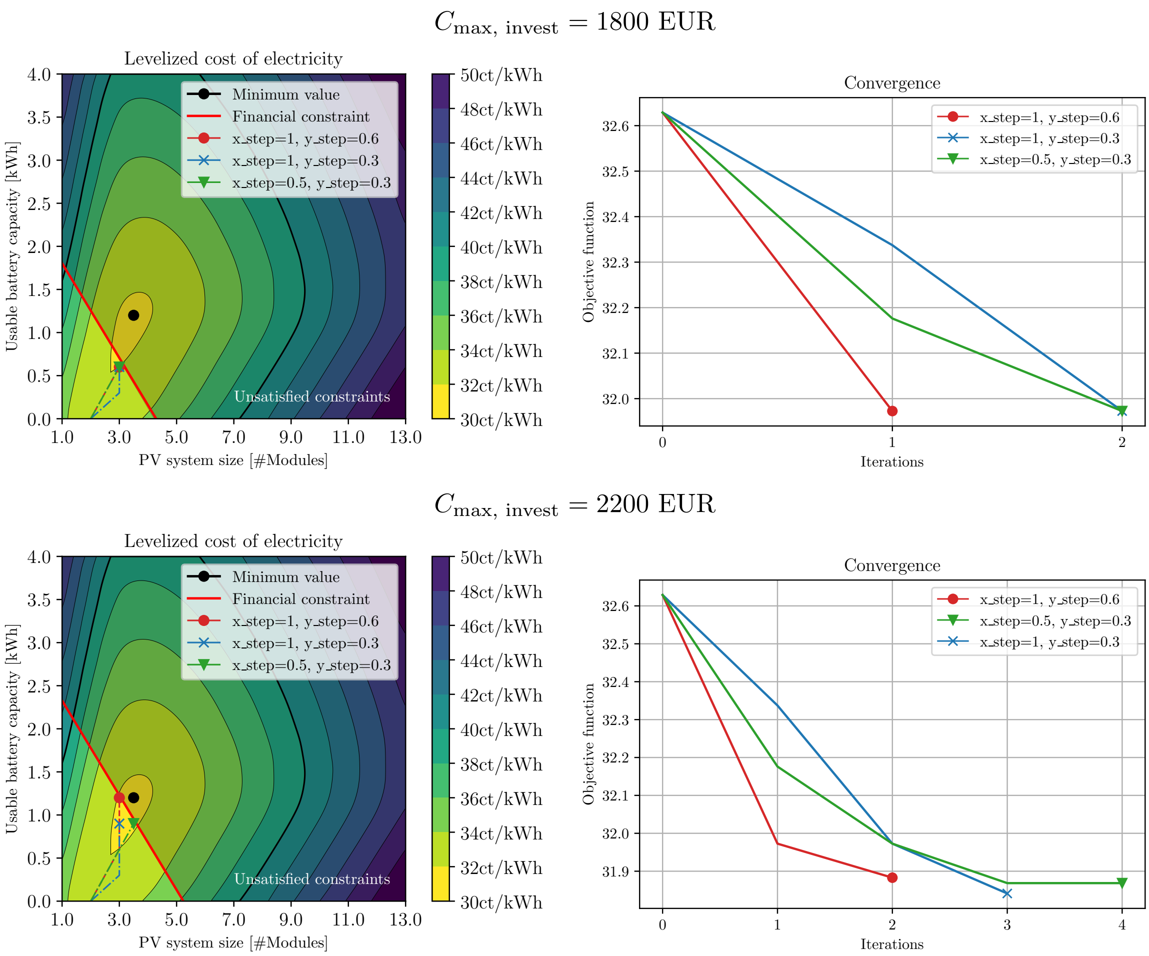


Figure 4.3: constrained optimization procedure using heuristic method with different resolutions and different constraints.

It can be seen in Figure 4.3, that the algorithm does not need many iterations to find an optimum even with constraints. The results of each iteration are saved and the design with the minimum loss is returned. This is for the case the algorithm diverges because of the tolerance given.

### 4.3.2. Newton's Method

**Unonstrained optimization** In an unconstrained optimization, the algorithm's goal is to find an optimum in a 2-dimensional plane. We consider the first and the second derivatives of the target function, which are calculated as follows

$$\begin{aligned}\frac{\partial \mathcal{L}(x,y)}{\partial x} &= \frac{\mathcal{L}(x',y)-\mathcal{L}(x,y)}{x'-x}\\ \frac{\partial \mathcal{L}(x,y)}{\partial y} &= \frac{\mathcal{L}(x,y')-\mathcal{L}(x,y)}{y'-y}\end{aligned} \tag{4.4}$$

where $x' = x - x_0$, $y' = y - y_0$ and $x_0, y_0$ are small numbers and can be interpreted as the resolution of the optimization problem. Here we use $x_0 = 0.2, y_0 = 50$. Even though not any multiplicand of 0.2 is physically possible, but this could also be interpreted as the installed peak capacity of the PV. It is also important to calculate the hessians smoothly. The second derivative of the loss function is calculated analogously with respect to the first derivative. In the following, two optimization strategies are related. A financially unconstrained optimization and a financially constrained optimization. For every $i$-th step of the optimization routine, the hessians are calculated as follows

$$\begin{aligned}dx_i &:= \frac{\partial \mathcal{L}(x,y)}{\partial x} \Big/ \frac{\partial^2 \mathcal{L}(x,y)}{\partial x^2}\\ dy_i &:= \frac{\partial \mathcal{L}(x,y)}{\partial y} \Big/ \frac{\partial^2 \mathcal{L}(x,y)}{\partial y^2}\end{aligned} \tag{4.5}$$

Even though this section has no financial constraints, there are physical constraints, i.e. there are no negative numbers of a battery's capacity or a negative number of panels. Additionally, the minimum number of panels is one. Therefore, the hessians are separately clipped if $x - dx_i < 1$ or if $y - dy_i < 0$

$$\begin{aligned}dx_i &:= x_{i-1} - 1, \quad \text{or}\\ dy_i &:= y_{i-1}\end{aligned} \tag{4.6}$$

In this way, the hessians will not point to "invalid" values. The variables are iteratively updated as

$$\begin{aligned}x_i &:= x_{i-1} - \alpha \cdot dx_i\\ y_i &:= y_{i-1} - \alpha \cdot dy_i\end{aligned} \tag{4.7}$$

where $\alpha$ is close to one, for example 0.95.

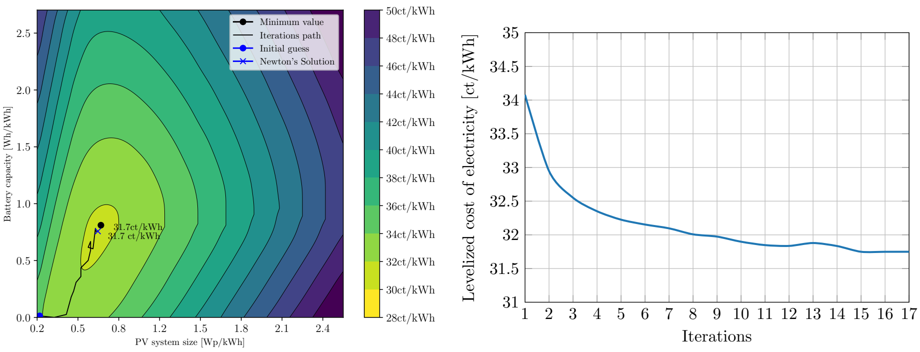


Figure 4.4: Trace and convergence of the optimization path using Newton's method. The algorithm needed 17 iterations.

As a convergence criterion, the optimization process stops once the difference in the target function smaller than a threshold $k_{\text{tres}}$ for the last $n_{\text{tres}}$ consecutive iterations. The size $(x, y)$ along with the corresponding target function $\mathcal{L}(x, y)$ are stored in every iteration. Finally, when the algorithm successfully terminates, the size with the minimum target function is returned. A maximum number of iterations guarantees the termination of the algorithm in a case of a divergence, see Figure 4.4.

**Constrained optimization** As described in Section 4.2, in most cases, an investor is tethered to a maximum possible investment $C_{\text{max, invest}}$ to be paid now. In this case, the search space is defined as

$$S = \{(N_{\text{modules}}, C_{\text{nom}}) | N_{\text{modules}} \cdot C_{\text{module}} + C_{\text{nom}} \cdot c_{\text{BESS}} \leq C_{\text{max, invest}}\} \tag{4.8}$$

Here assuming $C_{\text{max, invest}}$ does not include additional costs on equity such as installation costs and inverter costs. With this definition, the optimal design might exist outside the search space. If it is inside the search space, then not much changes from Section 4.3.2. But if it is outside the search space, then the optimal design with this regard, exists on the upper line, see Figure 4.5.

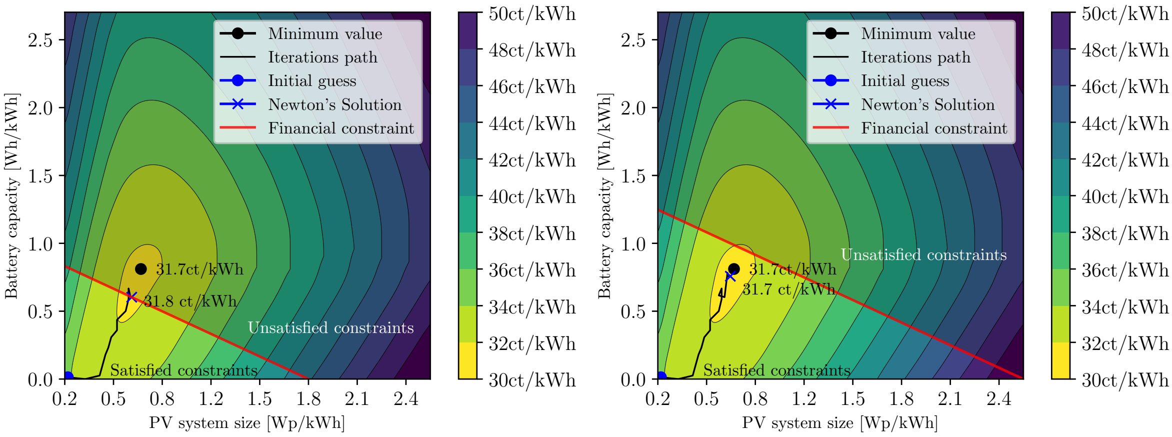


Figure 4.5: Optimization procedure using Newton's method with different financial constraints.

The algorithm proceeds here as in 4.3.2. In every iteration, the algorithm checks whether the equity of the new design exceeds the maximum investment. If not, then nothing is done. Otherwise, the algorithm becomes a 1-dimensional optimization along one axis, i.e. the $x$-axis. The values of the $y$-axis are evaluated using the linear equation of the upper limit of the investment $C_{\text{max, invest}}$.

A comparison between both the heuristic method and Newton's method are compared along with other optimization strategies in Section 5.4.2.

# 5. Case Study

In this section, three scenarios are generated using buildings from the cadaster. The results of finding an optimal design for this scenario are then discussed. The assessment period considered here is 25 years as given in Table 3.15. Input and efficiency parameters are given in Table 5.1.

| Parameter | Symbol | Value |
|---|---|---|
| Price of PV panels | $C_{\text{module}}/P_{\text{max, ref}}$ | 1400 EUR/kWp |
| Battery round-trip efficiency | $\eta_{\text{BESS}}$ | 92% |
| Inverter efficiency | $\eta_{\text{inverter}}$ | 97% |
| Panel size | | 1m×1.6m |
| Panel maximum power point in SRC | $P_{\text{max, ref}}$ | 300 Wp |
| Operation and maintenance (annually) | $C_{\text{O\&M}}$ | $1\% \cdot C_{\text{equity, PV}}$ [1] |
| Additional costs | $C_{\text{additional}}$ | 200 EUR |
| Real battery discount rate | $r_{\text{dr, bat, real}}$ | 3% |
| Real PV discount rate | $r_{\text{dr, real}}$ | 4% |
| inflation rate | $r_{\text{infl}}$ | 2.5% |
| Monthly shrinking rate of feed-in tariff | $i_{\text{feed-in, monthly}}$ | 1.457% |

Table 5.1: Simulation parameters.

The minimum and maximum state of charge optimized for are ($\text{SOC}_{\text{min}} = 10\%$ and $\text{SOC}_{\text{max}} = 95\%$) respectively.

## 5.1. Case study 1

**Input data** The considered annual load of 4500 kWh/a corresponds to four residents living in an apartment with an electrically heated water, see Table 2.4.

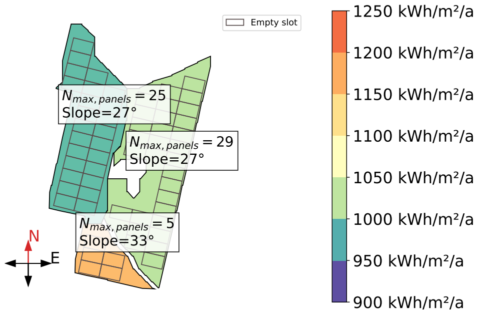


Figure 5.1: Surfaces of the given building by annual radiation and possible slots for PV panels.

| Parameter | Value |
|---|---|
| Address | Eupener Str. 270<br>52076 Aachen |
| Annual load | 4500 kWh |

Table 5.2: Simulation parameters for case study 1.

[1] https://www.solaranlage-ratgeber.de/photovoltaik/photovoltaik-wirtschaftlichkeit/photovoltaik-kosten accessed on Apr 12, 2022.

Table 5.2 provides the address of the building and the annual load. Given the cadastral and meteorological data, the annual irradiation of each surface is calculated using steps described in Sections 2.2, 2.3 and 3.1. As can be seen in Figure 5.1, a maximum of five panels can fit in the surface with maximum irradiation.

**Overview** The system is evaluated with different system designs as can be seen in Figure 5.3. The most profitable design is $\hat{C}_{\text{nom}}$=4.2 kWh of usable battery storage and 3.0kWp of installed PV power, i.e. $\hat{N}_{\text{modules}}$ =10 modules. With this design the levelized cost of electricity is $c_{\text{LCOE}}$=32.37 ct/kWh. The stakeholder consumes 80% of the generated power and 54% of the load is covered by the system.

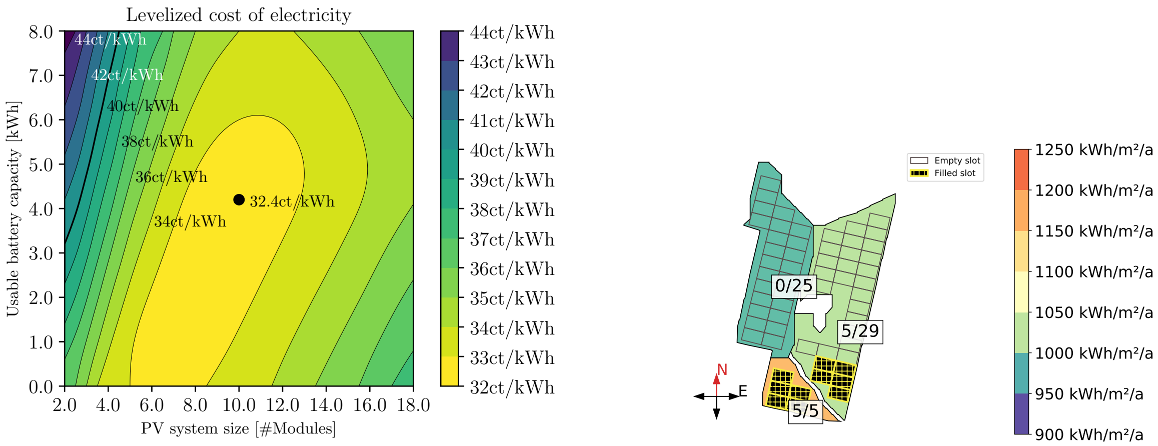


Figure 5.2: Levelized cost of electricity by design with a profitability limit of 39.83 ct/kWh on the left and assignment of panels for each surface of the rooftop for the optimal design on the right.

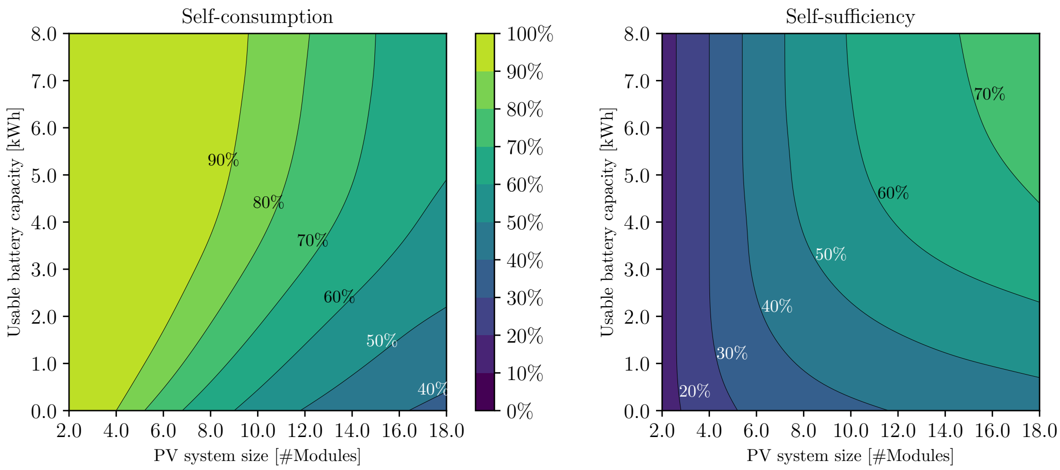


Figure 5.3: Self-consumption and self-sufficiency by design.

| **Parameter** | **Symbol** | **Value** |
|---|---|---|
| Number of modules | $N_{\text{modules}}$ | 10 modules (3 kWp) |
| Battery's capacity | $C_{\text{nom}}$ | 4.2 kWh |
| Equity | $C_{\text{equity}}$ | 6705.09 EUR |
| Mean battery estimated price | $c_{\text{BESS}}$ | 549 EUR/kWh |
| Levelized cost of electricity | $c_{\text{LCOE}}$ | 32.37 ct/kWh |
| Levelized cost of solar energy | $c_{\text{LCOE, PV}}$ | 13.51 ct/kWh |
| Levelized cost of stored energy | $c_{\text{LCOE, BESS}}$ | 31.40 ct/kWh |
| Self-consumption | $r_{\text{self-consumption}}$ | 80.3% |
| Self-sufficiency | $r_{\text{self-sufficiency}}$ | 53.7% |
| Estimated battery life | $N_{\text{BESS, years}}$ | 13 years and 3 months |
| DC output energy | $E_{\text{DC, annual}}$ | 3182.3 kWh |
| AC output energy | $E_{\text{AC, annual}}$ | 3086.8 kWh |
| Energy covered by the PV | $E_{\text{PV}\rightarrow\text{Load}}$ | 1717.9 kWh |
| Energy covered by the battery | $E_{\text{BESS}\rightarrow\text{Load}}$ | 698.8 kWh |
| Energy exported to grid | | 609.3 kWh |
| Energy imported from grid | | 2083.3 kWh |
| Battery loss | | 60.8 kWh |
| DC-AC conversion loss | | 95.5 kWh |
| Annual bill without system (levelized) | | 1792.35 EUR |
| Net annual bill with system (levelized) | | 820.38 EUR |
| Annual investment in electricity with system | | 1456.65 EUR |

Table 5.3: The annual results of the optimal design.

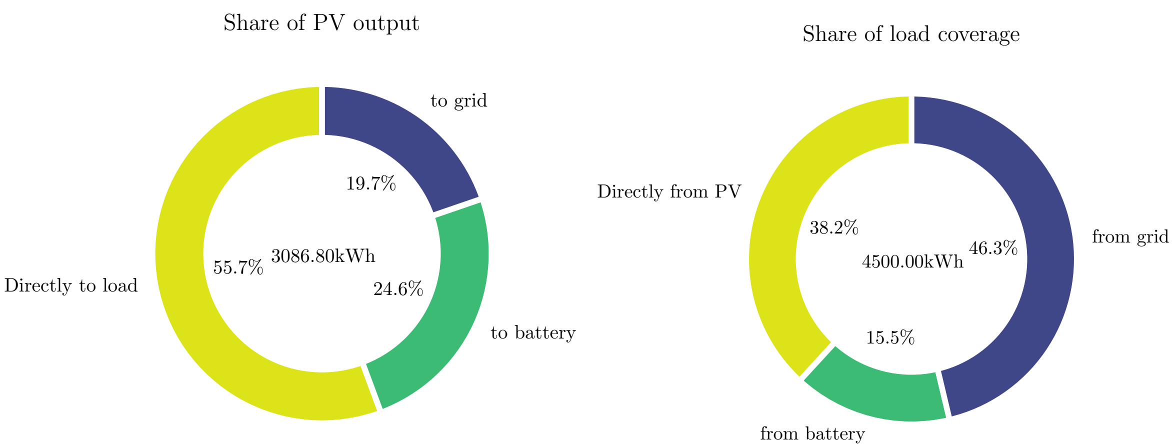


Figure 5.4: Share of PV output power by destination on the left and share of load by source on the right.

As can be seen in Table 5.3 with the optimal design, it is estimated that 335 EUR can be spared annually by investing in such a design. The grid bill is also reduced down to 45.8%. Figure 5.7 provides a visual overview on the energy distribution.

## 5.2. Case study 2

**Input data** The considered building here is a the Moss bakery in Ahornstr of Aachen, Germany. Its estimated area is 50m$^2$ yielding an annual load of 25,000 kWh, see Table 2.3. The corresponding load curve is (g0), see Figure 2.5.

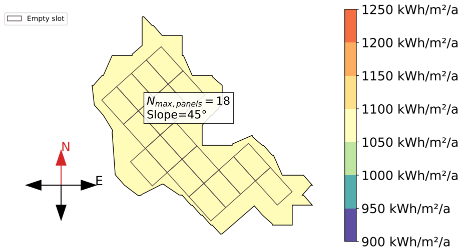


Figure 5.5: Surfaces of the given building by annual radiation and possible slots for PV panels.

| Parameter | Value |
|---|---|
| Address | Ahornstr 35<br>52074 Aachen |
| Annual load | 25,000 kWh |

Table 5.4: Simulation parameters for case study 2.

Similar to study case 1, the incident radiation for each of the surfaces is calculated first. Since there is only one usable surface of the rooftop here, only this surface is taken into account.

**Overview** The levelized cost of electricity is evaluated with the range up to investing in 28 panels. However, as can be seen in Figure 5.5, a maximum of 18 panels can be installed according to the shape given by the cadastral data. Thus, the simulation assumes a maximum of only 18 operating panels. This, in a way, acts as a "penalty function" for the optimization process. It could be seen in Figure 5.6 that the most profitable design is using the maximum capacity and no battery installed. The reason for this, is because the self-consumption of this design is already 95%. The self-sufficiency is, however, only 21%, see Figure 5.7.

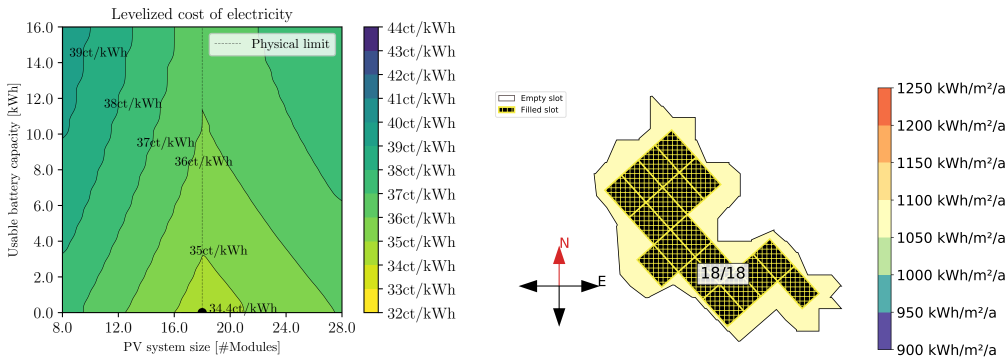


Figure 5.6: Levelized cost of electricity by design with a profitability limit of 39.77 ct/kWh on the left and assignment of panels for each surface of the rooftop for the optimal design on the right.

| Parameter | Symbol | Value |
|---|---|---|
| Number of modules | $N_{\text{modules}}$ | 18 modules (5.4 kWp) |
| Battery's capacity | $C_{\text{nom}}$ | 0 kWh |
| Equity | $C_{\text{equity}}$ | 7760.00 EUR |
| Mean battery estimated price | $c_{\text{BESS}}$ | - |
| Levelized cost of electricity | $c_{\text{LCOE}}$ | 34.44 ct/kWh |
| Levelized cost of solar energy | $c_{\text{LCOE, PV}}$ | 13.46 ct/kWh |
| Levelized cost of stored energy | $c_{\text{LCOE, BESS}}$ | - |
| Self-consumption | $r_{\text{self-consumption}}$ | 95.4% |
| Self-sufficiency | $r_{\text{self-sufficiency}}$ | 20.9% |
| Estimated battery life | $N_{\text{BESS, years}}$ | - |
| DC output energy | $E_{\text{DC, annual}}$ | 5647.3 kWh |
| AC output energy | $E_{\text{AC, annual}}$ | 5477.9 kWh |
| Energy covered by the PV | $E_{\text{PV}\rightarrow\text{Load}}$ | 5227.9 kWh |
| Energy covered by the battery | $E_{\text{BESS}\rightarrow\text{Load}}$ | 0 kWh |
| Energy exported to grid | | 249.9 kWh |
| Energy imported from grid | | 19,772.1 kWh |
| Battery loss | | - |
| DC-AC conversion loss | | 169.4 kWh |
| Annual bill without system (levelized) | | 9957.50 EUR |
| Net annual bill with system (levelized) | | 7871.34 EUR |
| Annual investment in electricity with system | | 8610.0 EUR |

Table 5.5: The annual results of the optimal design.

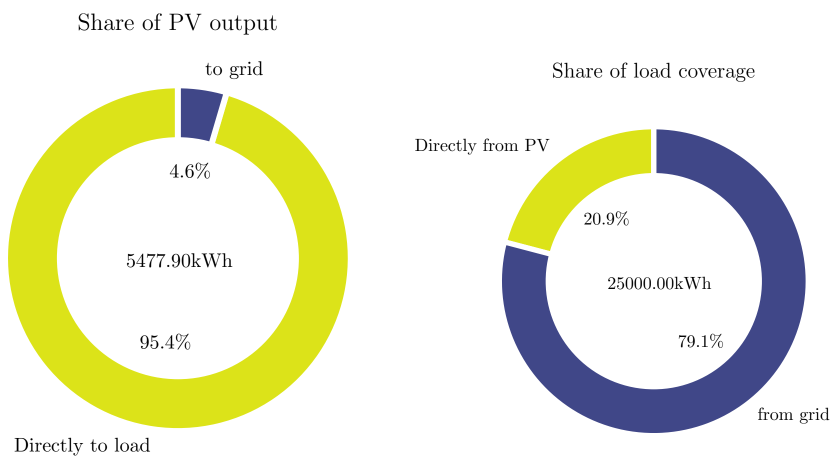


Figure 5.7: Share of PV output power by destination on the left and share of load by source on the right.

Table 5.5 shows that with the optimal design, roughly 1348 EUR can be spared annually by investing in such a design. The grid bill is also reduced down by 21%.

## 5.3. Case study 3

**Input data** The considered scenario here is three families of annual load 4500 kWh each. The corresponding load curve is the residential curve (h0), see Figure 2.5.

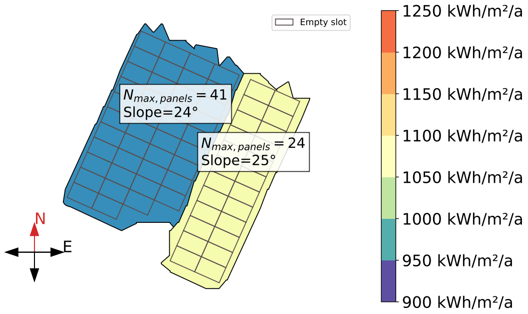


Figure 5.8: Surfaces of the given building by annual radiation and possible slots for PV panels.

| Parameter | Value |
|---|---|
| Address | Am Neuenhof 7<br>52074 Aachen |
| Annual load | 13,500 kWh |

Table 5.6: Simulation parameters for case study 3.

As can be seen in Figure 5.8, the maximal number of PV panels that could fit on the rooftop are 34 panels.

**Overview** As can be seen in Figure 5.9, the optimal design is investing in 33 panels (9.9 kWp) and a size of the Li-ion battery is 16 kWh. This design will result in a levelized cost of electricity of 31.36 ct/kWh.

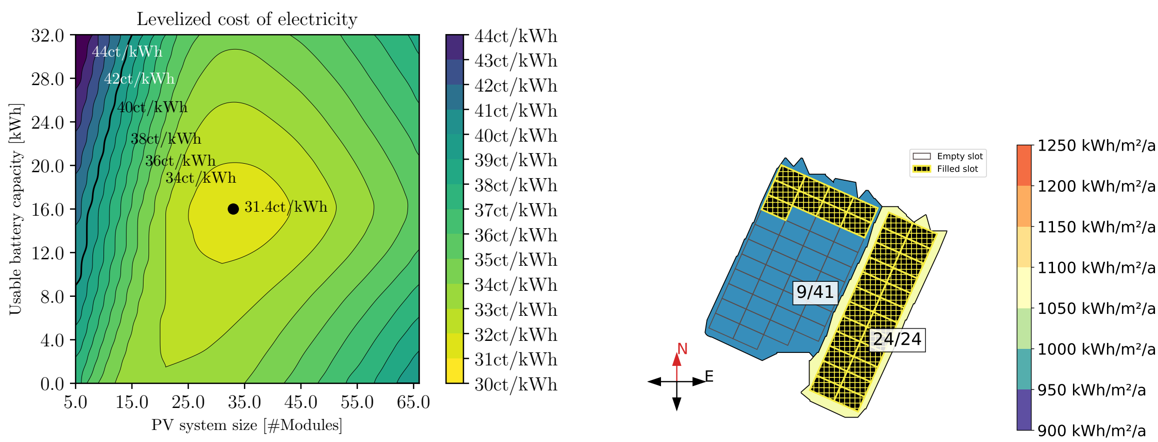


Figure 5.9: Levelized cost of electricity by design with a profitability limit of 39.83 ct/kWh on the left and assignment of panels for each surface of the rooftop for the optimal design on the right.

In such a design, the achieved self-consumption and self-sufficiency are 87% and 34% respectively as can be seen in Figure 5.10 and Figure 5.11. A value of 1144 EUR can be annually spared by investing in such a system.

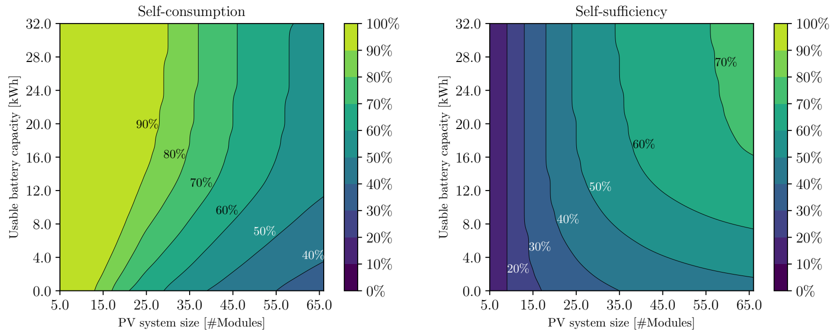


Figure 5.10: Self-consumption and self-sufficiency by design.

| **Parameter** | **Symbol** | **Value** |
|---|---|---|
| Number of modules | $N_{\text{modules}}$ | 33 modules (9.9 kWp) |
| Battery's capacity | $C_{\text{nom}}$ | 16 kWh |
| Equity | $C_{\text{equity}}$ | 20,199.36 EUR |
| Mean battery estimated price | $c_{\text{BESS}}$ | 384 EUR/kWh |
| Levelized cost of electricity | $c_{\text{LCOE}}$ | 31.36 ct/kWh |
| Levelized cost of solar energy | $c_{\text{LCOE, PV}}$ | 13.94 ct/kWh |
| Levelized cost of stored energy | $c_{\text{LCOE, BESS}}$ | 24.22 ct/kWh |
| Self-consumption | $r_{\text{self-consumption}}$ | 80.8% |
| Self-sufficiency | $r_{\text{self-sufficiency}}$ | 56.0% |
| Estimated battery life | $N_{\text{BESS, years}}$ | 14 years and 4 months |
| DC output energy | $E_{\text{DC, annual}}$ | 9896.5 kWh |
| AC output energy | $E_{\text{AC, annual}}$ | 9599.6 kWh |
| Energy covered by the PV | $E_{\text{PV}\rightarrow\text{Load}}$ | 5257.8 kWh |
| Energy covered by the battery | $E_{\text{BESS}\rightarrow\text{Load}}$ | 2302.2 kWh |
| Energy exported to grid | | 1839.4 kWh |
| Energy imported from grid | | 5940.0 kWh |
| Battery loss | | 200.2 kWh |
| DC-AC conversion loss | | 296.9 kWh |
| Annual bill without system (levelized) | | 5377.05 EUR |
| Net annual bill with system (levelized) | | 2337.48 EUR |
| Annual investment in electricity with system | | 4233.6 EUR |

Table 5.7: The annual results of the optimal design.

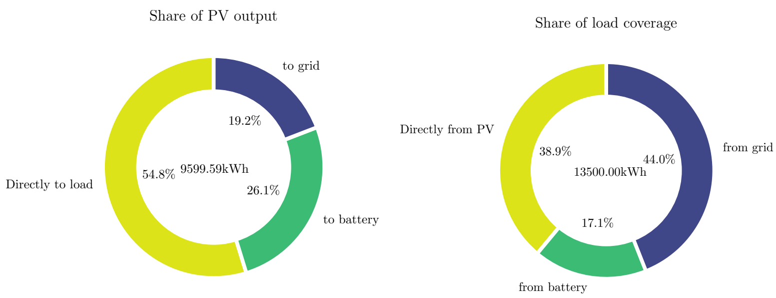


Figure 5.11: Share of PV output power by destination on the left and share of load by source on the right.

## 5.4. Discussion of Results

In this section, the results from previous sections are first compared another online tool and then the optimization process is discussed.

### 5.4.1. Comparison with other tools

In the following, the results are compared with the tool provided by rechnerphotovoltaik[1] with "Photovoltaik Rechner (Experte)" calculator. This tool simulates the photovoltaic system by installed peak power $N_{\text{modules}} \cdot P_{\text{max, ref}}$ and self-consumption. The self-consumption rate was set to the nearest ten, as only this is allowed by this tool. The other inputs are set as in accordance with optimal design for each case study.

| Case study | Parameter | Symbol | Mean Value | |
|---|---|---|---|---|
| | | | Rechnerphotovoltaic | This work |
| 1 | AC output energy | $E_{\text{AC, annual}}$ | 3097.3 kWh | 3086.8 kWh |
| | Energy covered by the system | $E_{\text{PV, BESS}\to\text{Load}}$ | 2477.8 kWh | 2416.7 kWh |
| | Energy exported to grid | | 619.5 kWh | 609.3 kWh |
| | Annual bill reduced by | | 981.6 EUR | 972.0 EUR |
| 2 | AC output energy | $E_{\text{AC, annual}}$ | 5290.3 kWh | 5477.9 kWh |
| | Energy covered by the system | $E_{\text{PV, BESS}\to\text{Load}}$ | 5025.8 kWh | 5227.9 kWh |
| | Energy exported to grid | | 264.5 kWh | 249.9 kWh |
| | Annual bill reduced by | | 1991.0 EUR | 2086.2 EUR |
| 3 | AC output energy | $E_{\text{AC, annual}}$ | 9909.48 kWh | 9599.6 kWh |
| | Energy covered by the system | $E_{\text{PV, BESS}\to\text{Load}}$ | 7927.6 kWh | 7560.0 kWh |
| | Energy exported to grid | | 1981.9 kWh | 1839.4 kWh |
| | Annual bill reduced by | | 3140.6 EUR | 3039.6 EUR |

Table 5.8: Comparison of results with the tool rechnerphotovoltaik.

Table 5.8 compares the results in this work for the previously introduced case studies with the results by the Rechnerphotovoltaic tool. A noticeable deviation emerges when the annual load energy is bigger as in case study 1 and 2.

[1] https://www.rechnerphotovoltaik.de

### 5.4.2. Optimization strategies

in the following, four different optimization strategies are compared, among of which the heuristic method described in Section 4.3.1. Each method was tested with different "initial guesses" (or initial designs). The results can be seen in Table 5.9. For all of the optimization strategies a local cache was used to reduce time needed for simulations in case of repetition of design. The methods are benchmarked with the first case study, see Section 5.1.

| Method | Initial design(s) [module, kWh] | Steps | Simulations | Time [s] | Optimal design [module, kWh] | Optimal cost [ct/kWh] |
|---|---|---|---|---|---|---|
| Newton | (12, 12) | 19 | 95 | 7.97 | (6.4, 0.42) | 32.60 |
| | (5, 5) | 9 | 45 | 3.69 | (6.2, 0.01) | 32.66 |
| | (4, 5) | 31 | 135 | 11.13 | (9.4, 2.86) | 32.85 |
| | (4, 1) | 12 | 60 | 5.15 | (6.2, 0.00) | 32.65 |
| | (2, 0) | 8 | 40 | 3.2 | (6.2, 0.00) | 32.65 |
| Secant | (3, 1), (2, 0.5) | 22 | 154 | 12.61 | (8.1, 2.33) | 32.41 |
| | (5, 5), (4, 4) | 18 | 126 | 11.13 | (7.7, 2.00) | 32.42 |
| | (6, 6), (4, 4) | 35 | 246 | 21.25 | (9.4, 3.96) | 32.39 |
| | (9, 9), (8, 8) | 28 | 196 | 17.6 | (9.2, 4.10) | 32.40 |
| | (20, 10), (19, 9) | 19 | 133 | 11.5 | (9.6, 4.14) | 32.38 |
| Powell | (5, 2.5) | 346 | 331 | 29.37 | (8.6, 2.78) | 32.40 |
| | (5, 5) | 216 | 192 | 16.09 | (10.1, 4.24) | 32.36 |
| | (2, 0) | 426 | 404 | 36.05 | (8.0, 2.14) | 32.41 |
| | (2, 2) | 229 | 205 | 17.55 | (7.8, 2.06) | 32.41 |
| | (5, 5) | 633 | 602 | 49.84 | (10.0, 4.22) | 32.36 |
| Heuristic1 | (15, 0) | 8 | 31 | 2.16 | (10.0, 4.20) | 32.37 |
| | (10, 0) | 8 | 25 | 1.71 | (10.0, 4.20) | 32.37 |
| | (5, 0) | 8 | 18 | 1.36 | (10.0, 4.20) | 32.37 |
| | (2, 0) | 9 | 14 | 1.09 | (10.0, 4.20) | 32.37 |
| Heuristic2 | (15, 0) | 9 | 36 | 2.88 | (8.0, 2.10) | 32.42 |
| | (10, 0) | 9 | 31 | 2.36 | (8.0, 2.10) | 32.42 |
| | (5, 0) | 9 | 24 | 1.96 | (8.0, 2.10) | 32.42 |
| | (2, 0) | 9 | 17 | 1.33 | (8.0, 2.10) | 32.42 |
| Heuristic3 | (15, 0) | 15 | 56 | 4.47 | (10.0, 4.20) | 32.37 |
| | (10, 0) | 16 | 46 | 3.65 | (10.0, 4.20) | 32.37 |
| | (5, 0) | 16 | 30 | 2.43 | (10.0, 4.20) | 32.37 |
| | (2, 0) | 49 | 24 | 2.02 | (10.0, 4.50) | 32.39 |
| Heuristic4 | (15, 0) | 12 | 26 | 1.92 | (10.0, 4.80) | 32.43 |
| | (10, 0) | 7 | 16 | 1.18 | (10.0, 4.80) | 32.43 |
| | (5, 0) | 5 | 10 | 0.73 | (9.0, 3.60) | 32.40 |
| | (2, 0) | 10 | 17 | 1.23 | (11.0, 7.20) | 33.34 |

Table 5.9: Results of different optimization strategies

For all the heuristic methods used, the tolerance `tol` was set to 0.01 ct/kWh and the steps of module numbers was set to one with the exception for method `Heuristic3` it was set to 0.5. Different steps of usable battery capacity were used. For the method `Heuristic1` a step of 0.6kWh, for `Heuristic2` and `Heuristic3` a step 0.3kWh, for `Heuristic4` a step of 1.2kWh were used.

The Newton's method is very dependent on the initial guess. As can be seen in Table 5.9, the number steps needed for Newton's method to converge is minimal when the initial guess is close to the optimum. However it converges sometimes to a local optimum and it take a long time to do so.

The Secant's method, on the other hand, delivers an optimum mostly very close to the global optimum. But it takes relatively more time than Newton's does.

One advanced method is the Powell's [46]. It can clearly be seen that the optimal design it delivers is very accurate. This, unfortunately, comes with a big time cost which is not very suitable for this online application. Moreover, optimizing over rational numbers is not the best option, since the number will be rounded to a natural number in the end, at least for the number of modules.

A realistic approach by heuristically optimizing over the natural numbers of modules and a multiplier of 0.6 of a usable capacity seems to provide a balance between the number of simulations and an acceptable optimal design.

The average simulation time is less than a tenth of a second, thus an exhaustive search with a maximum number of panels of $N_{\text{max, panels}}$ and a maximum capacity of the BESS of $C_{\text{nom, max}}$ would require less than $N_{\text{max, panels}} \cdot C_{\text{nom, max}} \cdot 0.1$ seconds.
To compare with the heuristic model, we assumed the maximum number of panels and maximum capacity correspond with the optimal design and the same resolution is used.

| **Resolution (Panels, kWh)** | **Exhaustive Search** | **Heuristic Method** |
|---|---|---|
| (1, 1.2) | 3s | <2s |
| (1, 0.6) | 6s | <3s |
| (1, 0.3) | 12s | <3s |
| (0.5, 0.3) | 24s | <5s |

Table 5.10: Time comparison between exhaustive search method and heuristic method.

As can be seen in Table 5.10, the exhaustive search method delivers an optimal model with a realistic resolution in the best case faster than Powell's method and ensures that the optimum with the given resolution is found. However, the fact that with unconstrained optimization, the capacity of the BESS is unconstrained. Despite, the fact that the maximum number of panels are constrained by the geometrical shape of the rooftop, the optimal design lies on average much less than that, resulting in even more simulations needed. The difference in the time is because the computational complexity of the exhaustive search is in $\mathcal{O}(N_{\text{max, panels}} \cdot C_{\text{nom, max}})$ while that of the heuristic search is in $\mathcal{O}(N_{\text{max, panels}} + C_{\text{nom, max}})$.

# 6. Conclusion

## 6.1. Summary

In this work, a simulation and optimization tool for estimating an optimal design of a grid-connected photovoltaic (PV) open rack panels system, optionally coupled with a battery energy storage system (BESS) was developed. Important data for the simulation of PV rooftops were collected and processed. These include hourly meteorological data over all Germany from the German Weather Agency (DWD), cadastral data for the rooftops of the buildings in the state of North Rhine-Westphalia (NRW) including geographical coordinates, tilt angle and orientation of each surface from Landesamt für Natur, Umwelt und Verbraucherschutz (LANUV), hourly parameterizable curve of the load power for both residential and commercial profiles. These data-sets, together with a sun position calculation algorithm, are the underlying data input used to simulate the hourly power of the different components of the PV systems, including a BESS.

A simulation of the PV modules was implemented using both an electrical model, namely the single-diode model (SDM) that approximates PV panels maximum power by their electrical parameters and a simple efficiency model that approximates the maximum power by an efficiency or a reference maximum power point. The results of the SDM were validated by a similar paper by NREL [58] and data-sheets, see Table 3.5 and Table 3.6. The simulation of the BESS was done using a simple model with a round-trip efficiency model and a simple dispatching strategy that allows one cycle a day for optimal lifetime of the battery. Furthermore, the hourly results of the system as a whole were successfully validated by the results of `SAM` tools in Section 3.4. Annual results were also compared to `PV*SOL`.

To optimize for a techno-financial objective, a financial model is incorporated to the system in Section 3.5. The financial model accounts both the present and future costs of the PV-BESS system as well as costs paid to the local grid and feed-in revenues from exporting excess energy to the local grid. To account for the costs of the BESS, a lifetime model of the BESS is incorporated to the financial model. Different iterative optimization algorithms were introduced in Section 4 a simple heuristic approach was introduced to optimize in a practical time. The optimization process is optionally constrained by a maximum amount of investment. Moreover, the optimization results were compared for the number of simulations needed and the optimal design achieved in Section 5.4.2.

Finally, a thorough case study on three different profiles was presented and compared with the results from a tool by `photovoltaicrechner`.

## 6.2. Future Work

**Input data** Only the cadastral data of the NRW state are included in this work. Users from other states will have to input three variables, the tilt, orientation and the usable area of each surface of their rooftop. Providing cadastral data-sets for the remaining states in Germany will save users from around Germany time to have an estimation of an optimal model for their needs.

Additionally, the temporal resolution used in this work is in an hourly intervals. Datasets with more temporal resolution help acquiring more stable results.

**Diffuse Radiation Model** The model used in this work to calculate the diffuse radiation is isotropic. It assumes that the sky radiates with the same intensity from all directions except for the sun itself. It, therefore, ignores the possibility that clouds might cover some parts of the sky. Implementing an anisotropic model such as Klucher [24] or Perez [44] would benefit from the cloud cover index provided in the meteorological data-set.

**Battery Model** The simple BESS model used in this thesis does not take into account the power of the battery and the chemical nature of the battery. A more detailed BESS model such as the model used in SAM [8] make incorporating a simulation of a battery's lifetime [57] and a battery management system (BMS) possible. Incorporating the simulation of a BMS allow for the use of today's used dispatching strategies of the battery such as the peak shaving strategy [27].

**Inverter Model** The simple efficiency model for the inverter implement in this work, ignores the maximum AC and DC power output or losses occuring because of consumption at night. A more accurate inverter model also accounts for the AC-DC conversion efficiency with respect to the output power. Such models are the inverter model by *Sandia* [23] or by *Inverter Park Load Curve* by NREL [14].

**Webservice** While the model is fully implemented, mainly in Python, and has a basic mock application programmin intergace (API). It is not yet accessible for end-users. Hence a fully integrated API and a web application are required to make it convenient of end-users to utilize.

# References


[1] Photovoltaics report. Fraunhofer Institute for Solar Energy Systems ISE, Jul 2021.

[2] RWTH Aachen. Speichermonitoring bw. 2019.

[3] A. Balouktsis, T. D. Karapantsios, A. Antoniadis, D. Paschaloudis, A. Bezergiannidou, and N. Bilalis. Sizing stand-alone photovoltaic system. 2005.

[4] M. Balzani and A. Reatti. Neural network based model of a pv array for the optimum performance of pv system. In *Research in Microelectronics and Electronics, 2005 PhD*, volume 2, pages 123–126, 2005. doi: 10.1109/RME.2005.1542952.

[5] Bundesministerium für Umwelt Naturschutz und nukleare Sicherheit co2online. Stromspiegel. 2021/22.

[6] W. DeSoto, S.A.Klein, and W.A.Beckman. Improvement and validation of a model for photovoltaic array performance. 2006.

[7] Nicholas DiOrio, Aron Dobos, Steven Janzou, Austin Nelson, and Blake Lundstrom. Technoeconomic modeling of battery energy storage in sam. 2015.

[8] Nicholas DiOrio, Aron Dobos, Steven Janzou, Austin Nelson, and Blake Lundstrom. Technoeconomic modeling of battery energy storage in sam. 2015.

[9] Aron P. Dobos. Pvwatts version 5 manual. Sep 2014.

[10] Jérémy Dulout, Bruno Jammes, Corinne Alonso, Amjad Anvari-Moghaddam, Adriana Luna, and Josep M. Guerrero. Optimal sizing of a lithium battery energy storage system for grid-connected photovoltaic systems. In *2017 IEEE Second International Conference on DC Microgrids (ICDCM)*, pages 582–587, 2017. doi: 10.1109/ICDCM.2017.8001106.

[11] Homer Energy. Homerő pro version 3.7 user manual. 8 2016.

[12] Jan Figgener, David Haberschusz, Kai-Philipp Kairies, Oliver Wessels, Benedikt Tepe, and Dirk Uwe Sauer. Wissenschaftliches mess- und evaluierungsprogramm solarstromspeicher 2.0. page 12, 2018.

[13] Jan Figgener, Peter Stenzel, Kai-Philipp Kairies, Jochen LinSSen, David Haberschusz, Oliver Wessels, Georg Angenendt, Martin Robinius, Detlef Stolten, and Dirk Uwe Sauer. The development of stationary battery storage systems in germany, a market review. *Journal of Energy Storage*, 29:101153, 2020. ISSN 2352-152X. doi: https://doi.org/10.1016/j.est.2019.101153.

[14] Paul Gilman. Solar advisor model user guide for version 2.0. Aug 2008.

[15] Inmaculada Guaita-Pradas and Ana Blasco-Ruiz. Analyzing profitability and discount rates for solar pv plants. a spanish case. 04 2020.

[16] Mehreen Gul, Yash Kotak, Tariq Muneer, and Stoyanka Ivanova. Enhancement of albedo for solar energy gain with particular emphasis on overcast skies. *Energies*, 11(11), 2018. ISSN 1996-1073. doi: 10.3390/en11112881.

[17] C. Fünfgeld H. Meier, T. Adam, and B. Schieferdecker. Repräsentative vdew-lastprofile. 2005.

[18] Clifford W. Hansen. Parameter estimation for single diode models of photovoltaic modules. Sandia National Laboratories, 2015.

[19] J. Hay and J. Davies. Calculation of the solar radiation incident on an inclined surface. 10, 1980.

[20] Wei He, Michael Pecht, David Flynn, and Fateme Dinmohammadi. A physics-based electrochemical model for lithiumion battery state-of-charge estimation solved by an optimised projection-based method and movingwindow filtering. 2018.

[21] M. M. Ismail, W. R. Anis, and R. Ghoneim. Comparative study between silicon and gallium arsenide on grid pv system. 2017.

[22] William A. Beckman John A. Duffie. Solar engineering of thermal processes. 2013.

[23] D. King, S. Gonzalez, G. Galbraith, and W. Boyson. Performance model for grid-connected photovoltaic inverters. 2007.

[24] T.M. Klucher. Evaluation of models to predict insolation on tilted surfaces. *Solar Energy*, 23(2):111–114, 1979. ISSN 0038-092X. doi: https://doi.org/10.1016/0038-092X(79)90110-5.

[25] Pericles S. Koronakis. On the choice of the angle of tilt for south facing solar collectors in the athens basin area. *Solar Energy*, 36(3):217–225, 1986. ISSN 0038-092X. doi: https://doi.org/10.1016/0038-092X(86)90137-4.

[26] CHRISTOPH KOST, SHIVENES SHAMMUGAM, VERENA FLURI, DOMINIK PEPER, ASCHKAN DAVOODI MEMAR, and THOMAS SCHLEGL. Stromgestehungskosten erneuerbare energien. 237, 07 2021.

[27] Daniel Kucevic, Leo Semmelmann, Nils Collath, Andreas Jossen, and Holger Hesse. Peak shaving with battery energy storage systems in distribution grids: A novel approach to reduce local and global peak loads. *Electricity*, 2(4):573–589, 2021. ISSN 2673-4826. doi: 10.3390/electricity2040033.

[28] M. Kumar and Nallapaneni. Simulation tools for technical sizing and analysis of solar pv systems. Aug 2017.

[29] S. Catalanotti L. Barra, F. Fontana, and F. Lavorante. An analytical method to determine the optimal size of a photovoltaic plant. pages 509 – 514, 1984.

[30] M. Szindler A. Drygaa L.A. Dobrzaski, M. Szczsna*. Electrical properties mono- and polycrystalline silicon solar cells. 2013.

[31] Chun Sing Lai, Youwei Jia, Zhao Xu, Loi Lei Lai, Xuecong Li, Jun Cao, and Malcolm D. McCulloch. Levelized cost of electricity for photovoltaic/biogas power plant hybrid system with electrical energy storage degradation costs. *Energy Conversion and Management*, 153:34–47, 2017. ISSN 0196-8904. doi: https://doi.org/10.1016/j.enconman.2017.09.076.

[32] Umwelt und Verbraucherschutz Nordrhein-Westfalen Landesamt für Natur. Das landesweite solarkataster nordrhein-westfalen. Jul 2012.

[33] Patrik Larsson and Philip Börjesson. Cost models for battery energy storage systems. 2018.

[34] B Liu and R Jordan. Daily insolation on surfaces tilted towards equator. *ASHRAE J.; (United States)*.

[35] Kevin Mallon, Francis Assadian, and Bo Fu. Analysis of on-board photovoltaics for a battery electric bus and their impact on battery lifespan. *Energies*, 10:943, 07 2017. doi: 10.3390/en10070943.

[36] Gilbert M. Masters. Renewable and efficient electric power systems. 2004.

[37] Jean Meeus. Astronomical algorithms. 1998.

[38] A. Mermoud and B. Wittmer. Pvsyst users manual. Jan 2014.

[39] Roger A. Messenger and Jerry Ventre. Photovoltaic systems engineering. 2004.

[40] Joseph J. Michalsky. The astronomical almanac's algorithm for approximate solar position (1950 2050). *Solar Energy*, 40(3):227–235, 1988. ISSN 0038-092X. doi: https://doi.org/10.1016/0038-092X(88)90045-X.

[41] K. Nishioka, N. Sakitani, Y.Uraoka, and T. Fuyuki. Analysis of multicrystalline silicon solar cells by modified 3-diode equivalent circuit model taking leakage current through periphery into consideration. pages 1222 – 1227, 2007.

[42] Björn Nykvist and Måns Nilsson. Rapidly falling costs of battery packs for electric vehicles. *Nature Climate Change*, 5:329–332, 03 2015. doi: 10.1038/nclimate2564.

[43] Chibuisi Okorieimoh, Brian Norton, and Michael Conlon. Long-term durability of solar photovoltaic modules. 10 2019.

[44] Richard Perez, Pierre Ineichen, Robert Seals, Joseph Michalsky, and Ronald Stewart. Modeling daylight availability and irradiance components from direct and global irradiance. *Solar Energy*, 44(5):271–289, 1990. ISSN 0038-092X. doi: https://doi.org/10.1016/0038-092X(90)90055-H.

[45] Piyasak Poonpun and Ward Jewell. Analysis of the cost per kilowatt hour to store electricity. *Energy Conversion, IEEE Transactions on*, 23:529 – 534, 07 2008. doi: 10.1109/TEC.2007.914157.

[46] M. J. D. Powell. An efficient method for finding the minimum of a function of several variables without calculating derivatives. *The Computer Journal*, 7(2): 155–162, 01 1964. ISSN 0010-4620. doi: 10.1093/comjnl/7.2.155.

[47] PVGIS. Pvgis version 5 manual.

[48] R. Pässler. Parameter sets due to fittings of the temperature dependencies of fundamental bandgaps in semiconductors. 1999.

[49] A.D. Rajapakse and Dharshana Muthumuni. Simulation tools for photovoltaic system grid integration studies. pages 1 – 5, 11 2009. doi: 10.1109/EPEC.2009.5420370.

[50] Ibrahim Reda and Afshin Andreas. Solar position algorithm for solar radiation applications. 2008.

[51] PVsyst SA. User's guide pvsyst contextual help. pages 1222 – 1227, 2012.

[52] Chih-Tang Sah, Robert N. Noyce, and William Shockley. Carrier generation and recombination in p-n junctions and p-n junction characteristics. pages 1228–1243, 1957.

[53] P. K. Sarswat and M. L. Free. A study of energy band gap temperature relationships for cu2znsns4 thin films. 2011.

[54] W. Shockley and H. J. Queisser. Detailed balance limit of efficiency of pn junction solar cells. 1960.

[55] Walter Short, Daniel J. Packey, and Thomas Holt. A manual for the economic evaluation of energy efficiency and renewable energy technologies. 03 1995.

[56] Valetin Software. Pv*sol expert 6.0.

[57] R. Spotnitz. Simulation of capacity fade in lithium-ion batteries. *Journal of Power Sources*, 113(1):72–80, 2003. ISSN 0378-7753. doi: https://doi.org/10.1016/S0378-7753(02)00490-1.

[58] H. Tian, F. Mancilla-David, K. Ellis, P. Jenkins, and E. Muljadi. A detailed performance model for photovoltaic systems. NREL, Jul 2012.

[59] B.K. Das V. Khanna, D. Bisht, and P.K. Singh Vandana. A three diode model for industrial solar cells and estimation of solar cell parameters using pso algorithm. 2015.

[60] K.V. Vidyanandan. An overview of factors affecting the performance of solar pv systems. *Energy Scan (A house journal of Corporate Planning, NTPC Ltd.)*, 27: 3–8, Feb 2017.

[61] Johannes Weniger, Tjarko Tjaden, and Volker Quaschning. Sizing of residential pv battery systems. *Energy Procedia*, 46:78–87, 2014. ISSN 1876-6102. doi: https://doi.org/10.1016/j.egypro.2014.01.160. 8th International Renewable Energy Storage Conference and Exhibition (IRES 2013).

[62] Muhammad Fahad Zia, Elhoussin Elbouchikhi, and Mohamed Benbouzid. Optimal operational planning of scalable dc microgrid with demand response, islanding, and battery degradation cost considerations. *Applied Energy*, 237:697–707, 03 2019. doi: 10.1016/j.apenergy.2019.01.040.

# List of Figures

2.1. The Sun's geocentric and topocentric altitude . . . 9
2.2. The structure of cadaster data after processing. . . . 11
2.3. An example of a random building in the cadaster provided by LANUV 12
2.4. Illustration of maximum panels fitting in a rooftop . . . 13
2.5. An hourly based residential and commercial load curve . . . 14
2.6. The residential load curve over the year . . . 15
3.1. Angle of incidence, the Sun's altitude, PV surface inclination and azimuth angles . . . 17
3.2. Share of the components of incident radiation by inclination angle . . . 18
3.3. Illustration of a photovoltaic cell . . . 19
3.4. Equivalent circuit of a three-diode model . . . 20
3.5. Equivalent circuit of a single-diode model . . . 21
3.6. I-U curve by incident radiation and temperature . . . 21
3.7. Comparison of a I-V curve predicted by the single-diode model implemented in the thesis and a data-sheet . . . 27
3.8. Comparison of the linear approximation of the MPP by temperature and radiation . . . 29
3.9. Illustration of power balance over the year for a residential profile . . . 30
3.10. Comparison between annual energy output and annual energy output delivered to the load in different cities in Germany. The data was simulated by the simple efficiency model for the typical load of one person living in a house with a 120W MPP module. . . . 31
3.11. Comparison of annual energy output in different cities . . . 32
3.12. Overview of the data flow in the system . . . 32
3.13. Approximation of the cycle lifetime of the Li-ion battery . . . 34
3.14. Power balance throughout a day and battery SOC . . . 36
3.15. Comparison of power output AC and energy delivered to the load . . . 38

3.16. The error of incident radiation between SAM tools and this work. . . . 39
3.17. The error of cell temperature between SAM tools and this thesis. . . . 39
3.18. The error of DC output between SAM tools and this work. . . . . . . . 40
3.19. The error of AC output between SAM tools and this work. . . . . . . . 40
3.20. The error of electricity delivered to load between SAM tools and this work. . . . . . . . . . . . . . . . . . . . . . . . . . . . . . . . . . . . . 41
3.21. The error of power balance between SAM tools and this work. . . . . . 41
3.22. Comparison of monthly energy delivered by the BESS to the load. . . . 43
3.23. The error of the battery state of charge. . . . . . . . . . . . . . . . . . 44
3.24. State-of-charge throughout the year as predicted by SAM and this work 44
3.25. Annual energy flow compared to SAM for use case 1 . . . . . . . . . . . 45
3.26. Annual energy flow compared to SAM for use case 2 . . . . . . . . . . . 46
3.27. Distribution of energy surplus and deficit . . . . . . . . . . . . . . . . . 49
3.28. On the left, the cost of storage by profile using $60W_p$ modules and their optimal capacity, i.e. with minimum levelized cost of stored energy. On the right, the cost of stored energy by year of operation with an expected lifetime of 7 years. . . . . . . . . . . . . . . . . . . . . . . . . . . . . . . . . . 50
3.29. Cost of electricity imported from the grid annually and average cost of imported electricity within the scope of 25, 15 and 10 years on the left. Change of feed-in tariff on an annual basis and the average feed-in tariff on the right. 51
3.30. Feed-in tariff in Germany since 2021 . . . . . . . . . . . . . . . . . . . . 51
3.31. Illustration of monthly feed-in by monthly decreasing feed-in tariffs . . 52
3.32. Cost of energy storage per kWh by year of operation. . . . . . . . . . . 52
3.33. Cost of energy storage per kWh by capacity . . . . . . . . . . . . . . . 53
3.34. Mean cost of electricity by the size of system and assessment period . . 54
3.35. Levelized cost of electricity by the cyclic lifetime of the battery. . . . . 55
3.36. Lifetime of the battery by the cyclic lifetime of the battery. . . . . . . . 55
3.37. Levelized cost of electricity by load curve. . . . . . . . . . . . . . . . . 55
3.38. Levelized cost of electricity by inflation rate. . . . . . . . . . . . . . . . 56
3.39. Levelized cost of electricity by cost of battery. . . . . . . . . . . . . . . 56
3.40. Levelized cost of electricity by feed-in tariff. . . . . . . . . . . . . . . . 57
3.41. Levelized cost of electricity by minimum self-consumption rule. . . . . . 57
3.42. Self-consumption and self-efficiency by system size. . . . . . . . . . . . 58
4.1. Heuristic search in pseudocode. . . . . . . . . . . . . . . . . . . . . . . 61
4.2. Optimization procedure using heuristic method with different resolutions and starting points. . . . . . . . . . . . . . . . . . . . . . . . . . . 62
4.3. constrained optimization procedure using heuristic method with different resolutions and different constraints. . . . . . . . . . . . . . . . . . . 63
4.4. Trace and convergence of the optimization path using Newton's method. The algorithm needed 17 iterations. . . . . . . . . . . . . . . . . . . . . 64
4.5. Optimization procedure using Newton's method with different financial constraints. . . . . . . . . . . . . . . . . . . . . . . . . . . . . . . . . . 65
5.1. Surfaces of the rooftop by annual radiation and maximum number of panels . . . . . . . . . . . . . . . . . . . . . . . . . . . . . . . . . . . . 66

5.2. Levelized cost of electricity by design on the left and assignment of panels for each surface of the rooftop on the right. . . . . . . . . . . . . 67
5.3. Self-consumption and self-sufficiency by design. . . . . . . . . . . . . . 67
5.4. Share of PV output power by destination and share of load by source . 68
5.5. Surfaces of the rooftop by annual radiation and maximum number of panels . . . . . . . . . . . . . . . . . . . . . . . . . . . . . . . . . 69
5.6. Levelized cost of electricity by design on the left and assignment of panels for each surface of the rooftop on the right. . . . . . . . . . . . . 69
5.7. Share of PV output power by destination and share of load by source for case study 2 . . . . . . . . . . . . . . . . . . . . . . . . . . . . 70
5.8. Surfaces of the rooftop by annual radiation and maximum number of panels for case study 3 . . . . . . . . . . . . . . . . . . . . . . . . . 71
5.9. Levelized cost of electricity by design on the left and assignment of panels for each surface of the rooftop on the right. . . . . . . . . . . . . 71
5.10. Self-consumption and self-sufficiency by design. . . . . . . . . . . . . . 72
5.11. Share of PV output power by destination and share of load by source for case study 3 . . . . . . . . . . . . . . . . . . . . . . . . . . . . 72
A.1. Inflation rate in Germany from 2017 until 2022. . . . . . . . . . . . . . 91
A.2. Cost of a lithium-ion battery per kWh without BMS from 2010 until 2022. 92

# List of Tables

1.1. Related work . . . . . . . . . . . . . . . . . . . . . . . . . . . . . . 2
2.1. Features provided by different meteorological datasets . . . . . . . . . . 6
2.2. Relevant features provided in the cadaster . . . . . . . . . . . . . . . . 11
2.3. Annual energy load per meter squared of commercials . . . . . . . . . . 15
2.4. Annual energy load per number of residents . . . . . . . . . . . . . . . 16
2.5. Definition of seasons . . . . . . . . . . . . . . . . . . . . . . . . . . . 16
3.1. Physical parameters of various semiconductor materials . . . . . . . . . 20
3.2. Parameters of SRC and NOCT testing conditions . . . . . . . . . . . . 22
3.3. Availability of PV-Module parameters . . . . . . . . . . . . . . . . . . 25
3.4. Results of estiamted parameters of the single-diode model . . . . . . . . 27
3.5. Validation of the results of the single diode model in this work . . . . . 28
3.6. Comparison of the results of the model with data-sheets . . . . . . . . 28
3.7. System Parameters for the validation of the photovoltaic model . . . . 37
3.8. Comparison of annual results by different models . . . . . . . . . . . . 38
3.9. Error between this work and SAM tools for a standalone system . . . . 42
3.10. Comparison of error with different sub-models of the thesis . . . . . . . 42
3.11. Battery design parameters for the validation of the battery-coupled model 43
3.12. Error between this work and SAM tools for a battery coupled system for use case 1 . . . . . . . . . . . . . . . . . . . . . . . . . . . . . . . 44
3.14. Error between this work and SAM tools for a battery coupled system for use case 2 . . . . . . . . . . . . . . . . . . . . . . . . . . . . . . . 45

3.15. Levelized values of different parameters by assessment period. . . . . . . . . 53
5.1. Simulation parameters for all case studies . . . . . . . . . . . . . . . . . . 66
5.2. Simulation parameters for the case study 1 . . . . . . . . . . . . . . . . . 66
5.3. Annual results of optimal design for case study 1 . . . . . . . . . . . . . 68
5.4. Simulation parameters for case study 2 . . . . . . . . . . . . . . . . . . . 69
5.5. Annual results of optimal design for case study 2 . . . . . . . . . . . . . 70
5.6. Simulation parameters for case study 3 . . . . . . . . . . . . . . . . . . . 71
5.7. Annual results of optimal design for case study 3 . . . . . . . . . . . . . 72
5.8. Comparison of case study results with the tool rechnerphotovoltaik . . 73
5.9. Results of different optimization strategies . . . . . . . . . . . . . . . . . 74
5.10. Time comparison between exhaustive search method and heuristic method. 75
A.1. Default values for single value parameters of the system with references 91

# Nomenclature

| | |
|---|---|
| $I$ | PV cell's current, see Equation (3.12) |
| $I_0$ | Reverse saturation current, see Equation (3.21) |
| $I_{\mathrm{d}}$ | Diode (leakage) current, see Equation (3.14) |
| $I_{\mathrm{ph}}$ | Photocurrent, see Equation (3.17) |
| $I_{\mathrm{sh}}$ | Shunt current, see Equation (3.13) |
| $I_{0,\mathrm{ref}}$ | Reverse saturation current in SRC |
| $R_{\oplus}$ | Radius of Earth's orbit, see Section 2.2 |
| $\mu_{\mathrm{P}}$ | The relative power temperature coefficient, see Table 3.3 |
| $\mu_{I_{\mathrm{sc}}}$ | The relative short-circuit current temperature coefficient, see Table 3.3 |
| $\mu_{U_{\mathrm{oc}}}$ | The relative open-circuit voltage temperature coefficient , see Table 3.3 |
| $h$ | Planck's constant |
| $k$ | The Boltzmann constant |
| $q$ | The elementary charge of an electron |
| $d_{\mathrm{julian}}$ | Julian day, see Section 2.2 |
| $N_{\mathrm{BESS,\ days}}$ | Lifetime of the battery in days, see Equation (3.69) |
| $\alpha_{\odot,\mathrm{geo}}$ | The Sun's geocentric right ascension, see Equation (2.5) |
| $\alpha_{\odot,\mathrm{topo}}$ | The Sun's topocentric right ascension, see Equation (2.11) |

| | |
|---|---|
| $\Delta\varepsilon$ | The nutation in the obliquity of the ecliptic, see Section 2.2 |
| $\Delta\lambda_{\odot,\text{geo}}$ | The nutation in Sun's longitude, see Section 2.2 |
| $\delta_{\odot,\text{geo}}$ | The Sun's geocentric declination, see Equation (2.5) |
| $\delta_{\odot,\text{topo}}$ | The Sun's topocentric declination, see Equation (2.13) |
| $\lambda$ | The observer's geographical longitude angle |
| $\lambda_{\odot}$ | The Sun's apparent longitude, see Equation (2.4) |
| $\lambda_{\odot,\text{geo}}$ | The Sun's geocentric longitude, see Equation (2.1) |
| $\lambda_{\oplus,\text{helio}}$ | Earth's heliocentric longitude, see Section 2.2 |
| $\phi$ | The observer's geographical latitude angle |
| $\phi_{\odot,\text{geo}}$ | The Sun's geocentric latitude, see Equation (2.1) |
| $\phi_{\oplus,\text{helio}}$ | Earth's heliocentric latitude, see Section 2.2 |
| $\theta_{\text{HRA, geo}}$ | The observer's geocentric hour angle, see Equation (2.6) |
| $\theta_{\text{HRA, topo}}$ | The observer's topocentric hour angle, see Equation (2.12) |
| $\varphi'_{\odot}$ | The Sun's topocentric altitude angle without correction for atmospheric refraction, see Equation (2.15) |
| $v$ | The apparent sidereal time at Greenwich, see Equation (2.3) |
| $\beta$ | Surface inclination (tilt), see Table 2.2 |
| $\gamma$ | Surface azimuth (orientation), see Table 2.2 |
| $\gamma_{\odot}$ | The Sun's azimuth angle, see Equation (2.17) |
| $\theta_{\text{incidence}}$ | Angle of incidence, see Equation (3.3) |
| $\varphi_{\odot}$ | The Sun's altitude angle, see Equation (2.17) |
| $\eta_{BESS}$ | Battery's round-trip efficiency |
| $\eta_{\text{inverter}}$ | Inverter's DC-AC efficiency |
| $\eta_{\text{PV}}$ | Solar cell efficiency, see Equation (3.39) |
| $C_{\text{max, invest}}$ | Maximum amount of investment |
| $C_{\text{additional}}$ | Additional costs, including inverter and installation costs |
| $C_{\text{BESS}}$ | Annual costs of energy storage |

| | |
|---|---|
| $C_{\text{equity, BESS}}$ | Equity of the BESS system, see Equation (3.73) |
| $C_{\text{equity, PV}}$ | Equity of the PV system, see Equation (3.65) |
| $C_{\text{equity}}$ | Equity of the PV-BESS system, see Equation (3.73) |
| $C_{\text{feed-in}}$ | Annual reveneues from exporting to grid, see Equation (3.55) |
| $C_{\text{import}}$ | Annual costs from importing from grid, see Equation (3.54) |
| $C_{\text{O\&M, NPV}}$ | Net present value of future operation and maintenance costs |
| $C_{\text{O\&M}}$ | Annual operation and maintenance costs |
| $C_{\text{PV}}$ | Annual costs of solar energy |
| $C_{\text{system}}$ | Lifetime cost of the PV system including additional and future costs, see Equation (3.63) |
| $c_{\text{BESS, ref}}$ | Mean cost of one kWh of lithium-ion battery, see Equation (3.79) |
| $c_{\text{BESS, today}}$ | Current cost of one kWh of lithium-ion battery |
| $c_{\text{BESS}}$ | Mean cost of one kWh of lithium-ion battery adjusted with capacity, see Equation (3.80) |
| $c_{\text{feed-in, today}}$ | Current feed-in tariff |
| $c_{\text{feed-in}}$ | Mean feed-in tariff, see Equation (3.76) |
| $c_{\text{grid, today}}$ | Current electricity retail rate |
| $c_{\text{grid}}$ | Mean electricity retail price, see Equation (3.74) |
| $c_{\text{LCOE, BESS}}$ | Levelized cost of stored energy, see Equation (3.72) |
| $c_{\text{LCOE, PV}}$ | Levelized cost of solar energy, see Equation (3.66) |
| $c_{\text{LCOE}}$ | Levelized cost of electricity, see Equation (3.53) |
| $t$ | Hour of day |
| $t_{\text{end}}$ | The hour of day where charging the battery ends, see Equation (3.51) |
| $t_{\text{start}}$ | The hour of day where charging the battery begins, see Equation (3.51) |
| $p_{\text{ambient}}$ | Air pressure |
| $T_{\text{ambient}}$ | Ambient temperature |
| $T_{\text{cell}}$ | Cell temperature (operating temperature), see Equation (3.10) |

| | |
|---|---|
| $T_{\text{NOCT}}$ | Ambient temperature in NOCT, see Table 3.2 |
| $T_{\text{ref}}$ | Cell temperature in SRC, see Table 3.2 |
| $P_{\text{AC}}$ | AC power output, see Equation (3.41) |
| $P_{\text{balance}}$ | Power balance, see Equation (3.40) |
| $P_{\text{DC}}$ | DC power output, see Equation (3.42) |
| $P_{\text{load}}$ | Load power, see Equation (2.18) |
| $P_{\text{max}}$ | Maximum power of a solar cell, see Equation (3.38) |
| $E_{\text{PV}\rightarrow\text{Load}}$ | Energy delivered to load directly by the PV, see Equation (3.45) |
| $E_{\text{PV}\rightarrow\text{BESS}}$ | Annual energy delivered to the BESS by the PV system |
| $E_{\text{PV}\rightarrow\text{Load, BESS}}$ | Annual energy delivered to the load and the BESS by the PV system |
| $E_{\text{AC, annual}}$ | Annual AC energy output, see Equation (3.44) |
| $E_{\text{AC, lifetime}}$ | Lifetime AC energy output, see Equation (3.62) |
| $E_{\text{BESS, lifetime}}$ | Lifetime stored energy in the BESS, see Equation (3.71) |
| $E_{\text{DC, annual}}$ | Annual DC energy output, see Equation (3.43) |
| $E_{\text{load}}$ | Annual load energy, see Equation (2.19) |
| $E_{\text{photon}}$ | Energy of a photon, see Equation (3.8) |
| $E_g$ | Band gap energy, see Equation (3.9) |
| $A_{\text{module}}$ | Area of solar cell module |
| $v_{\text{wind}}$ | Wind speed |
| $N_{\text{modules, series}}$ | Number of solar modules connected in series |
| $N_{\text{modules}}$ | Number of solar modules |
| $N_{\text{p}}$ | Number of solar modules connected in parallel |
| $N_s$ | Number of solar cells connected in series in all modules, see Equation (3.18) |
| $N_{c,\text{module}}$ | Number of solar cells connected in series in a module |
| $R_{\text{sh}}$ | Shunt resistor in SDM |
| $R_{\text{s}}$ | Series resistor in SDM |

| | |
|---|---|
| $r_{\text{BESS}}$ | Annual decrease rate in the cost of the lithium-ion battery |
| $r_{\text{CRF, BESS}}$ | Cost recovery factor for the BESS system |
| $r_{\text{CRF, PV}}$ | Cost recovery factor for the PV system, see Equation (3.61) |
| $r_{\text{dr, BESS, real}}$ | Real discount rate of the BESS |
| $r_{\text{dr, PV, real}}$ | Real discount rate for PV |
| $r_{\text{dr, PV}}$ | Nominal discount rate for PV, see Equation (3.60) |
| $r_{\text{feed-in, annually}}$ | Annual decrease rate in feed-in tariff |
| $r_{\text{feed-in, monthly}}$ | Monthly decrease rate in feed-in tariff |
| $r_{\text{grid, annually}}$ | Annual increase rate in electricity retail rate |
| $r_{\text{inflation}}$ | Inflation rate |
| DOD | Battery's depth of discharge |
| SOC | Battery's state of charge |
| $\text{SOC}_{\text{max}}$ | Battery's maximum state of charge, see Equation (3.47) |
| $\text{SOC}_{\text{min}}$ | Battery's minimum state of charge, see Equation (3.49) |
| $r_{\text{albedo}}$ | Albedo (Ground reflectance ratio) |
| $U$ | PV cell's voltage |
| $U_T$ | The volt equivalent of temperature, see Equation (3.15) |
| $U_{\text{d}}$ | Voltage across a diode, see Equation (3.15) |
| $\mathcal{I}$ | Global incident irradiance, see Equation (3.7) |
| $\mathcal{I}_{\text{ref}}$ | Incident radiation in SRC, see Table 3.2 |
| $I_{\text{diffuse, H}}$ | Diffuse horizontal irradiance (DHI) |
| $I_{\text{diffuse, T}}$ | Diffuse irradiance on a tilted surface, see Equation (3.5) |
| $I_{\text{direct, H}}$ | Direct horizontal irradiance, see Equation (3.1) |
| $I_{\text{direct, N}}$ | Direct normal irradiance (DNI), see Equation (3.1) |
| $I_{\text{direct, T}}$ | Direct irradiance on a tilted surface, see Equation (3.4) |
| $I_{\text{global, H}}$ | Global horizontal irradiance (GHI), see Equation (3.2) |

$I_{\text{reflected, T}}$ Reflected irradiance on a tilted surface, see Equation (3.6)

$N_{\text{analysis}}$ Analysis period in years

$N_{\text{BESS, cal}}$ Calendar lifetime of the battery in years

$N_{\text{BESS, cyc}}$ Cycle lifetime of the battery in cycles

$N_{\text{BESS, years}}$ Lifetime of the battery in years, see Equation (3.70)

$N_{\text{PV, years}}$ Lifetime of the PV system in years

# Acronyms

| | |
|---|---|
| AC | Alternating Current |
| BDEW | Bundesverband der Energie und Wissenschaft |
| BESS | Battery Energy Storage System |
| BMS | Battery Management System |
| BMUV | Bundesministerium für Umwelt, Naturschutz, nukleare Sicherheit und Verbraucherschutz |
| CRF | Cost Recovery Factor |
| DC | Direct Current |
| DDM | Double Diode Model |
| DHI | Diffuse Horizontal Irradiance |
| DNI | Direct Normal Irradiance |
| DOD | Depth of Discharge |
| DWD | Deutsche Wetterdienst |
| EEG | Erneuerbare Energien Gesetz (Renewable Energy Sources Act) |
| ETRS98 | European Terrestrial Reference System 1989 |
| GHI | Global Horizontal Irradiance |
| GIS | Geographical Information System |
| JSON | JavaScript Object Notation |
| LANUV | Landesamt für Nature, Umwelt und Verbraucherschutz |
| LCOE | Levelized Cost of Energy |
| LIDAR | Laser Detection and Ranging |
| MAE | Mean Absolute Error |
| MPP | Maximum Power Point |
| MPPT | Maximum Power Point Tracker |
| NOCT | Nominal Operating Cell Temperature |
| NPV | Net Present Value |
| NREL | National Renewable Energy Laboratory (USA) |
| NRW | North Rhine-Westphalia |
| O&M | Operation and Maintenance |
| PV | Photovoltaic |
| SAM | System Advisor Model |
| SDM | Single Diode Model |
| SOC | State of Charge |
| SPA | Sun Position Algorithm |
| SRC | Standard Reference Conditions |
| TDM | Three Diode Model |
| TRY | Test Reference Years |
| WGS84 | World Geodetic System of 1984 |

# A. Appendix

| Parameter | Symbol | Unit | Value | Reference |
|---|---|---|---|---|
| Albedo | $r_{\text{albedo}}$ | % | 0.2 | [16] |
| Inverter efficiency | $\eta_{\text{inverter}}$ | % | 96 | [9] |
| Battery's round-trip efficiency | $\eta_{\text{BESS}}$ | % | 92 | [10] |
| Cost of a PV module | $C_{\text{module}}$ | EUR | $1400 \cdot P_{\text{max, ref}}$ | [2] |
| Current cost of one kWh of a lithium-ion battery | $c_{\text{BESS, today}}$ | EUR | 850 (500 - 1200) | [26] |
| Operation and maintenance costs | $C_{\text{O\&M}}$ | EUR | $1\% \cdot C_{\text{equity, PV}}$ | [1] |
| Additional costs | $C_{\text{additional}}$ | EUR/kW$_\text{p}$ | 185 (150-220) | [2] |
| Current electricity rate | $c_{\text{grid, today}}$ | ct/kWh | 31.09 | [3] |
| Current feed-in tariff | $c_{\text{feed-in, today}}$ | ct/kWh | 6.53 | [4] |
| Annual decrease rate in the cost of a lithium-ion battery | $r_{\text{BESS}}$ | % | 8 | [42] |
| Real discount rate of the PV | $r_{\text{dr, PV, real}}$ | % | 4 | [15] |
| Real discount rate of the BESS | $r_{\text{dr, BESS, real}}$ | % | 3 | [33] |
| Inflation rate | $r_{\text{inflation}}$ | % | 2.6 | [5] |
| Annual increase rate in electricity rate | $r_{\text{grid, annually}}$ | % | 2 | [61] |
| Annual decrease rate in feed-in tariff | $r_{\text{feed-in, annually}}$ | % | 15 | [4] |
| Monthly decrease rate in feed-in tariff | $r_{\text{feed-in, monthly}}$ | % | 1.457 | [4] |
| Calendar lifetime of the BESS | $N_{\text{BESS, cal}}$ | year | 25 | [10] |
| Lifetime of the PV | $N_{\text{PV, years}}$ | year | 25 | [43] |

Table A.1: Default values for single value parameters of the system.

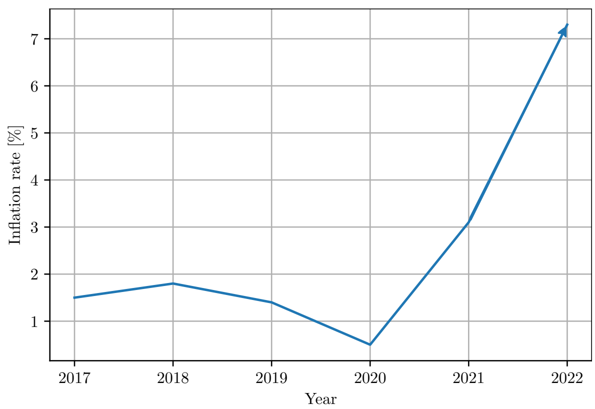


Figure A.1: Cost of the lithium-ion battery without BMS from 2010 until 2022[5] .

[1] https://www.solaranlage-ratgeber.de/photovoltaik/photovoltaik-wirtschaftlichkeit/photovoltaik-kosten accessed on Apr 12, 2022.

[2] https://www.photovoltaik-angebotsvergleich.de/photovoltaik-kosten.html accessed on Apr 20, 2022.

[3] https://www.stawag.de/fileadmin/stawag/content/Dokumente/Strom/Preisblatt_StromSTAR_2021.pdf accessed on Apr 12, 2022.

[4] Based on historical data from https://www.wegatech.de/ratgeber/photovoltaik/foerderung-finanzierung/einspeiseverguetung/ accessed on Apr 20, 2022.

[5] Averaged annually from year 2017 to 2022 from data by https://de.statista.com/statistik/daten/studie/1046/umfrage/inflationsrate-veraenderung-des-verbraucherpreisindexes-zum-vorjahr/ and https://de.statista.com/statistik/daten/studie/1045/umfrage/inflationsrate-in-deutschland-veraenderung-des-verbraucherpreisindexes-zum-vorjahresmonat/ accessed on Apr 20, 2022.

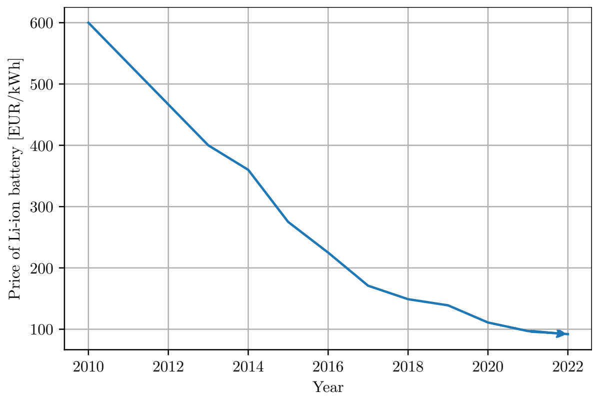


Figure A.2: Cost of the lithium-ion battery without a BMS from 2010 until 2022[1].

[1] `https://de.statista.com/statistik/daten/studie/534429/umfrage/weltweite-preise-fuer-lithium-ionen-akkus/` accessed on Apr 20, 2022.